A STUDY OF THE INTERACTIONS OF MOLTEN SODIUM NITRATE–POTASSIUM NITRATE 50 MOL % MIXTURE WITH WATER VAPOR AND CARBON DIOXIDE IN AIR

FINAL REPORT

June 2, 1980 - June 30, 1981

S. H. White
U. M. Twardoch

951 3351

EIC Laboratories, Inc.
55 Chapel Street
Newton, Massachusetts 02158

September 1981

Work Performed for
U.S. Department of Energy
Under Contract to
Sandia Laboratories, Livermore, California
CONTRACT NO. 20-2991

DISCLAIMER

SAND--80-8182

DE82 010033

EXECUTIVE SUMMARY

The interactions of aerial components such as water, carbon dioxide and oxygen with the binary 50 mol% mixture of sodium nitrate and potassium nitrate (a potential thermal storage fluid) have been studied in the temperature range 300-600°C using electrochemical methods. In addition, the behavior of nitrite ions in this melt was investigated electrochemically because these ions are a major thermal decomposition product of nitrate and, therefore, represent a further possible reactant with atmospheric components. Essentially it was planned to apply electrochemical techniques as in situ methods to monitor directly any interactive chemistry of the melt-atmosphere system. However, it was recognized early in the program that the electrochemical behavior of water, carbon dioxide, carbonate ions (a product of the interactive chemistry) and nitrite ions was rather complex. Nevertheless, by judicial choice of techniques, in situ electroanalysis was possible and the necessary relevant data to accomplish this has been developed, as well as some new insights into the corresponding electrochemical mechanisms associated with the electroactive species. A feature of this electrochemistry is the coupling of fast multi-order chemical reactions following the electrochemical steps.

By the use of selected inert materials such as alumina and gold, extrinsic reactions were minimized. This, together with the purification techniques developed in this work for the melt, ensured that any observed reactivity would be related confidently to the interaction of the melt (nitrate dilute in nitrite) with atmospheric components. The influence of each atmospheric component was examined separately.

On the basis of the results obtained during these studies, a number of conclusions can be drawn which are relevant to the thermal storage program.

Although nitrite ions can be detected at low temperature in melted commercial salts, their formation can be ascribed to the influence of reducing impurities in the nitrate salts. Suitable purification methods described ensured that their concentration was less than 10^{-3} mol-kg^{-1} below 300°C. As the temperature is raised above this level, nitrite ions begin to accumulate due to thermal decomposition of the nitrate. Measurements at 500°C showed that the equilibrium concentration of nitrite expected at this temperature under oxygen is reached at a time greater than one day although initial buildup (20% of the equilibrium amount) is rapid. Nitrite ions can be removed temporarily by treating the melt with nitrogen dioxide. The presence of nitrite ions may have a deleterious effect as there is a strong possibility that they are the site at which carbon dioxide can attack the melt. Water has a significant solubility in the binary nitrate melt which depends upon the humidity in the supernatant

atmosphere and the melt temperature. Although the direct measurement of water solubility by combined electrochemical methods of lower precision than direct manometry, the data of Zambonin have been confirmed. It is suggested that these results can be extrapolated with confidence to 600°C. No electrochemical evidence for hydrolytic reactions was obtained. Water can be rapidly and reversibly taken up or removed from the melt up to 600°C. Two methods of in situ analysis for water are described. The most insidious component of the atmosphere in relation to nitrate thermal storage liquids is carbon dioxide. Pure carbon dioxide attacks the melt at all temperatures above 250°C. The product of this reaction is carbonate. The reaction is probably diffusion controlled. It is to be expected that carbonate will be a major impurity in spite of the low carbon dioxide content of the atmosphere, because of the long term exposure. The solubility of carbonate is strongly temperature dependent and thermal cycling may result in precipitation of carbonate which could cause problems in piping. It is expected that any hydroxide will be converted to carbonate in the presence of air. If carbonate buildup is a significant problem, then regeneration of clean melt can be achieved with NO_2 (or better NO_2/O_2) treatment. Carbonate ions in the form of 1.1 wt% potassium carbonate in the melt were removed by bubbling (100 ml/min) NO_2 gas through the melt at 500°C for less than one hour.

Carbonate ions, dissolved water and less easily nitrite ions can be detected by direct in situ electrochemical measurements and relevant data to achieve this are included in the text.

DEFINITION OF SYMBOLS

Symbol	Physical Quantity	Units
ν	kinematic viscosity	(cm^2-sec^{-1})
η	viscosity	gm-cm^{-1}-sec^{-1} (poise)
ρ	density	gm-cm^{-3}
D	diffusion coefficient	cm^2-sec^{-1}
C	concentration	m (molal) mol-kg^{-1} M (molar) mol-ℓ^{-1}
F	Faraday	Cb-mol^{-1}
k	chemical rate constant	
i	current	amperes
j	current density	amp-cm^{-2}
A	area	cm^2
E	potential (versus reference electrode)	V
p	partial pressure	mM
v	scan rate	V-sec^{-1}
ω	rotation rate $2\pi f$ f = revolutions sec^{-1}	rad-sec^{-1}
t	temperature	°C
T	temperature T = t + 273	°K
n	number of electrons in overall reaction	
n_a	number of electrons in rate determination step (n_a = 1)	
R	gas constant	8.316 joule mol^{-1}°K^{-1}
τ	transition time	seconds
i_p	peak current (voltammetry)	amps
i_L	limiting current	amps
RP	rest potential (zero current)	volts
K	equilibrium constant	

TABLE OF CONTENTS

Section		Page
	EXECUTIVE SUMMARY	i
1.0	INTRODUCTION	1
2.0	PREVIOUS STUDIES	2
3.0	EXPERIMENTAL PROCEDURES	14
	3.1 Materials	14
	3.2 Experimental Apparatus and Electrochemical Cell Assemblies	17
	3.2.1 General	17
	3.2.2 Electrodes	17
	3.2.3 Other Probes	19
	3.2.4 Electrochemical Techniques	21
	3.2.5 Procedure	21
4.0	RESULTS AND DISCUSSION	23
	4.1 General Chemistry and Electrochemistry of the Equimolar Sodium-Nitrate Potassium-Nitrate Mixture	23
	4.2 Nitrite - The Chemical and Electrochemical Behavior of Nitrite Ions in Equimolar Sodium Nitrate Potassium Nitrate Mixture	25
	4.2.1 Introduction	25
	4.2.2 Electrochemical Study of the Oxidation of Nitrite Ions	26
	4.2.3 Mechanism of the Nitrite Oxidation	41
	4.2.4 The Chemical Behavior of Nitrite Ions	46
	4.3 Water - The Chemical and Electrochemical Behavior of Water in Equimolar Sodium Nitrate-Potassium Nitrate Mixture	48
	4.3.1 Electrochemical Study of the Reduction of Water	50
	4.3.2 The Physical and Chemical Properties of Water in Contact with the Nitrate Mixture	70
	4.4 Carbon Dioxide - The Interaction of Carbon Dioxide with the Equimolar Molten Sodium Nitrate-Potassium Nitrate Mixture	76
	4.4.1 Introduction	76
	4.4.2 Electrochemistry of Carbonate Ion Oxidation on Stationary Gold Electrodes	76
	4.4.3 The Chemistry of Carbon Dioxide and Carbonate Formation in the Equimolar Nitrate Mixture	85
	REFERENCES	92

LIST OF FIGURES

		Page
Fig. 1	Plot of Henrian constant for water as a function of temperature.	13
Fig. 2	Apparatus for the purification of molten nitrates. . . .	15
Fig. 3	Vacuum line and auxiliary gas lines.	16
Fig. 4	Electrodes and cells used in experimental work	18
Fig. 5	Electrodes and cell inserts.	20
Fig. 6	Binary nitrate melt, range of electroinactivity as detected by cyclic voltammetry on gold electrodes. . . .	24
Fig. 7	Current reversal chronopotentiogram at low concentration of NO_2^- ions 3.316×10^{-3} molal at Au electrode 0.365 cm^2, applied current 1.50 mA, t = 350°C	27
Fig. 8	Sand plot for the oxidation of nitrite ions in sodium nitrate-potassium nitrate (50 mol%) at different concentrations and temperatures	28
Fig. 9	Sand plot for nitrite ion oxidation at gold electrode. .	29
Fig. 10	Karaoglanoff plot for the oxidation of nitrite ions on a Au electrode at 325°C.	30
Fig. 11	Arrhenius plot of the diffusion coefficient of nitrite ions in equimolar sodium nitrate-potassium nitrate determined from Sand's equation.	33
Fig. 12	Voltammetric peak current as a function of the square root of scan rate for the oxidation of nitrite ions at different concentrations and temperatures on gold. . . .	35
Fig. 13	Voltammetric peak current as a function of the square root of the scan rate at different nitrite concentrations and melt temperatures.	36
Fig. 14	Plot of peak potential versus logarithm of the scan rate at different concentrations and temperatures for the oxidation of nitrite ions on gold electrodes	37
Fig. 15	Current reversal chronopotentiogram at high concentration of NO_2^- ions (17.10×10^{-3} molal) at Au electrodes . . .	39

LIST OF FIGURES
(Continued)

		Page
Fig. 16	Determination of order of following chemical reaction and influence of temperature and concentration	40
Fig. 17	Cyclic voltammogram for nitrite ion process at low concentration (3.316×10^{-3} molal) for different scan rates at Au electrode, 0.365 cm^2	42
Fig. 18	Cyclic voltammograms for nitrite ion process at high concentration 17.10×10^{-3} molal for two different scan rates at Au electrode 0.358 cm^2.	43
Fig. 19	Influence of concentration and temperature on the ratio of reverse peak current/forward peak current for nitrite oxidation	44
Fig. 20	Growth of nitrite ion concentration after purging nitrate melt with NO_2 gas at 500°C oxygen atmosphere	49
Fig. 21	Differential pulse voltammogram for water reduction at 300°C.	51
Fig. 22	Chronopotentiogram for the reduction of water on Au electrode at 525°C, p_{H_2O} = 19.3 mm	52
Fig. 23	Cyclic voltammograms for water reduction as a function of scan rate. Gold electrode, 350°C water partial pressure = 21 mm	53
Fig. 24	Series of cyclic voltammograms for the water processes at different scan rates.	54
Fig. 25	Hydrodynamic voltammograms for the reduction of water at a rotating gold disc electrode (0.021 cm^2) at 405°C in KNO_3-$NaNO_3$ (50 mol%)	55
Fig. 26	Current function versus scan rate at constant temperature at three water partial pressures.	57
Fig. 27	Peak current function versus scan rate for four different temperatures	58
Fig. 28	Plot of peak potential as function of ℓn scan rate for three different water partial pressures and constant temperature (300°C).	60

LIST OF FIGURES
(Continued)

		Page
Fig. 29	Plot of $-i_L/mA$ versus the square root of the rotation rate at 295°C and three water partial pressures.	62
Fig. 30	Plot of $E(i_L/2)$ versus $\ell n\omega$ at 405°C and a partial pressure of 16.48 mm. Theoretical slope for EC mechanism.	63
Fig. 31	Limiting current data analysis for E.C.E. mechanism. . .	65
Fig. 32	Temperature dependence of the diffusion coefficient of water	66
Fig. 33	Cyclic voltammograms on gold electrodes for water. . . .	69
Fig. 34	Development of water peak, 300°C p_{H_2O} = 19.35 mm	71
Fig. 35	Increase of water content during equilibration process under different conditions	72
Fig. 36	Plot of log water concentration ($mol\text{-}kg^{-1}$) versus time in min	74
Fig. 37	Two chronopotentiograms at different current densities for the oxidation of carbonate ions at 530°C and 20.69×10^{-3} molal	77
Fig. 38	Typical voltammogram for the oxidation of carbonate ions on gold electrode (0.21 cm^2)	78
Fig. 39	Sand's plots for carbonate ion oxidation as a function of temperature and concentration	79
Fig. 40	Sand's plot for carbonate ion oxidation at 505°C	80
Fig. 41	Sand's constant as a function of carbonate ion concentration at 550°C	81
Fig. 42	Karaoglanoff plots for the oxidation of carbonate ions .	82
Fig. 43	Current reversal chronopotentiogram at gold electrode 0.21 cm^2 and 505°C	83

LIST OF FIGURES
(Continued)

		Page
Fig. 44	Arrhenius plot for carbonate ion diffusion.	86
Fig. 45	Buildup of carbonate ions in the binary nitrate melt in contact with dry carbon dioxide	87
Fig. 46	Anodic peak observed after CO_2 in contact with nitrate melt after 3 days	89
Fig. 47	Voltammograms showing the melts (1) containing carbonate and nitrate ions before NO_2 treatment and (2) after NO_2 treatment and showing developing NO_2^- ion peak.	90
Fig. 48	Cyclic voltammograms showing background during removal of CO_2/water; showing background 15 hours after dry argon; after addition of 30.8×10^{-3} molal $NaNO_2$ and 12.5×10^{3} molal K_2CO_3	91

LIST OF TABLES

		Page
Table 1	Physical Properties of 50 Mol% Sodium Nitrate-Potassium Nitrate Mixture.	3
Table 2	Electrochemical Data Relating to Oxidic and Other Species in Nitrates ($NaNO_3$-KNO_3)	5
Table 3	Thermodynamic Data Relevant to Possible Reactions in Molten Nitrates.	7
Table 4	Solubility Limit for Carbonate in the Sodium-Nitrate, Potassium-Nitrates Equimolar Mixture	8
Table 5	H_2O Solubility in Molten Nitrates/Nitrites	12
Table 6	Value of $E_{\tau/4}$ at Different Temperatures.	31
Table 7	Diffusion Coefficient for NO_2^- in Molten Sodium Nitrate-Potassium Nitrate Mixture (50 mol%) as a Function of Temperature, Calculated from the Sand's Equation	32
Table 8	Comparison of Experimental and Literature Data for Nitrate Ion Diffusion Coefficients in Molten KNO_3-$NaNO_3$ 50 mol%.	32
Table 9	Comparison of the Observed Half Peak Width with the Value for a Reversible Process (Soluble Product) at Several Different Temperatures	38
Table 10	Estimate of the Linear Sweep Voltammetric Function Based on Experimentally Measured $i_p v^{-\frac{1}{2}}$ and the Experimental Sand Constant $it^{\frac{1}{2}}$.	38
Table 11	Some Thermodynamic Data Relating to Reactions (35) and (36) Over the Temperature Range 230°C to 600°C	47
Table 12	CV Data for the Reduction of Water in Molten $NaNO_3$-KNO_3 (50-50 mol%) Mixture at 295°C on Stationary Gold Electrode (0.21 cm^2)	56
Table 13	HDV Data for Reduction of Water on Au Disc, 0.21 cm^2 and a Scan Rate 2 $mV\text{-}sec^{-1}$, t°C = 295.	56
Table 14	Half Peak Width Data (E_p-$E_{p/2}$) for Water Reduction Peak Compared with that Expected for Reversible-Irreversible/ Chemical Complication at Several Temperatures.	61

LIST OF TABLES
(Continued)

		Page
Table 15	Results of the Combined Analysis of Hydrodynamic and Voltammetric Data for Water at 295°C.	64
Table 16	Diffusion Coefficient of Water Relevant Data.	67
Table 17	Examples of E_p Versus Ag/0.07m AgNO, $NaNO_3$-KNO_3 Reference Electrode at Scan Rate 0.100 V-sec^{-1} over the Temperature Interval 250-600°C for Range of Thermal Water Partial Pressure.	75
Table 18	Results for Karaoglanoff Plots for Carbonate Oxidation.	84

1.0 INTRODUCTION

A number of liquids have been suggested to bridge the solar energy/thermal storage interface. The more promising are simple high temperature liquids amongst which molten alkali metal nitrates appear the most attractive for heat transfer and energy storage. The Department of Energy has established a comprehensive development program in the area of thermal storage. Although alkali metal nitrates are used industrially as heat transfer and heat treatment media, and consequently some scientific and technological base exists, the more demanding needs of solar applications, such as higher operating temperatures (400-650°C), long term stability (30 years), and low corrosiveness required more extensive data than existed previously. A number of different liquid nitrate mixtures have been used previously, but the 50-50 molar mixture of sodium nitrate-potassium nitrate has been selected for extensive investigation. Among the areas of study are those concerning corrosion, salt composition changes, and thermophysical properties, specifically in the temperature range 300-600°C.

The objectives of the EIC program have been to examine the chemical behavior of components of the atmosphere such as water, carbon dioxide, and oxygen in contact with the 50 mol% mixture of sodium nitrate and potassium nitrate. These interactions have been investigated by the application of electrochemical procedures such as cyclic voltammetry, chronoamperometry, hydrodynamic voltammetry, pulse voltammetry, and chronopotentiometry. The above techniques enable the detection and identification of many ionic and molecular species in the concentration range 0.0002-0.2 weight percent to be made *in situ* in the molten salt phase. Thus, the direct measurement of solubility and chemical reaction reactants and products can, in principle, be made. As it will be shown later, the electrochemistry of the atmospheric components of interest is complicated by, *inter alia*, coupled chemical reactions involving nitrate and nitrite ions aided by the high temperatures involved, and the quantitative determination of solution species is no longer straightforward. Nevertheless, the data obtained have provided insight into the interactive chemistry of the nitrate solvent and atmospheric components, which will be presented and discussed in some detail both from the electrochemical and technological viewpoints.

2.0 PREVIOUS STUDIES

Although various aspects of molten alkali metal nitrate chemistry have been investigated in some detail previously, albeit at lower temperatures, it is convenient to bring together the relevant aspects of these studies in relationship to the objectives of this work. In particular, it is necessary to present some of the chemical and electrochemical results on which the present methodology is based. It is possible to make use of some of the earlier results to unravel the complex chemistry and electrochemistry which results from the interaction of oxygen, water, and carbon dioxide with the sodium nitrate-potassium nitrate liquid mixture.

Alkali metal nitrates have commonly been employed as solvents in high temperature studies. Their physical properties and those of the lower melting mixtures have been studied extensively, particularly in the case of sodium nitrate-potassium nitrate mixtures (1). Table 1 shows some typical properties, particularly the kinematic viscosity which is required for the application of hydrodynamic voltammetry to these systems.

Thermodynamically, pure alkali nitrates are rather stable even at moderately high temperatures (<650°C); the most important of the decomposition reactions

$$2NO_3^- \rightleftarrows 2NO_2^- + O_2 \qquad (1)$$

has an equilibrium constant around 5.7×10^{-2} at one atmosphere of oxygen (2). The rate of the reaction

$$2NO_2^- + O_2 \rightleftarrows 2NO_3^- \qquad (2)$$

was shown to be significant above 500°C. Data will be presented (vide infra) on the reverse of this reaction, obtained during the course of this work for a melt from which carbonate and nitrite ions had been eliminated by NO_2 treatment. The buildup of nitrite could then be observed.

At higher temperatures, nitrite may thermally decompose but little is known about these reactions, particularly over long periods of time. Janz et al. (1) indicate that the reaction

$$2NO_2^- \rightarrow O^{2-} + NO + NO_2 \qquad (3)$$

may occur under gas flow conditions, at temperatures above 650°C. No oxide ions have been detected in the melt at lower temperatures in this work.

TABLE 1

PHYSICAL PROPERTIES OF 50 MOL% SODIUM NITRATE-POTASSIUM NITRATE MIXTURE

Melting Point	220°C
Viscosity	$10^2\eta = 90.8112 - 35.1716 \times 10^{-2}T + 46.64877 \times 10^{-5}T^2 - 20.8610 \times 10^{-8}T^3$
Density	$\rho = 2.2860 - 6.72864 \times 10^{-4}T + 9.5 \times 10^{-9}T^2$
Kinematic Viscosity	$10^2\nu = 0.380083 - 1.2996 \times 10^{-3}T + 1.283 \times 10^{-6}T^2 - 3.9805 \times 10^{-13}T^4 + 1.6182 \times 10^{-11}T^3$
Potential Stability Range vs. 0.07m Ag/Ag(1)	
300°C	-1.45V to + 0.4V
500°C	-1.1V to + 0.4V
Based on $\Delta G°_{250}$ $NaNO_3$	3.018V

The moderation of these intrinsic reactions in the presence of other reagents is a subject of some concern technologically. It is known for heat treatment baths that carbonate ions and hydroxide ions build up, suggesting that carbon dioxide and water can interact either directly with the nitrate melt itself or via the thermal decomposition products. On the other hand, little or no evidence exists for oxygen derivatives such as O_2^- or O_2^{2-} being formed in the melt. This has been confirmed by the studies reported here. The role of oxygen is essentially confined to that of controlling equilibrium (1). At low temperatures, oxygen solubility has been measured manometrically in oxide-free melts (3). It is implicit in these measurements, in the temperature range 240-330°C, that reaction (1) does not occur. The results of Nissen (4) and observations reported in this work suggest that the oxygen solubility will be unaffected by chemical effects during the time period of these measurements. Thus, the physical solubility of oxygen was obtained. This is confirmed by the linearity of the calculated Henrian constant with temperature. From Zambonin's results, a positive heat of solution was obtained and the solubility S, in mol kg^{-1} at one atmosphere oxygen is given by

$$\ln S_{O_2}(T_2) = -12.289 - \frac{4.2 \times 10^3}{R}\left(\frac{1}{T_2} - \frac{1}{T_1}\right) \qquad (4)$$

where

$$S_{O_2} = K_H p_{O_2} \qquad (5)$$

and $T_1 = 511°K$.

In parallel work, Zambonin (5) and Jordan and Zambonin and co-workers (6,7) have studied the electroreduction of oxygen in wet and dry melts, respectively. The processes

$$O_2 + e \rightarrow O_2^- \qquad (6)$$

$$O_2^- + e \rightarrow O_2^= \qquad (7)$$

have been determined in dry melts. The relevant data are recorded in Table 2. On the other hand, a different electrochemical reaction was observed in wet melts which depended upon the oxygen solubility. This reaction, which was shown by massive electrolysis to be

$$O_2 + 2H_2O + 4e \rightleftarrows 4OH^-, \qquad (8)$$

was examined as a function of electrode rotation rate, oxygen concentration, and temperature (3). An activation energy for diffusion was reported as 5.0 kcal mol^{-1}. The evaluation of the diffusion coefficient was based upon a simple reversible diffusion-controlled model involving four electrons. At 550°K, D was 3.1×10^{-4} cm^2-sec^{-1}. This value for the

TABLE 2

ELECTROCHEMICAL DATA RELATING TO OXIDIC AND OTHER SPECIES IN NITRATES ($NaNO_3$-KNO_3)

Species	E(V)*	10^5D cm^2sec^{-1}	Temp. (°K)	Method	Reference
NO_2^-	$E_{\tau/4}^{NO_2/NO_2^-} = -0.44$	5.2**	571	Chronopotentiometry	25
	$E_{\frac{1}{2}} = -0.44$	0.525	502	Rotating Disc Electrode	21
		2.4 ± 0.7	523	Chronopotentiometry	23
H_2O	$E_{\frac{1}{2}} = -1.19$	1.9	502	Rotating Disc Electrode	30
O_2^-	$E_{\frac{1}{2}}^{O_2/O_2^-} = -0.74$	0.475	502	Rotating Disc Electrode	7
O_2^{2-}	$E_{\frac{1}{2}}^{O_2^-/O_2^{2-}} = -1.28$	0.31	502	Rotating Disc Electrode	7
OH^-	$E^{O_2H_2O/OH^-} = -0.495$	-	502	Potentiometry	8
O_2	$E_{\frac{1}{2}}^{O_2H_2O/OH^-} = -0.65$	31†	520††	Rotating Disc Electrode	3
Cl^-	$E_p = -0.27$	0.152	423	Linear Sweep Voltammetry Hg	42
	$E_{\frac{1}{2}} = -0.212$	0.691	518	Pulse Polarography Hg	68

*Versus 0.07 molal Ag^+/Ag reference electrode.

**The large discrepancy here may arise from the inadvertent presence of oxidic species which in the chronopotentiometric method consume current leading to τ being enhanced, hence resulting in D being too large cf. RDE technique.

†This based on (a) K_H 4.8 x 10^{-6} mol $kg^{-1}atm^{-1}$ and using wet oxygen.

††Measured over the temperature range 525-575°K.

diffusion coefficient is at least one order of magnitude larger than expected. The evaluation of D is critically dependent on a correct evaluation of n and the limiting current function. The implication here, given that the solubility data are correct, is that the reduction reaction is much more complex than that assumed by Zambonin. Since his work is based upon limited rotating disc measurements, little can be said concerning the mechanism. No value can be placed upon the value of D although the activation energy may be correct. At higher temperatures, it is to be expected that the solubility of oxygen will be influenced by the nitrate-nitrite equilibrium and hence ΔH would be expected to become more negative. Thus, extrapolation of Zambonin's solubility data for oxygen to the temperature range 400-600°C cannot be carried out, and for this reason and the reasons given above about the diffusion coefficient of oxygen, no transport data can be estimated at higher temperatures. Measurements made during the course of this work under oxygen atmospheres suggest that in the absence of oxide ion oxygen is inert to the melt with the exception of reaction (1), the nitrate-nitrite equilibrium.

Carbon dioxide is permanently present in the ambient atmosphere at the level of 0.033% (by volume dry air). The results reported by Zambonin and co-workers (9,10) rather implied that carbon dioxide is inert vis-à-vis nitrates at temperatures up to 350°C. Thermodynamic calculations for reactions (12) and (13) in Table 3 also support this conclusion. Nevertheless, these latter results show that at temperatures around 500°C in an open system the possibility exists for reaction between carbon dioxide and nitrate-nitrite. Experience with heat treatment baths confirms the buildup of carbonate ions in the melt (11).

Solubility measurements of carbon dioxide and carbonate in various nitrates have been reported in the literature (12-14). Recently (15) the phase diagrams have been reported for Na_2CO_2-$NaNO_3$ and K_2CO_3-KNO_3, which are at some variance with the earlier data (16). Zambonin, on the other hand, reported a number of solubility measurements in the 50 mol% sodium nitrate-potassium nitrate mixture at several temperatures between 220°C and 350°C. These results are expressed as

$$\log S_{Na_2CO_3} = 2.081 - 1.9446 \times 10^3 \, T^{-1} \qquad (14)$$

$$\Delta H = 8.9 \text{ kal} \quad \text{(note error in orgininal paper)}$$

where S is the solubility in mol Na_2CO_3 kg^{-1} melt. Solubilities predicted from these results at temperatures of interest in thermal storage are given in Table 4.

TABLE 3

THERMODYNAMIC DATA RELEVANT TO POSSIBLE REACTIONS IN MOLTEN NITRATES

Temp, °K	573	673	773	873
Reaction	ΔG°kcal / K	ΔG°kcal / K	ΔG°kcal / K	ΔG°kcal / K
9	52.99 / 6.1×10^{-21}	47.94 / 2.7×10^{-16}	42.90 / 7.4×10^{-13}	37.86 / 3.3×10^{-10}
10	33.50 / 1.7×10^{-13}	32.55 / 2.7×10^{-11}	31.61 / 1.2×10^{-9}	30.68 / 2.1×10^{-8}
11	-25.99 / 8.2×10^{9}	-24.86 / $1.2 \times 10^{+8}$	-23.72 / 5.1×10^{6}	-22.58 / $4.5 \times 10^{+3}$
12	26.99 / 5.1×10^{-11}	23.09 / 3.2×10^{-8}	19.18 / 3.8×10^{-6}	15.28 / 1.5×10^{-4}
13	7.49 / 1.4×10^{-3}	7.69 / 3.2×10^{-3}	7.89 / 5.9×10^{-3}	8.10 / 9.4×10^{-3}
1	11.72 / 3.4×10^{-5}	8.74 / 1.5×10^{-3}	5.76 / 2.3×10^{-2}	2.79 / 2.0×10^{-2}

Reaction 9: $2NaNO_3(\ell) + H_2O(g) \rightarrow 2NaOH(\ell) + 2NO_2(g) + \frac{1}{2}O_2(g)$

10: $NaNO_2(\ell) + H_2O(g) \rightarrow 2NaOH(\ell) + NO_2(g) + NO(g)$

11: $2NaOH(\ell) + CO_2(g) \rightarrow Na_2CO_3(\ell) + H_2O(g)$

12: $2NaNO_3(\ell) + CO_2(g) \rightarrow Na_2CO_3(\ell) + 2NO_2(g) + \frac{1}{2}O_2(g)$

13: $2NaNO_2(\ell) + CO_2(g) \rightarrow Na_2CO_3(\ell) + NO_2(g) + NO(g)$

1: $NaNO_3(\ell) \rightarrow NaNO_2(\ell) + \frac{1}{2}O_2(g)$

TABLE 4

SOLUBILITY LIMIT FOR CARBONATE IN THE SODIUM-NITRATE, POTASSIUM-NITRATE EQUIMOLAR MIXTURE

Temperature °C	10^3 Conc. Na_2CO_3 mol-kg^{-1}
230	16.4
300	48.6
400	155.4
500	367.5
600	713.7

Carbon dioxide solubilities obtained by the differential manometric method for equimolar sodium nitrate-potassium nitrate show that the heat of solution is still slightly positive in spite of the presence of ion-quadrapole interactions. The Henrian constant is given by

$$\ln K_H(T_2) = 15.32 - \frac{0.717}{R}\left(\frac{1}{T_2} - \frac{1}{T_1}\right) \qquad (15)$$

where $T_1 = 623°K$, K_H in mol-g^{-1}At^{-1}. Results in a number of other nitrate solvents were also reported (9).

The electroactivity of carbon dioxide and carbonate ions has also been examined. The results for carbon dioxide show that one or two reduction reactions can take place according to conditions:

(a) In the presence of oxygen, the reduction (10)

$$CO_2 + \tfrac{1}{2}O_2 + 2e \rightleftarrows CO_3^{=} \qquad (16)$$

has been observed. Results at low temperatures (250°C) at the rotating platinum disc electrode have shown that this reaction is irreversible. No specific interpretation of irreversibility was given.

(b) In the nitrate melt alone, the reduction is via

$$NO_3^- + CO_2 + 2e \rightleftarrows CO_3^{=} + NO_2^- \qquad (17)$$

No evidence of the reduction

$$2CO_2 + 2e \rightleftarrows CO_3^{=} + CO \qquad (18)$$

has been reported, although (17) could be thought of as the EC mechanism

$$2CO_2 + 2e \rightleftarrows CO_3^{=} + CO \qquad (18A)$$

$$NO_3^- + CO \rightleftarrows NO_2^- + CO_2 \qquad (18B)$$

Evidence for the reduction of nitrate by carbon monoxide has been presented by Desimoni and co-workers (17). Electrochemically, therefore, the behavior of carbon dioxide is not straightforward as was presented previously.

The electrochemistry of the carbonate anion is of interest because it provides a means of detecting carbonate ions in-situ in the melt and provides a way of monitoring the reaction of carbon dioxide with the nitrate melt. Zambonin reported the oxidation of carbonate ions takes place at around 0.4V versus $Ag/Ag^+(1)$ 0.07m reference electrode in the equimolar nitrate solvent. It was observed that, at concentrations above 6×10^{-3}M, the limiting currents at the rotating disc were distorted, but at lower concentrations well-defined limiting currents were observed. Assuming the reaction

$$CO_3^{=} \rightarrow CO_2 + \tfrac{1}{2}O_2 + 2e \qquad (19)$$

the Levich equation was applied

$$i_L = 0.62\ nFAD^{2/3}C\ \nu^{-1/6}\omega^{1/2} \qquad (20)$$

to the results at several different temperatures to obtain $D_{CO_3^{=}}$. This parameter can be expressed for the temperature range 220-300°C in the form

$$\ln D(T_2) = -4.60 - \frac{6.8 \times 10^3}{R}\left(\frac{1}{T_2} - \frac{1}{T_1}\right) \qquad (21)$$

where T_1 = 536°K. Other workers have added carbonate ions to nitrate melts as sources of oxide ions, assuming that carbonate ion undergoes the decomposition (18)

$$CO_3^{=} \rightarrow CO_2 + O^{2-} \qquad (22)$$

No evidence for this reaction was obtained by Zambonin (10), Romberger (19) or in the present studies between 250°-550°C.

The oxidation of carbonate ions occurs close to the oxidation of nitrite ions at low temperatures which complicates the electrochemistry if both are present. However, it is possible to prepare melts sufficiently low in nitrite ion content for reasonable results to be obtained for carbonate oxidation as were the conditions in Zambonin's experiments. On the other hand, at higher temperatures >450°C nitrite is continuously present and the oxidation processes may interact in a compromising manner.

Fortunately, as our results show, the carbonate oxidation shifts cathodically as the temperature increases leading to some separation.

The oxidation of nitrite ion in this melt has been studied by a number of workers (20-27), either in its own right or to detect analytically nitrite ion formation from intrinsic reaction or from extrinsic interactions. Both stationary and rotating electrodes have been employed together with voltammetry or hydrodynamic voltammetry, and in the former case, chronopotentiometry. The results, obtained over the temperature interval 225-350°C, conclusively agree that

$$NO_2^- \rightleftarrows NO_2 + e \qquad (23)$$

occurs, and is a fast charge transfer. Complications in the mechanism due to electrode materials have been asserted by some workers (23,26,27). It is clear from the ensuing diffusion coefficients (see Table 2) that the reaction may be more complicated than implied by equation (23). Studies reported in the current work bear out this conjecture. Because nitrite ion is a decomposition product of the melt and may be formed or consumed during other interactions between atmospheric components and the nitrate melt, its chemistry and electrochemistry is important to the understanding of this liquid system.

Regenerative treatments of nitrate melt in thermal storage applications have received attention (28,29). The use of NO_2 gas appears favorable either in diluted form or as the pure component. In either case, nitrite will consume NO_2 via the reaction

$$NO_2^- + NO_2 \rightarrow NO_3^- + NO \qquad (24)$$

in a wasteful manner. The use of NO_2/O_2 mixture would overcome this by converting the nitric oxide into nitrogen dioxide. Nevertheless, nitrite ion would build up again in the melt after treatment. Carbonate ions and hydroxide ions can be removed by NO_2 gas treatment according to the reactions

$$CO_3^= + 3NO_2 \rightleftarrows 2NO_3^- + CO_2 + NO \qquad (25)$$

$$2OH^- + 3NO_2 \rightleftarrows 2NO_3^- + H_2O + NO \qquad (26)$$

Again NO_2/O_2 mixtures would be favored to pure or inert gas diluted NO_2. These techniques have been advocated in the literature for the preparation of high purity nitrate solvents and the current work has used such techniques. Under these conditions, the buildup of nitrite in the melt at temperatures in the range 400-600°C can be studied electrochemically if the nitrite ion oxidation mechanism is understood.

Perhaps the most contentious of the alkali metal nitrate-atmosphere interactions revolves around the presence of water in the

atmosphere. From the point of view of thermal storage, the solubility of water, any chemical interaction between water and the melt, or water-atmosphere and the melt, are of greatest importance. The solubilities of water in a number of nitrate melts have been investigated by various techniques (29-35). The results have been discussed in recent reviews (29). Those relevant to the thermal storage are presented in Table 5. Manometric measurements at different water partial pressures (5-30 mm) were used to obtain the water solubilities and Henrian constants. The heat of solution was obtained from the temperature dependence of the Henrian constant. These important data (30) are expressed by

$$\log_{10} K_H = -6.720088 + 1.844874 \times 10^3 \, T^{-1} \qquad (27)$$

and are illustrated in Figure 1.

The reduction of water in this melt has been reported by several workers (36-41). It provided a convenient means of monitoring water in nitrate melts at temperatures between 120-300°C. These studies suggested a method by which water could be quantitatively measured at higher temperatures (39). It was proposed that the coupling of cyclic voltammetry, chronopotentiometry and hydrodynamic voltammetry could provide direct measurements of the water content of the melt. The results from this approach are discussed at length later, but suffice to say here that the results obtained at 300-450°C support the data given by Zambonin (30) suggesting that his data may be extrapolated with confidence to the higher temperatures. Furthermore, both the hydrodynamic voltammetry and the cyclic voltammetry provide means of monitoring water in the melt at 500+°C. On the basis of Zambonin's results, the water content of a nitrate melt in contact with a humid atmosphere at 300°C could be considerable (see Table 5). Estimates based upon thermodynamic data for the pure compounds show that hydrolysis of nitrate melts (reactions (9) and (10)) should be insignificant (see Table 3) as will be the hydrolysis of carbonate ions (reverse of reaction (11)). These data also imply that in the presence of humid air, any hydroxide arising through extrinsic processes will be converted to carbonate in spite of the high p_{H_2O}/p_{CO_2} ratio.

In summary, the literature data together with the findings of the research reported here suggest that chemical interactions between the atmosphere and the binary equimolar mixture of sodium nitrate-potassium nitrate will be minimal except for the slow buildup of carbonate in the melt due to carbon dioxide activity. The long time period anticipated for the operation with these melts might suggest that regenerative processing will be necessary.

TABLE 5

H_2O SOLUBILITY IN MOLTEN NITRATES/NITRITES

Solvent	T,°C	Henry's Constant μmol $mol^{-1}mm^{-1}$	Range of HL	ΔH_{soln} kcal-mol^{-1}	10^5D cm^2sec^{-1}	Reference
$LiNO_3$	265	232	30 mm			31
	280	165				31
	275	161	30 mm	-9.35		40
	335	59				40
$NaNO_3$	310	22	30 mm	-8.15		40
	342	15	30 mm			
KNO_3	337	2	30 mm			40
	335	20 ± 7				32,33
	360	15 ± 7				32,33
	335	20 ± 2				34,33
$NaNO_3$-KNO_3	227	176	20 mm	-8.4	1.90*	30
50:50 mol%	294	63	20 mm			
$LiNO_3$-KNO_3						
75 25	230	278	30 mm			
	265	137	30 mm			
50 50	230	162	30 mm			31
	265	82	30 mm			
25 75	230	99	30 mm			
	265	54	30 mm			
$LiNO_3$-$NaNO_3$	230	354	30 mm			
75 25	265	165	30 mm			
	280	118	30 mm			
50 50	230	242	30 mm			31
	265	110	30 mm			
	280	81	30 mm			
25 75	265	84	30 mm			
	280	64	30 mm			
$NaNO_2$	281	80	38 mm**			35
$NaNO_2$-KNO_3	143	610	20 mm	-8.4		33
	201	167	20 mm			
	260	59	20 mm			

*Diffusion coefficient at 229°C.

**Solubility limit reached at ∿38 mm pressure H_2O.

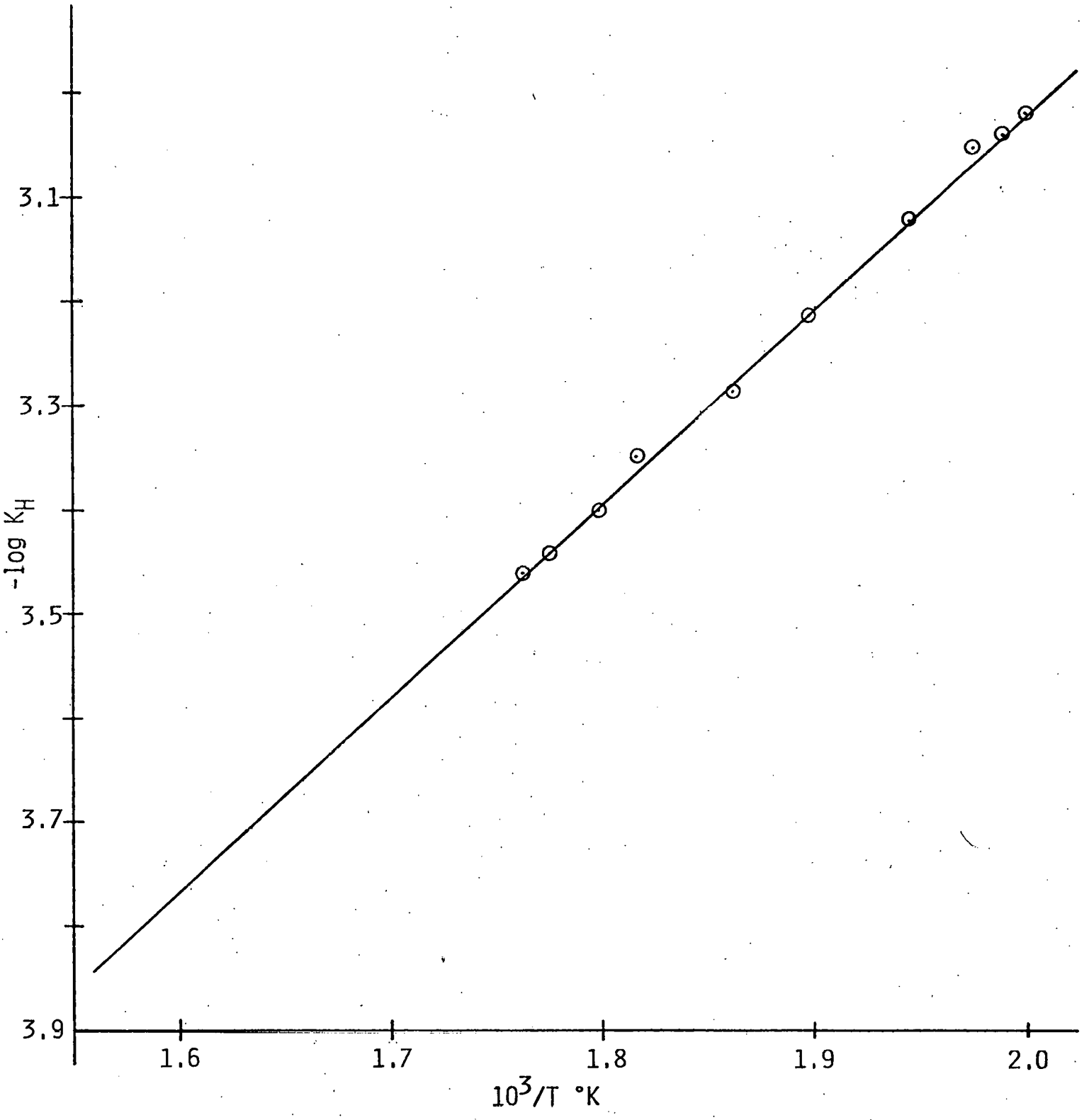

Fig. 1. Plot of Henrian constant for water as a function of temperature. Manometric data of Zambonin (30).

3.0 EXPERIMENTAL PROCEDURE

3.1 Materials

ACS grade sodium nitrite was twice recrystallized from distilled water before drying under vacuum over phosphorus pentoxide. The product was pale yellow. ACS grade potassium carbonate dried over P_2O_5 was used directly for carbonate pilot ion additions. Twice recrystallized lithium nitrate trihydrate was prepared from anhydrous Alfa Ventron $LiNO_3$. It was kept below 29°C during storage.

The salt sources used to prepare the sodium nitrate-potassium nitrate solvent were:

Source 1 -	Ultrapure	$NaNO_3$
Source 2 -	Puratronic	KNO_3
Source 3 -	AR Mallinckrodt	$NaNO_3$ and KNO_3
Source 4 -	ACS	$NaNO_3$ and KNO_3

In the earliest experiments, equimolar sodium nitrate-potassium nitrate was prepared directly in the electrochemical cell from sources 1 and 2, respectively. The salts were handled in the dry box before loading into the experimental cell A. The cell was then evacuated and the temperature raised to 300°C via a series of temperature plateaus at which the pressure was allowed to reach a minimum. Once molten, the pressure was raised to 1 atmosphere argon, and the experiment commenced. Most experiments were conducted using melt which had been prepared by the following method.

AR or ACS grade sodium nitrate and potassium nitrate, twice recrystallized from water, were weighed out separately and dried over P_2O_5 *in vacuo*. These materials were mixed thoroughly in a plastic jar. The apparatus in Figure 2 had been prepared previously by cleaning tubes A, B and cup C in 50:50 H_2SO_4:HNO_3, water and distilled water. The apparatus could sustain a pressure less than 2μ. The mixture was transferred to tube A which was located above the filter disc (porosity fine) on a pyrex ring. The cap was placed on the "O" ring grooved flange with the breaker rod and gas bubbler withdrawn. The lower part of the apparatus was evacuated first followed by evacuation of the upper section, Figure 3. This procedure ensured no "bumping" of the powdered salts. The apparatus was pumped until it reached a minimum pressure of ∿2-5μ (usually overnight). The temperature was raised to ∿120°C, then 170°C allowing the pressure to achieve a minimum value before proceeding to the next temperature plateau. At ∿190°C, the pressure was brought up to 1 atmosphere with argon before replacing this gas with NO_2. The salts were melted under NO_2 and then this gas was bubbled through the liquid for ∿1 hour. Nitrogen dioxide was finally replaced by

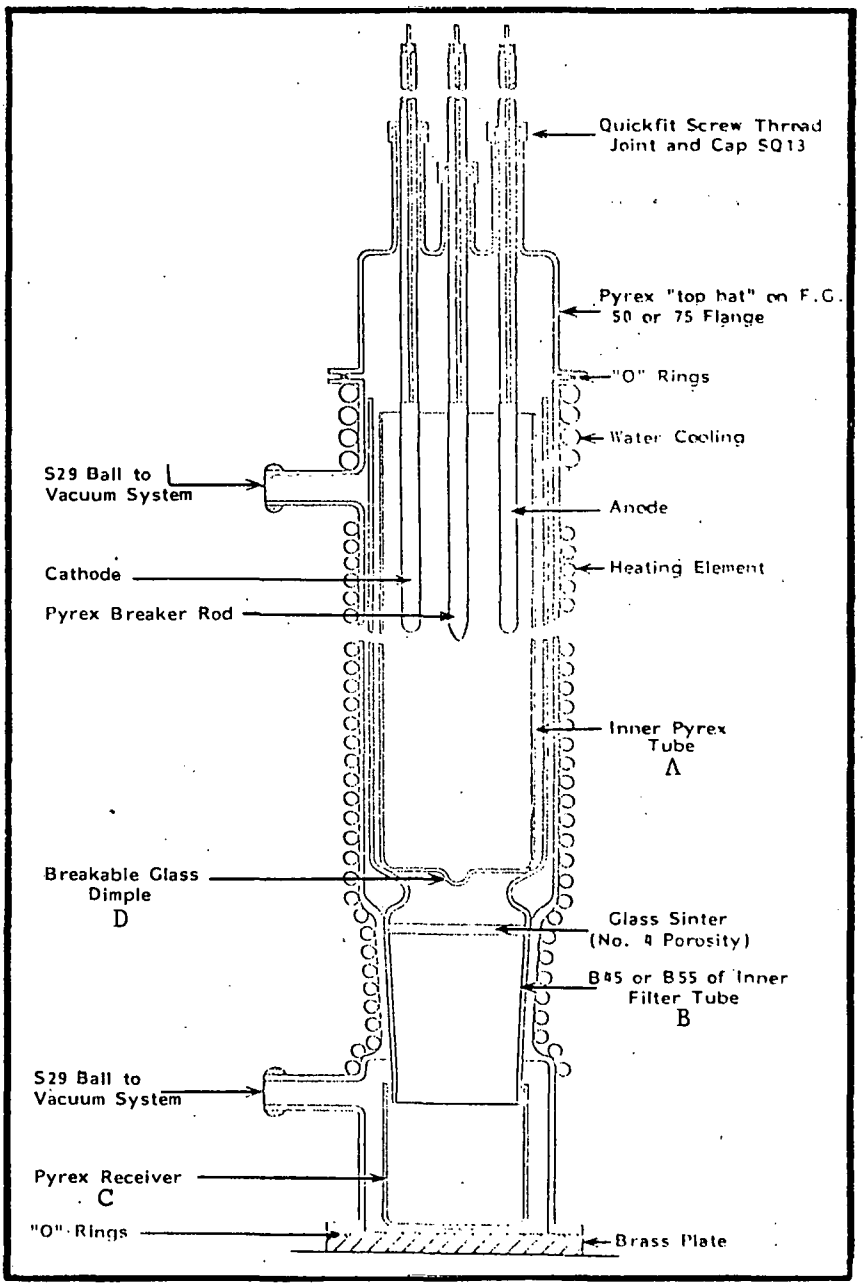

Fig. 2. Apparatus for the purification of molten nitrates.

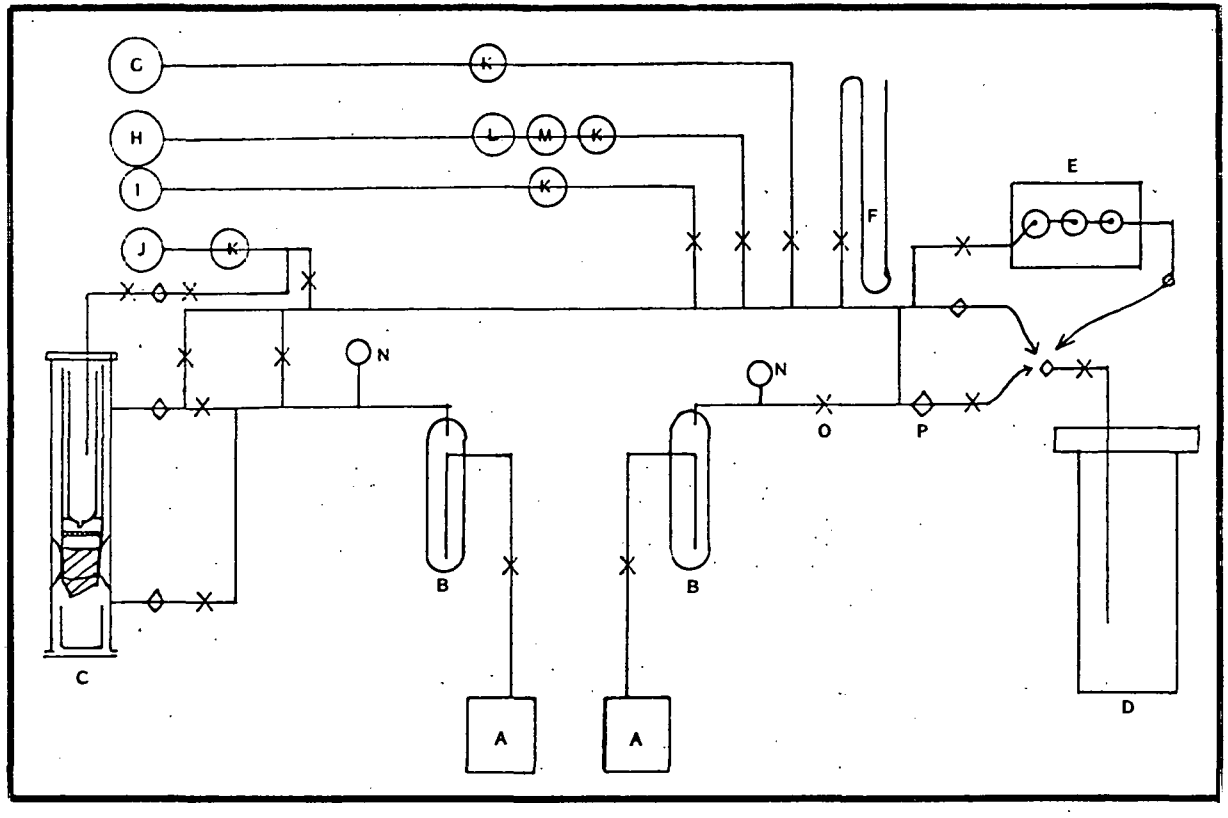

Fig. 3. Vacuum line and auxiliary gas lines.

Glossary

A - Rotary Pump
B - Cold Trap
C - Purification Cell
D - Electrochemical Cell
E - Water-Gas Saturator Train
F - Manometer
G - Carbon Dioxide Tank
H - Argon Tank
I - Oxygen Tank
J - Nitrogen Dioxide Tank
K - Molecular Sieve Tower
L - Sofnalite Tower
M - Copper Deoxygenating Tower Furnace
N - Thermocouple Vacuum Gauge
O - Rotoflow (Teflon) Stopcocks
P - Greasless Ball Joint

argon which was also used to push the salt through the frit after breaking bubble D with the rod. Reduced pressure was maintained in the lower half of the cell to ensure rapid filtration. The filtrate was collected in cup C. The argon flow was stopped and the apparatus evacuated while cooling to room temperature. The mixture produced was water clear when hot and white in the solid state. The material was transferred to the dry box and stored in a capped bottle.

An earlier batch of salt was prepared in which oxygen replaced nitrogen dioxide. The material used to prepare the reference salt mixture was taken from sources 1 and 2 and treated by vacuum heating. At 250°C, the atmosphere was returned to argon and the ACS grade $AgNO_3$ added to produce a 0.07 molal solution. This concentration was confirmed by subsequent AA analysis of the crushed material.

3.2 Experimental Apparatus and Electrochemical Cell Assemblies

3.2.1 General

Two cells were used in this work: Cell A which is shown in Figure 4A and Cell B in Figure 4B. The latter cell enabled the rotating disc electrode to be used. The envelopes were either pyrex or silica tubes closed at one end, 7.5 cm in diameter and approximately 38 cm long for Cell A, and 28 cm long for Cell B. Cell A was capped by a water cooled brass head accommodating six Ace screw cap joints by which electrodes, bubbler, thermocouple, etc. could be introduced in the cell. Cell B was similar but the head was made from aluminum. The rotating disc electrode passed through a SGA (JA 6910) screw cap fitting mounted on a Cajon VCR coupling with a Teflon gasket. This arrangement enabled vacuum to be achieved except when the electrode was rotated.

The cell assembly was located above the furnace in a water cooled aluminum block. The block was mounted below an X-Y table which enabled the drive unit for the disc electrode to be precisely aligned above the central electrode assembly. The furnace was of the counter weight design enabling viewing of the cell and contents on lowering the furnace. The furnace was powered by a pair of nichrome elements wound upon a 12.5 cm silica tube. Each element was controlled separately with a 10 ampere variac. The temperature could be monitored by thermocouples placed alongside the windings. The temperature setting for the variacs were determined with a dummy cell in position.

3.2.2 Electrodes

Counter Electrode. The counter electrode was a gold foil (99.99%) approximately 2 cm x 2 cm rolled in the form of a semi-cylinder. It was supported on a short gold wire fused to a pure silver lead wire. Figure 5A shows the total assembly. This electrode was usually contained in a

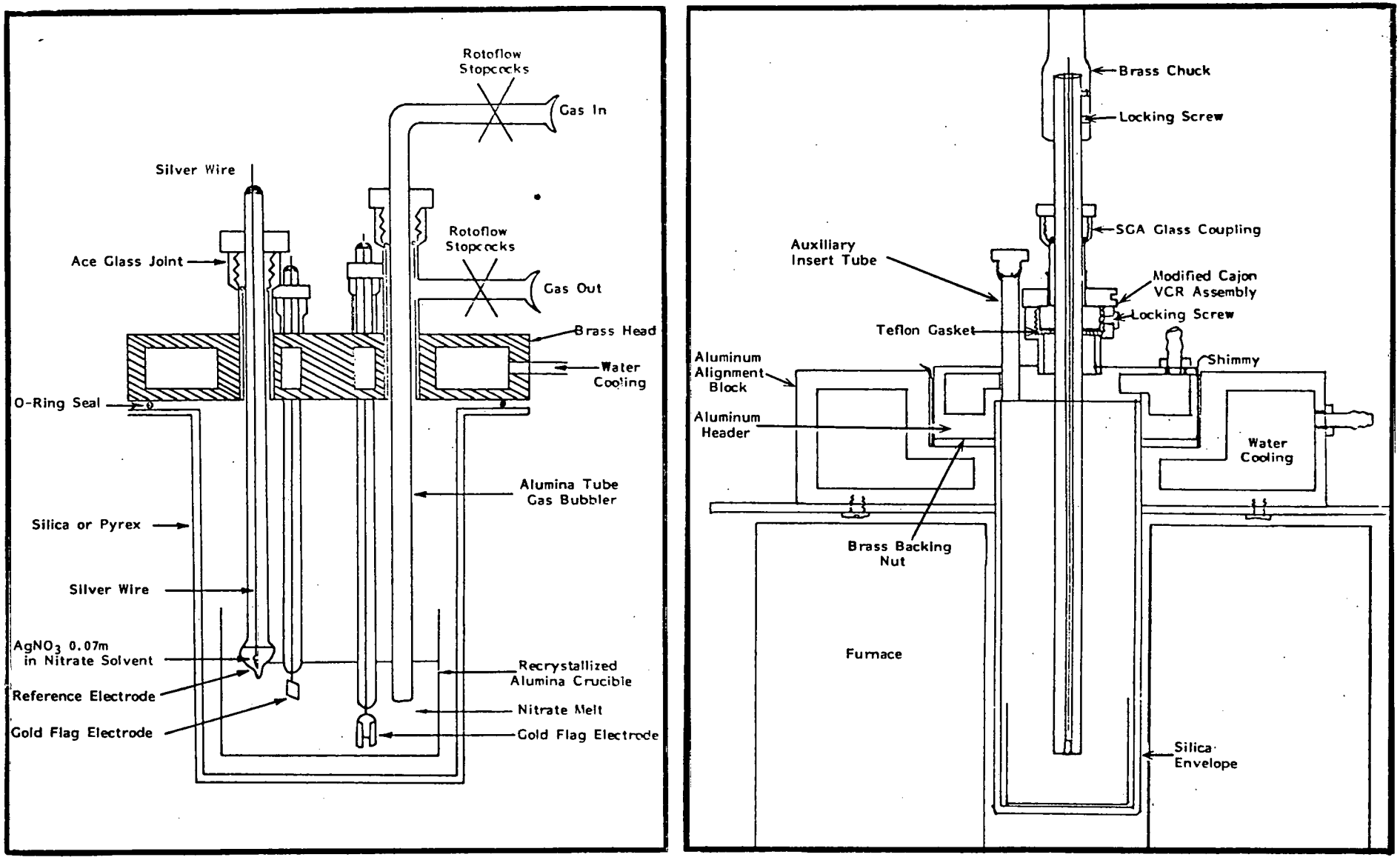

Cell A

Cell B

Fig. 4. Electrodes and cells used in experimental work.

separate alumina compartment. Electrical contact was maintained through the liquid film between crucible bottom and the end of the alumina tube.

Working Electrodes. Working electrodes were either gold flags made from Matthey Bishop 99.99% gold foil, 0.005 cm thick or gold wires. The flags were approximately 0.2 cm x 0.2 cm square, welded to gold wires sealed in alumina capillary. The main lead was again silver. The wire electrodes were short gold wires 0.002 cm diameter, and with 0.2-0.3 cm protruding from alumina capillary tubes into which the gold was sealed.

The rotating disc electrode was constructed from an alumina tube 0.75 cm diameter at the end of which a gold plug ($\sim$0.16 cm diameter) was formed, maintaining a gold-silver lead wire. The end of the tube was subsequently polished using 600 paper and fine cloth with wet No. 2 Buehler alumina. Attempts to polish, using jewelers' rouge, led to contamination and was discontinued. Details of all these electrodes are illustrated in Figures 5A and 5B. The areas of all working electrodes were estimated from optical micrograph pictures prior to the experiment and were measured experimentally using the method of Caton (43) after each experiment. Good agreement was generally found between geometrical and electrochemical areas.

Reference Electrode. A number of different electrode designs were employed. Initially, electrodes based upon the conventional design (44) were used but they were separated from the bulk melt by a sodium β alumina membrane. This ensured that the experimental melt was never in direct contact with the pyrex glass (a possible oxide ion source) of the reference electrode. These electrodes worked well above 275°C but below this temperature had a rather high impedance which caused problems with the electrochemical instrumentation. Above 425°C, changes occurred in this reference electrode system which was attributed to Ag(l) ion exchanging with the pyrex. To overcome this, the pyrex tube and β alumina were replaced by membranes of porcelain or mullite. These electrodes again functioned well above 275°C and below 450°C, but irreversible changes appeared to take place when used above this temperature (vide infra). The general structure of these electrodes is shown in Figures 5A and 5B. The reference electrode is summarized by the half cell representation

$$Ag\,|\,AgNO_3(0.07m)\ KNO_3\text{-}NaNO_3\ 50\ mol\%\,\|\,membrane$$

3.2.3 Other Probes

A number of other inserts were used which included an addition tube, a gas bubbler and outlet system and a thermocouple. The latter was a Omega chromel-alumel calibrated thermocouple contained in a closed end alumina tube. These items are illustrated in Figures 5A and 5B.

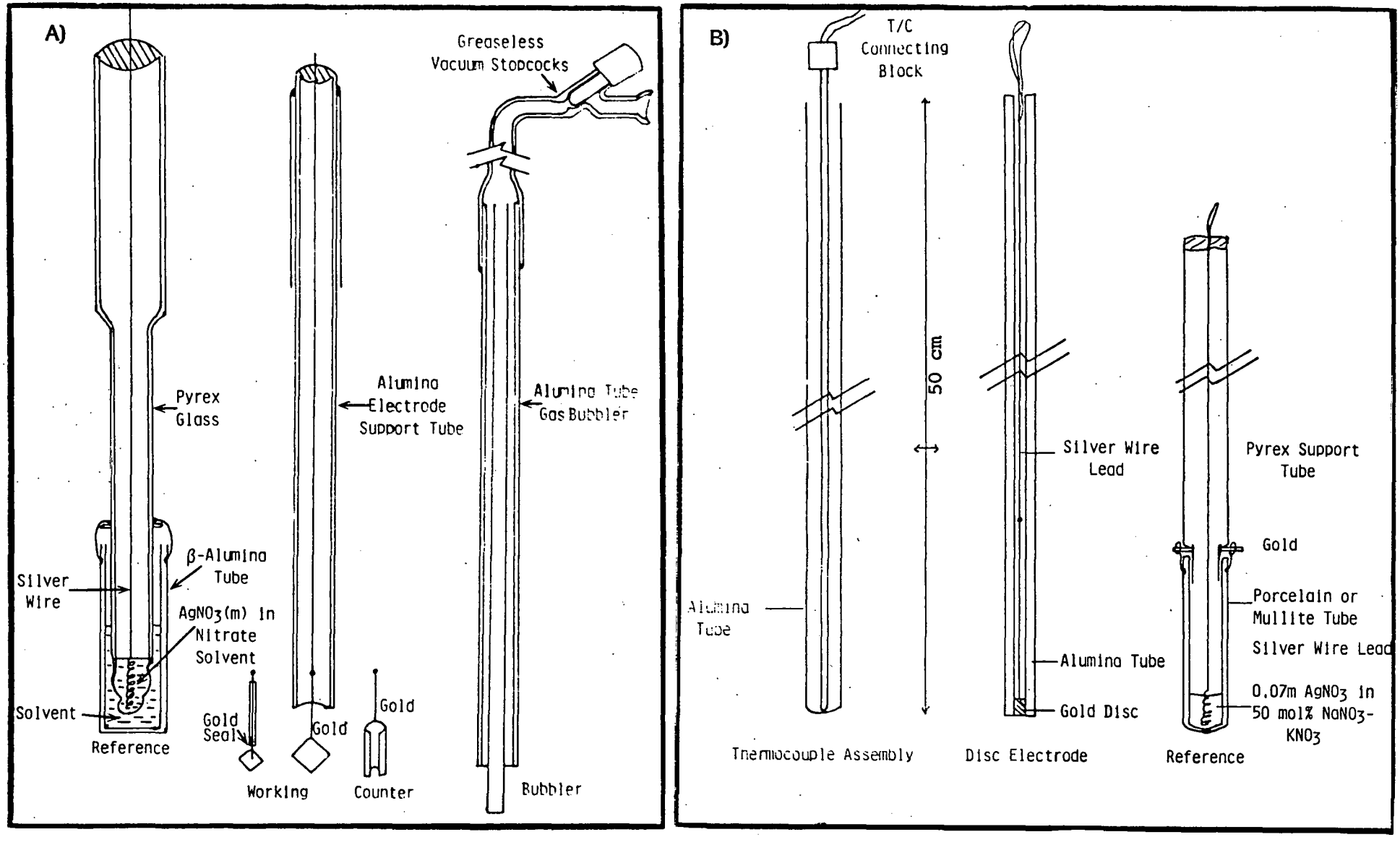

Fig. 5. Electrodes and cell inserts.

3.2.4 Electrochemical Techniques

During the course of the work a number of electrochemical methods were applied to investigate the various problems. The electrochemical measurements were based upon the use of an Amel 551 potentiostat which was coupled with a PAR 175 wave form generator. The current output of the 551 was recorded via a PAR 4201 transient recorder, a Hewlett-Packard 7045A X-Y recorder or a Bascom-Turner 8000 series microprocessor controlled X-Y recorder. Data was stored on the latter on floppy discs. This system enabled voltammetry, chronoamperometry and chronopotentiometry to be used. Additionally, a PAR 174A was used in the limited situations where low currents were observed and for pulse voltammetric measurements. Descriptions of these methodologies are to be found in standard reference books (45-47).

3.2.5 Procedure

Although the objectives of the various experiments carried out were somewhat different, a single description will suffice to illustrate the procedures employed for this work.

The materials which came into contact with the melt or the gas atmosphere were cleaned for each experiment. The brass or alumina cell heads were carefully cleaned with water and acetone and dried in the air. The pyrex or silica envelope, the alumina crucible, alumina and pyrex tubes were cleaned in 50% H_2SO_4-50% HNO_3 mixture, water and distilled water before drying in the oven and under reduced pressure. The electrodes were individually tested for vacuum tightness after construction. Bubblers, thermocouple tubes, etc. were similarly checked. The cell was assembled and tested as a whole for vacuum tightness before introducing the crucible containing a weighed sample of melt from the dry box.

The cell was mounted above the furnace. Cell B was aligned with the disc drive unit by adjusting the X-Y table, and the rotating electrode was then connected to the drive shaft. Cell A or B was finally evacuated at room temperature usually reaching 5-10μ. The temperature was then raised to the working temperature under vacuum before backfilling the cell with argon. The experiment was generally commenced at 250-300°C to enable the background condition of the melt to be assessed by cyclic voltammetry.

The appropriate experiment was then performed; for example, water was introduced on an argon gas stream at a known partial pressure. The water partial pressure was maintained by passing argon through boiled distilled water held in a thermostat at temperatures between 5 and 30°C. The required electrochemical measurements were carried out using various techniques as a function of water partial pressure and temperature. In the case of nitrite studies, known weights of sodium nitrite were added at different temperatures. Carbon dioxide/carbonate studies were performed

by introducing carbon dioxide, carbon dioxide-water mixtures, carbon dioxide-oxygen mixtures via the gas bubbler either above or through the melt. Additions of carbonate were made as weighed amounts of potassium carbonate.

During the course of these measurements, the applications of NO_2 directly into the electrochemical cell was carried out to assess the ability to remove NO_2^-, $CO_3^=$, OH^- ions and renew the melt for further studies. The behavior of the melt was monitored electrochemically during such operations to determine the effectiveness of these procedures.

Typically, the experimental run would last between 3 and 5 weeks. Termination of an experiment usually resulted from electrode failure.

4.0 RESULTS AND DISCUSSION

4.1 General Chemistry and Electrochemistry of the Equimolar Sodium-Nitrate Potassium-Nitrate Mixture

Molten alkali metal nitrates are generally thermally stable up to 400°C when significant amounts of nitrite are detected. Electrochemically, the range of inactivity, as suggested by the free energies of formation, is around 2.5-3.5V. However, this range is not achieved because the nitrate ion itself can be reduced before alkali metal ion reduction takes place (48). Figure 6 shows the range of solvent inactivity at 300°C and 535°C. The formation of peak limited currents arises because the cathodic reaction products are partially soluble in the melt. The peak current is then some function of the balance between the rate of formation of the film and the rate of dissolution. At low temperatures, it was proposed that the film was that of sodium oxide (49). It is clear from the results here that at high temperature not only is the solubility of that film greatly enhanced, but another filming reaction takes place. It was shown that sodium peroxide is limited in its solubility in nitrate compositions (50). The appearance of peak 2 parallels the increase in nitrite ion content of the melt and it is tempting to ascribe it to a reaction involving this species. However, further studies are required to confirm such an hypothesis.

Background measurements are important to the electrochemical studies to be discussed later, and as it will be emphasized rather critical in resolving low concentrations of, for example, water (see Section 4.3.1). The preparation of melt is critical in minimizing extrinsic effects on the magnitude of the background. The formation of nitrite ions from oxidative reactions between nitrate and organic residues is well-documented in the literature (22,51). The application of recrystallization procedures, nitrogen dioxide treatment of the melt, and minimizing the initial thermal cycle has enabled nitrite concentrations to be held generally at or below 1 mM. The problem of background corrections at higher temperatures is exceedingly difficult requiring extensive measurements which are stored digitally and the corrections applied to subsequent measurements using software programs.

A requirement for such work is the availability of a stable reproducible reference electrode system. During the course of this work it became apparent that conventional reference electrodes (44) based upon pyrex, or fibre junctions, silver-silver (1) in the nitrate melt were increasingly unsuitable at higher temperatures (>450°C). The use of mullite and/or porcelain certainly improved the reproducibility but the marked decomposition of nitrate to nitrite at these temperatures also caused problems. Reference electrodes based upon nitrite solvent such as:

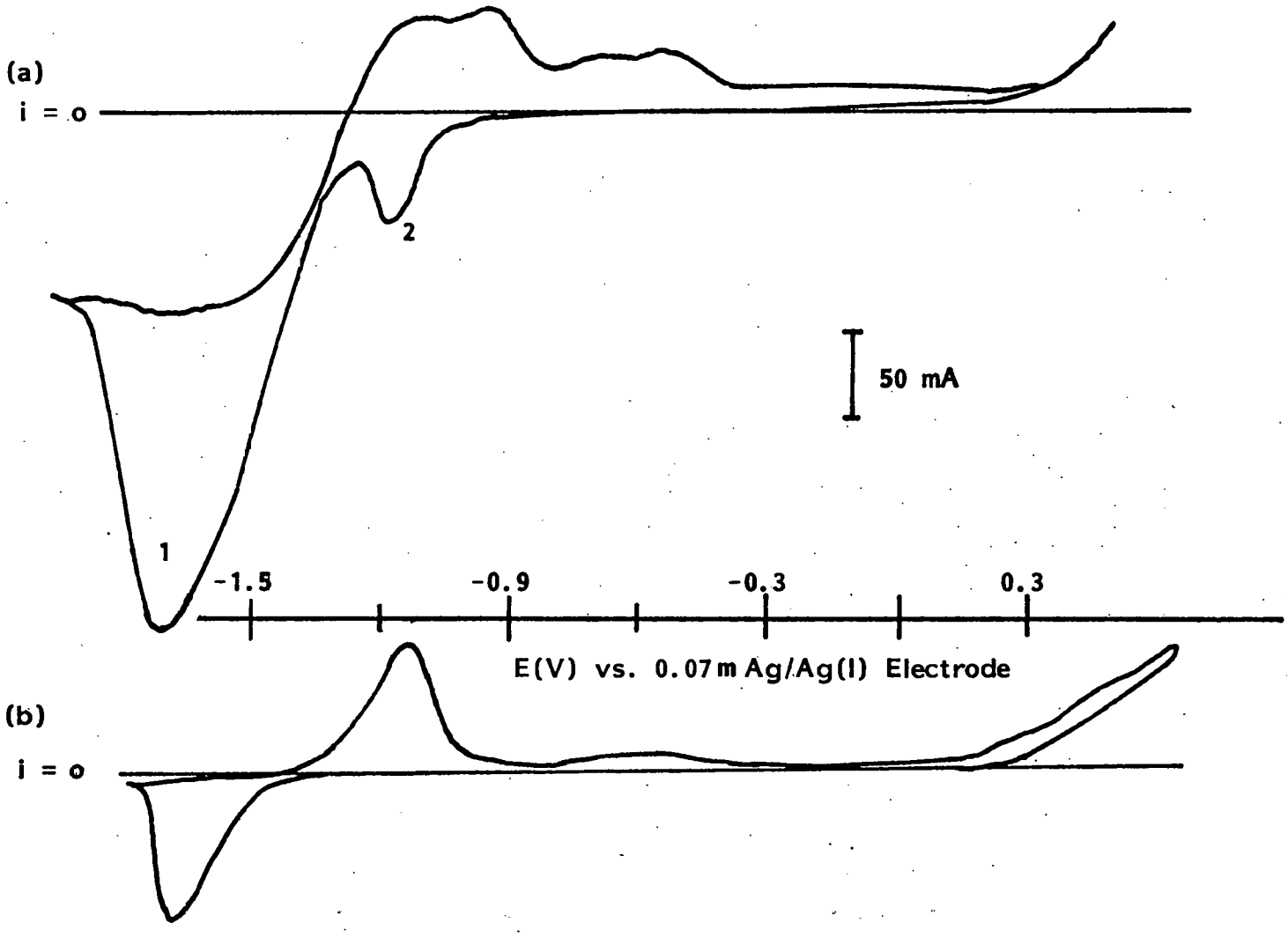

Fig. 6. Binary nitrate melt, range of electroinactivity as detected by cyclic voltammetry on gold electrodes (0.21 cm^2): (a) t = 535°C, (b) t = 300°C. Scan rate 100 $mV\text{-}sec^{-1}$.

$$Ag/Ag(l)\ 0.07m\ KNO_2\text{-}NaNO_2 \parallel$$

offer a working alternative. Corrections were applied in this work by measuring the reference electrode used versus a new Ag/Ag(l) 0.07m nitrate electrode and from a knowledge of the peak potentials for different processes in the melt.

4.2 Nitrite - The Chemical and Electrochemical Behavior of Nitrite Ions in Equimolar Sodium Nitrate Potassium Nitrate Mixture

4.2.1 Introduction

Because the thermal decomposition of nitrates at higher temperatures (>400°C) gives rise to nitrite ions, a study of the electrochemical behavior of nitrite was essential to monitor any interaction with other aerial components. Unfortunately, although the electro-oxidation of nitrite ions has been reported previously (20-27), no measurements have been made at temperatures higher than 350°C. Careful examination of these studies showed inconsistencies in the results, but all workers agree that nitrite ions are oxidized according to

$$NO_2^- \rightleftarrows NO_2 + e \qquad (28)$$

However, Arvia et al. (26,27) indicated that such a mechanism represented only part of the story because the electrode material played a prominent role. Although their chemical interpretation, involving dimerization of nitrogen dioxide in the following reaction, must be treated with some skepticism in view of the instability of N_2O_4 above 150°C (52), they did make the important point that follow-up chemistry after the electro-oxidation step was involved, and this was dependent on the nature of the electrode material, i.e., electrocatalysis was involved. Inman, Spencer and White (23) had previously observed a difference in behavior between chronopotentiograms recorded using platinum and gold electrodes. The present work has confirmed these observations (and those of Arvia).

These complications and those recently reported by Zambonin et al. (53) for nitrite ion oxidation in the presence of trace water, result in an oxidative process which is far from the simplicity expressed by equation (28). While it has been possible to monitor nitrite ions at low concentrations and low temperatures, 300-400°C, the hitherto mentioned objective of characterizing the apparently simple nitrite behavior to aid in unravelling the chemical interactions between atmospheric components and the nitrate and nitrite ions has not been possible at high temperatures. The results obtained, however, have provided some insight into the oxidation of nitrite ions per se and its thermal formation.

4.2.2 Electrochemical Study of the Oxidation of Nitrite Ions

Chronopotentiometry, current reversal chronopotentiometry, linear sweep voltammetry, cyclic voltammetry and pulse polarography have been applied to study the oxidation of nitrite ions in the concentration range 0.5 to 100 x 10^{-3}M over the temperature interval 250°C to 550°C. Generally speaking, gold electrodes were used, although brief use of platinum electrodes was made.

Chronopotentiometric Results on a Stationary Electrode. A typical chronopotentiogram for the oxidation of nitrite ion in this melt is shown in Figure 7. Anodic transition times were recorded as a function of current density, concentration of nitrite ions and temperature. Plots of $\tau^{\frac{1}{2}}$ versus 1/i are shown in Figures 8 and 9 for the various experimental conditions. The linearity of these plots is consistent with the Sand equation

$$i\tau^{\frac{1}{2}} = 0.5\ nFACD^{\frac{1}{2}}\pi^{\frac{1}{2}} \tag{29}$$

Analysis of the potential time curves was carried out. A linear relationship between E and $\ln \tau^{\frac{1}{2}} - t^{\frac{1}{2}}/t^{\frac{1}{2}}$ was obtained and illustrated in Figure 10. Such a result is consistent with a fast oxidation process involving the formation of a soluble product or followed by a fast equilibrium dimerization process. For both of these cases, $E_{\tau/4}$ is independent of current density and concentration as was observed here. For the fast following dimerization equilibrium

$$m\ Red \rightleftarrows p\ Ox + ne$$

$$p\ OX \rightarrow Prod$$

for which

$$E = E_{\tau/4} - \frac{RT}{nF} \ln \frac{(\tau^{\frac{1}{2}} - t^{\frac{1}{2}})^m}{t^{p/2}} \tag{30A}$$

for m = p = 2

$$E = E_{\tau/4} - \frac{2RT}{nF} \ln \frac{\tau^{\frac{1}{2}} - t^{\frac{1}{2}}}{t^{\frac{1}{2}}} \tag{30}$$

The slope of Figure 10 is consistent with equation (30) when n = 2 per two mols of nitrite.

Distinction between this case and the simple soluble product case requires further information such as that obtained in current reversal

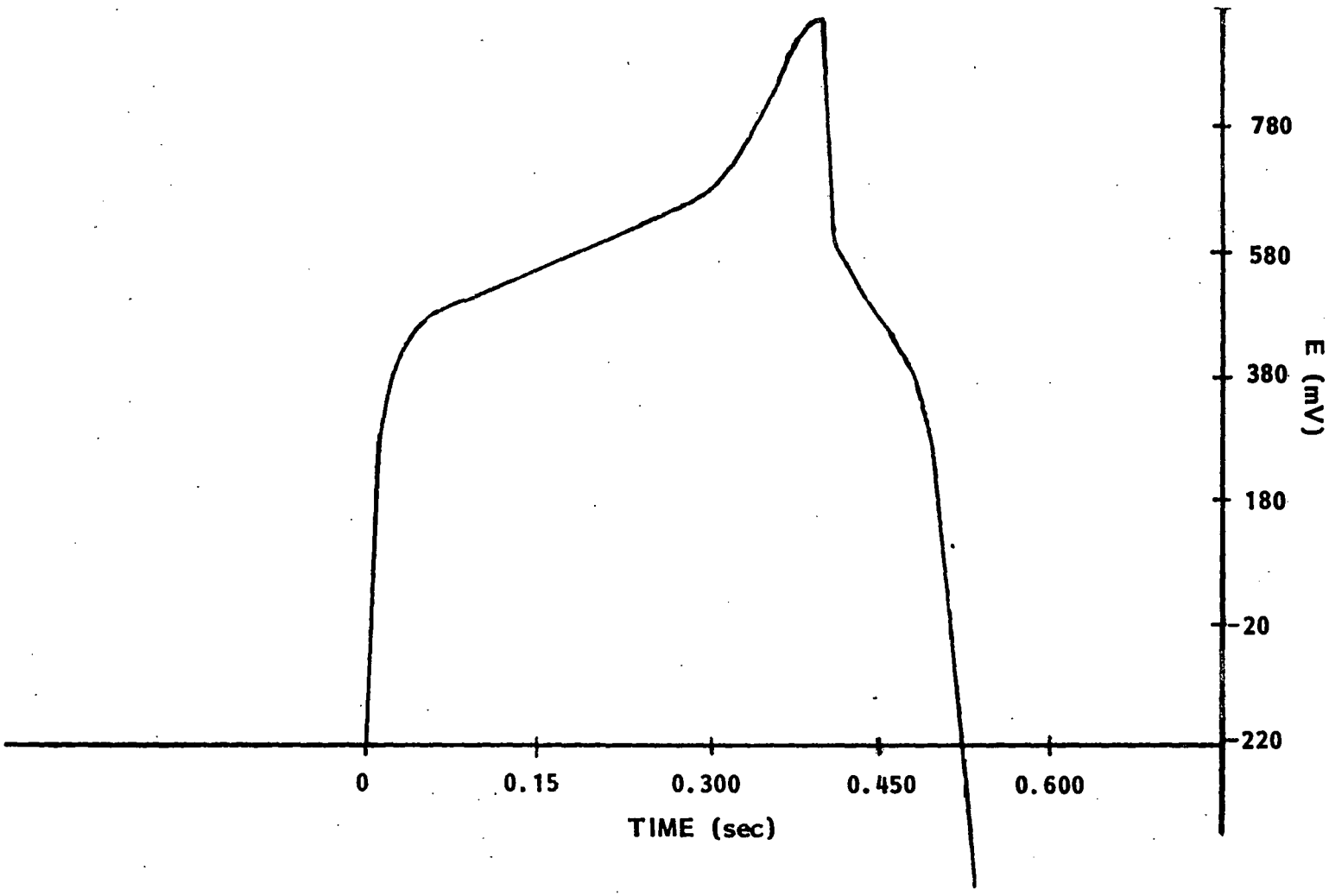

Fig. 7. Current reversal chronopotentiogram at low concentration of NO_2^- ions 3.316×10^{-3} molal at Au electrode 0.365 cm^2, applied current 1.50 mA, t = 350°C.

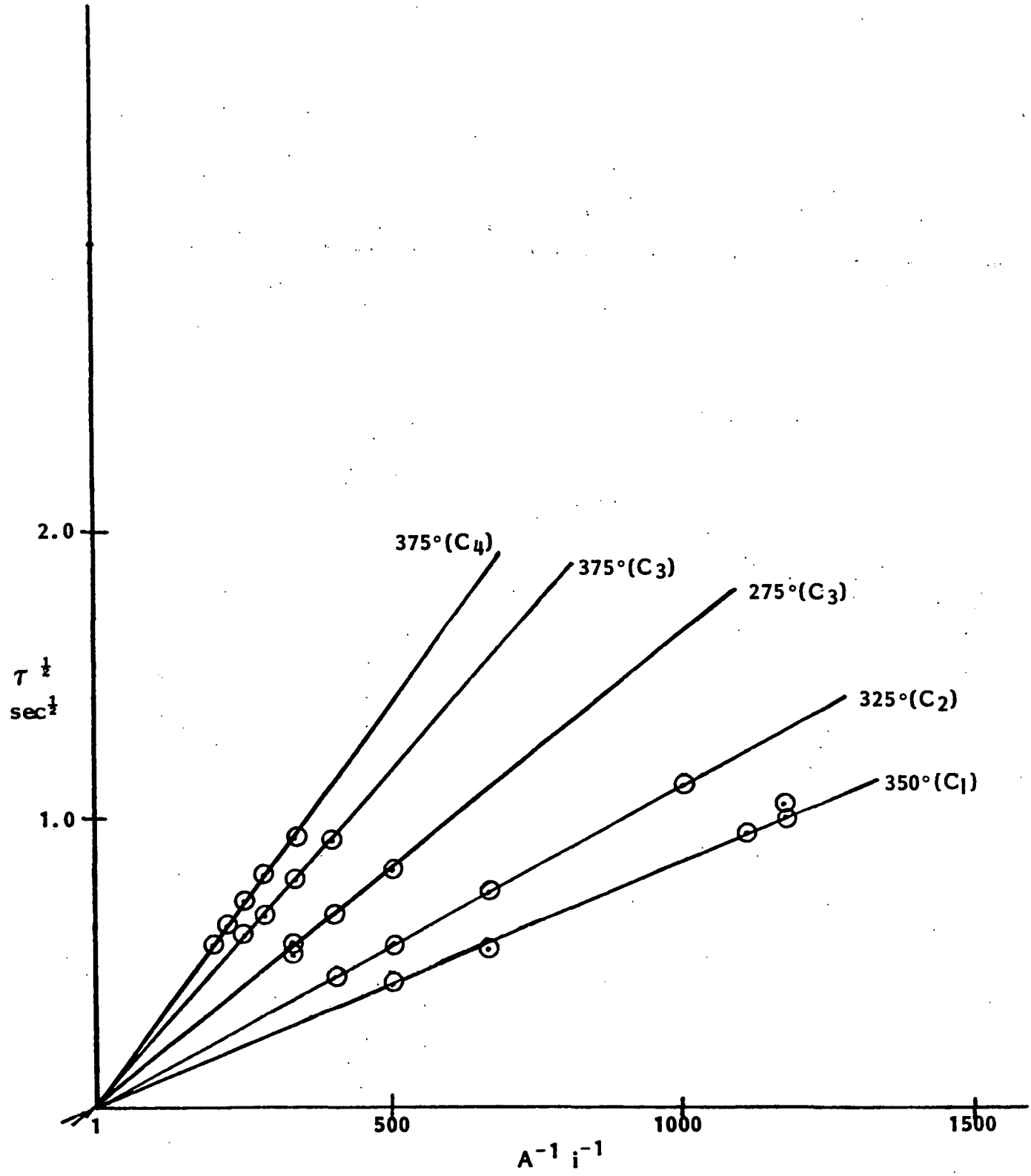

Fig. 8. Sand plot for the oxidation of nitrite ions in sodium nitrate-potassium nitrate (50 mol%) at different concentrations and temperatures. Au electrode 0.365 cm^2.

$C_1 = 3.316 \times 10^{-3}$ mol-kg^{-1}
$C_2 = 5.110 \times 10^{-3}$ mol-kg^{-1}
$C_3 = 9.330 \times 10^{-3}$ mol-kg^{-1}
$C_4 = 11.326 \times 10^{-3}$ mol-kg^{-1}

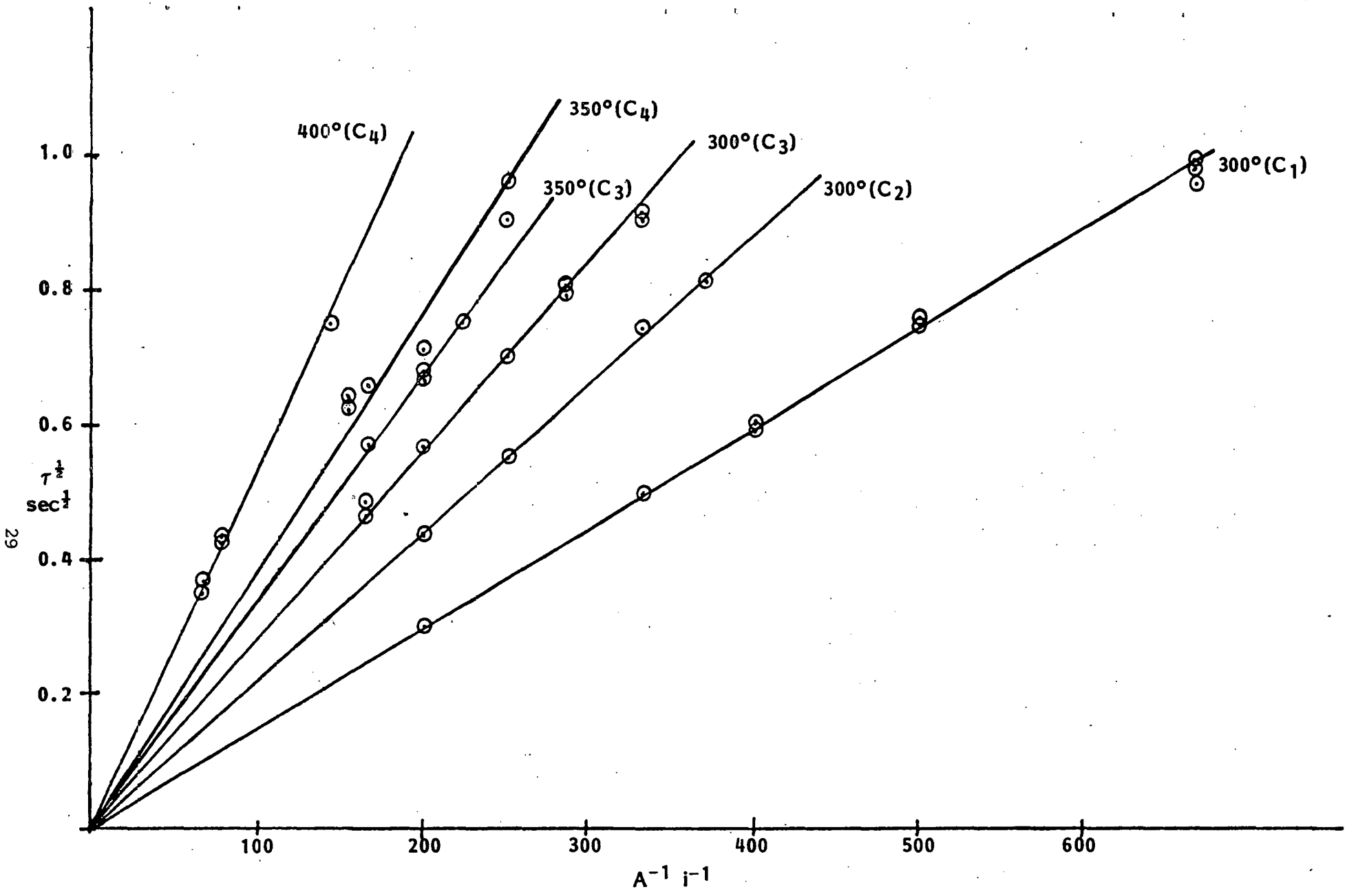

Fig. 9. Sand plot for nitrite ion oxidation at gold electrode (0.358 cm^2).

C_1 = 6.766 x 10^{-3} mol-kg^{-1}
C_2 = 10.251 x 10^{-3} mol-kg^{-1}
C_3 = 13.194 x 10^{-3} mol-kg^{-1}
C_4 = 17.099 x 10^{-3} mol-kg^{-1}

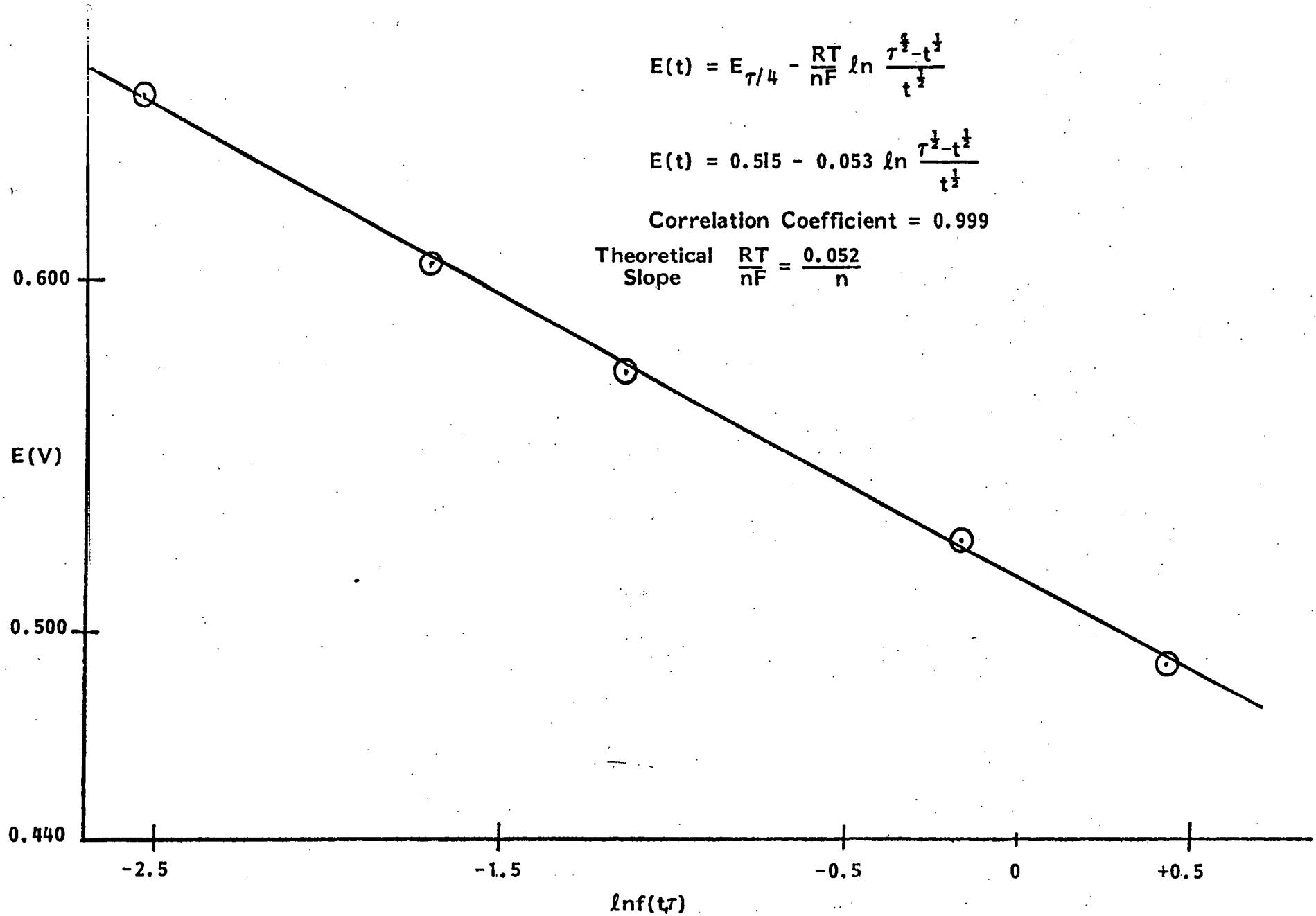

Fig. 10. Karaoglanoff plot for the oxidation of nitrite ions on a Au electrode at 325°C.

measurements (loc. cit.). Table 6 records $E_{\tau/4}$ versus Ag/Ag(1) 0.07m reference electrode at different temperatures. The Sand equation (29) can be used to calculate the diffusion coefficients of the nitrite ions at various temperatures in spite of the possible complications in the mechanism. A value of n = one electron per mol of nitrite ion was used. The diffusion coefficients obtained are plotted in Arrhenius form in Figure 11 and tabulated in Table 7. The least squares equation representing the temperature dependence of the diffusion coefficients is

$$\ln D = -5.674 - 3.252 \times 10^{3} T^{-1} \qquad (31)$$

The activation energy for nitrite ion diffusion is 6.5 ± 1.0 kcal-mol^{-1}. Using the least squares equation diffusion coefficients were calculated at temperatures where data had been previously reported and these results are compared in Table 8.

Zambonin reported an activation energy of -5.4 kcal-mol^{-1} (error in sign) obtained over the temperature range 227-287°C from rotating disc measurements. This value is in good agreement with the more extensive results obtained here. Both values are consistent with activation energies reported for ionic diffusional processes in molten nitrates. The value of the actual diffusion coefficients are also in good agreement in the case of Zambonin's results, but his and the present measurements are about five times smaller than the other reported values. This difference probably arises from inadequate background corrections as well as possible oxide film formation contributing to the observed transition times, or enhancing the true surface area. Gold electrodes (less prone to oxide formation) were used in the present work and their areas determined electrochemically after the experiment (43).

TABLE 6

VALUE OF $E_{\tau/4}$ AT DIFFERENT TEMPERATURES

Temp, °C	275	325	350	375
$E_{\tau/4}$ vs. 0.07m Ag(1) Reference	0.485 ± 0.003	0.506 ± 0.004	0.509 ± 0.004	0.550 ± 0.004

Linear Sweep Voltammetric Results on a Stationary Electrode. The anodic oxidation peak for nitrite ions was studied as a function of sweep rate, concentration and temperature simultaneously with the

TABLE 7

DIFFUSION COEFFICIENT FOR NO_2^- IN MOLTEN SODIUM NITRATE-POTASSIUM NITRATE MIXTURE (50 mol %) AS A FUNCTION OF TEMPERATURE, CALCULATED FROM THE SAND'S EQUATION

Temp., °C	275	300	325	350	375	400
$10^5 \cdot D$ $cm^2 sec^{-1}$	0.86 ± 0.05	1.24 ± 0.10	1.70 ± 0.18	1.74 ± 0.16	1.83 ± 0.18	3.18 ± 0.18

TABLE 8

COMPARISON OF EXPERIMENTAL AND LITERATURE DATA FOR NITRATE ION ION DIFFUSION COEFFICIENTS IN MOLTEN KNO_3-$NaNO_3$ 50 MOL %

Temp, °K	D x 10^6 This Work cm^2-sec^{-1}	D x 10^6 Literature Data cm^2-sec^{-1}	Electrode	Reference
571	11.5 ± 0.5	44 ± 2	Pt wire	25
523	6.8 ± 0.3	24.8 ± 7	Pt wire	23
523	6.8 ± 0.3	27.5	Pt wire	20
523	6.8 ± 0.3	49.9	Pt wire	69
510	5.8 ± 0.3	5.25 ± 0.1	Polished Pt disc	21

$$\ln D = -5.6747 - 3.252 \times 10^3 \, T^{-1}$$

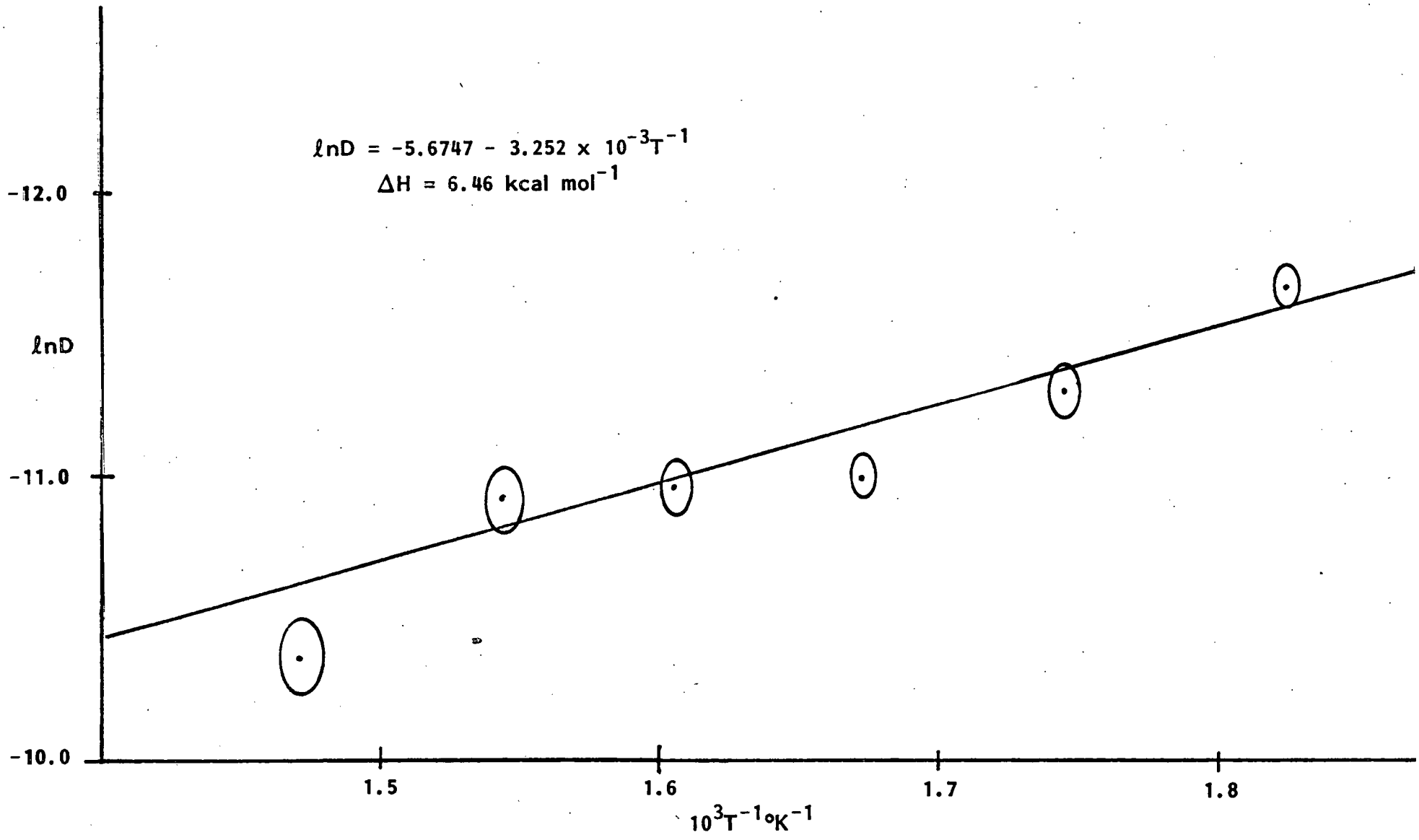

Fig. 11. Arrhenius plot of the diffusion coefficient of nitrite ions in equimolar sodium nitrate-potassium nitrate determined from Sand's equation. Ellipse represents error as determined by measurements at different concentration (corrected for background) at each temperature.

chronopotentiometric measurements. The linear dependence of peak current on the scan rate under various conditions are shown in Figures 12 and 13. Although this apparent linearity supports the chronopotentiometric results, the behavior of the peak potential as a function of scan rate (Figure 14) and the half peak width (Table 9) show that the diffusion process is moderated by other phenomena. The observed slopes in Figure 14 suggest that quasi-reversible or irreversible reactions can be discounted (compare $E_{\tau/4}$ vs. i data), and suggest that a second order following chemical reaction model might be appropriate. However, the peak potential independence of concentration and the half peak width imply additional complications.

The χ_{max} function in sweep voltammetry is a characteristic of the particular model. An attempt to evaluate this ($\sqrt{\pi}\chi_{max}$) value (which might point to the mechanism), was considered. For the case of chemical reactions following the electrochemical process, the Sand equation is valid which enables the two sets of data (LV and CP) to be combined using equation (29) and the Randles-Sevcik equation in the form

$$i_p v^{-\frac{1}{2}} = nFD^{\frac{1}{2}}CA \left(\frac{nF}{RT}\right)^{\frac{1}{2}} \left(\sqrt{\pi}\,\chi_{max}\right) \qquad (32)$$

to evaluate $\left(\sqrt{\pi}\,\chi_{max}\right)$. The results are shown in Table 10. Homogeneous fast irreversible dimerization can produce values of $\sqrt{\pi}\,\chi_{max}$ which increase with increasing concentration and temperature. The results in Table 10 show no trend as functions of either of these variables. At the same time, the magnitude of $\sqrt{\pi}\,\chi_{max}$ is smaller than expected for this and related models and no further mechanistic information can be deduced.

Chronopotentiometry with Current Reversal. Figures 7 and 15 show typical current reversal chronopotentiograms. More than one cathodic transition time can be observed under certain circumstances, particularly high concentrations and lower temperatures. The diagnostic parameter in this technique is the ratio of $\tau_{back}/\tau_{forward}$. For simple diffusion controlled processes, this ratio is equal to 0.333 (54). The results for the nitrite ion process show that $\tau_b(1)/\tau_f$ is always less than 0.333 indicating loss of product by processes other than diffusion, i.e., following chemical reactions.

Dracka (55) has shown that following chemical reactions may be resolved by the convenience of plotting ln τ_{back} versus ln i_{back}. From the slope of this linear dependence, the order of reaction may be deduced. For a second order homogeneous reaction, the expected slope is -2/3. Figure 16 shows the results obtained in the present studies; clearly the observed slopes are greater than that predicted. Additionally, the plots are dependent on concentration and temperature. Dracka has further shown that the slope of plots of ln τ_{back} versus ln i are greater than

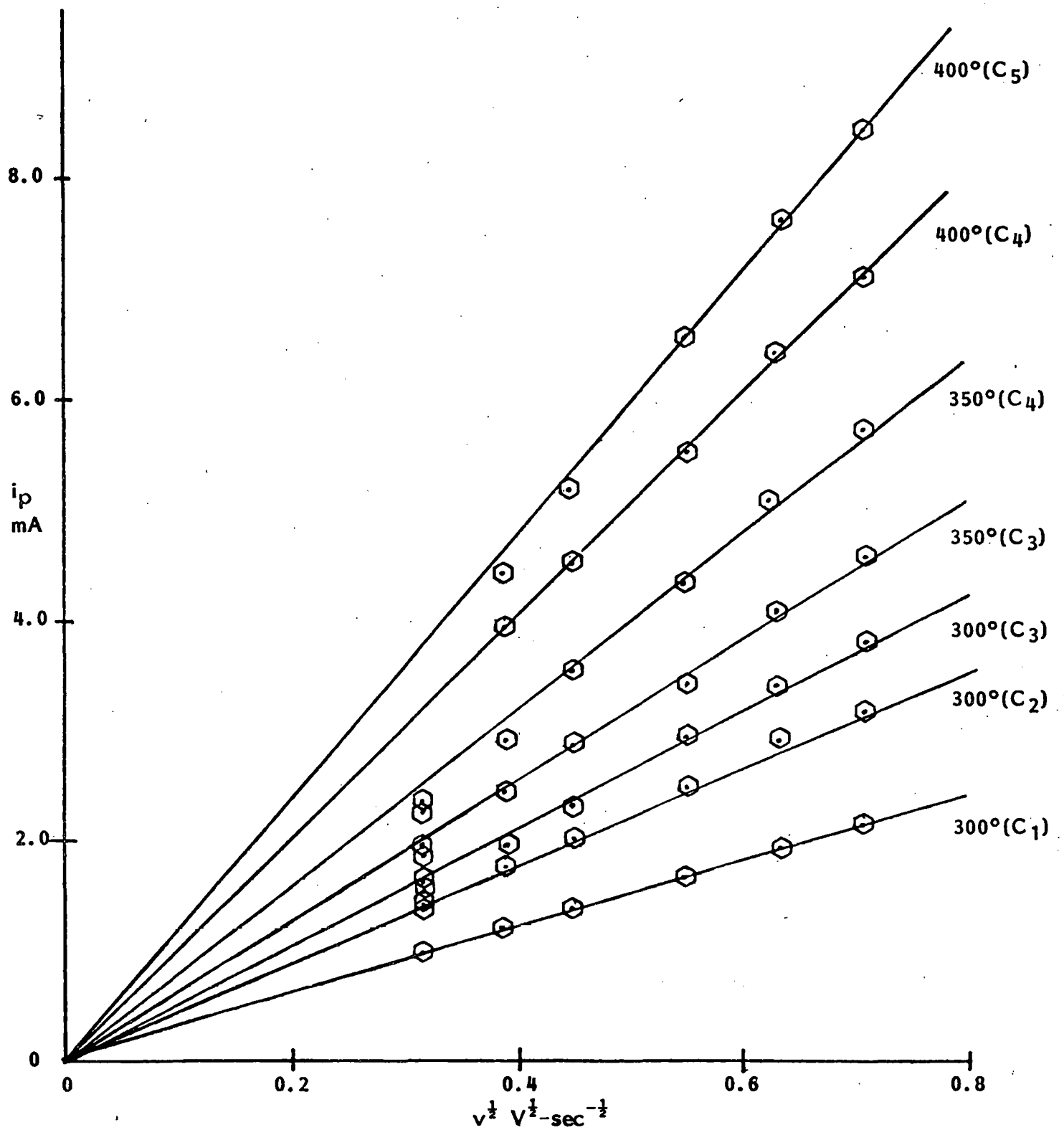

Fig. 12. Voltammetric peak current as a function of the square root of scan rate for the oxidation of nitrite ions at different concentrations and temperatures on gold; Au = 0.358 cm^2.

C_1 = 6.766 x 10^{-3} molal
C_2 = 10.251 x 10^{-3} molal
C_3 = 13.194 x 10^{-3} molal
C_4 = 17.095 x 10^{-3} molal
C_5 = 19.920 x 10^{-3} molal

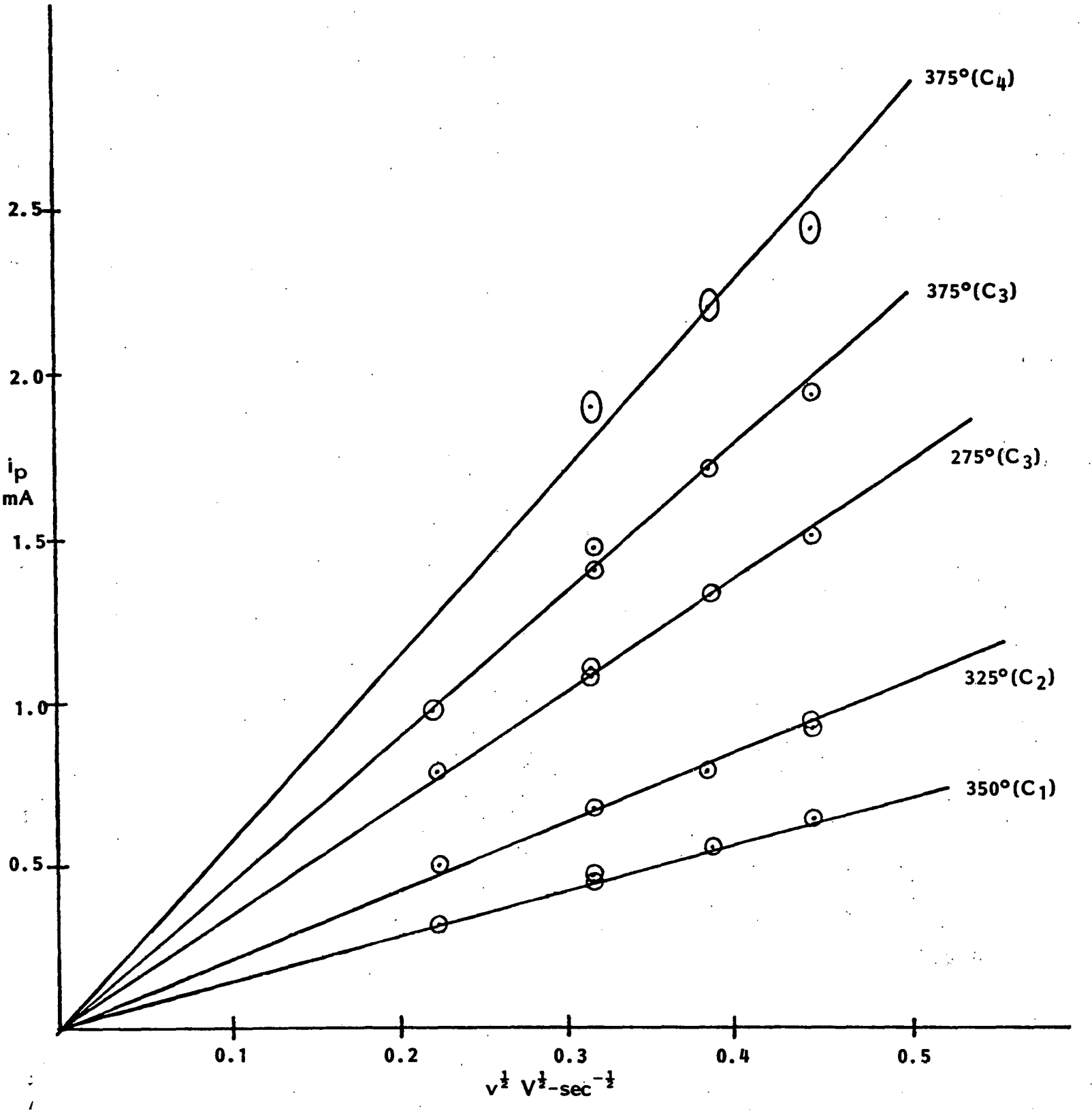

Fig. 13. Voltammetric peak current as a function of the square root of the scan rate at different nitrite concentrations and melt temperatures. Au electrode 0.365 cm2.

C_1 = 3.316 x 10^{-3} molal C_3 = 9.330 x 10^{-3} molal
C_2 = 5.110 x 10^{-3} molal C_4 = 11.326 x 10^{-3} molal

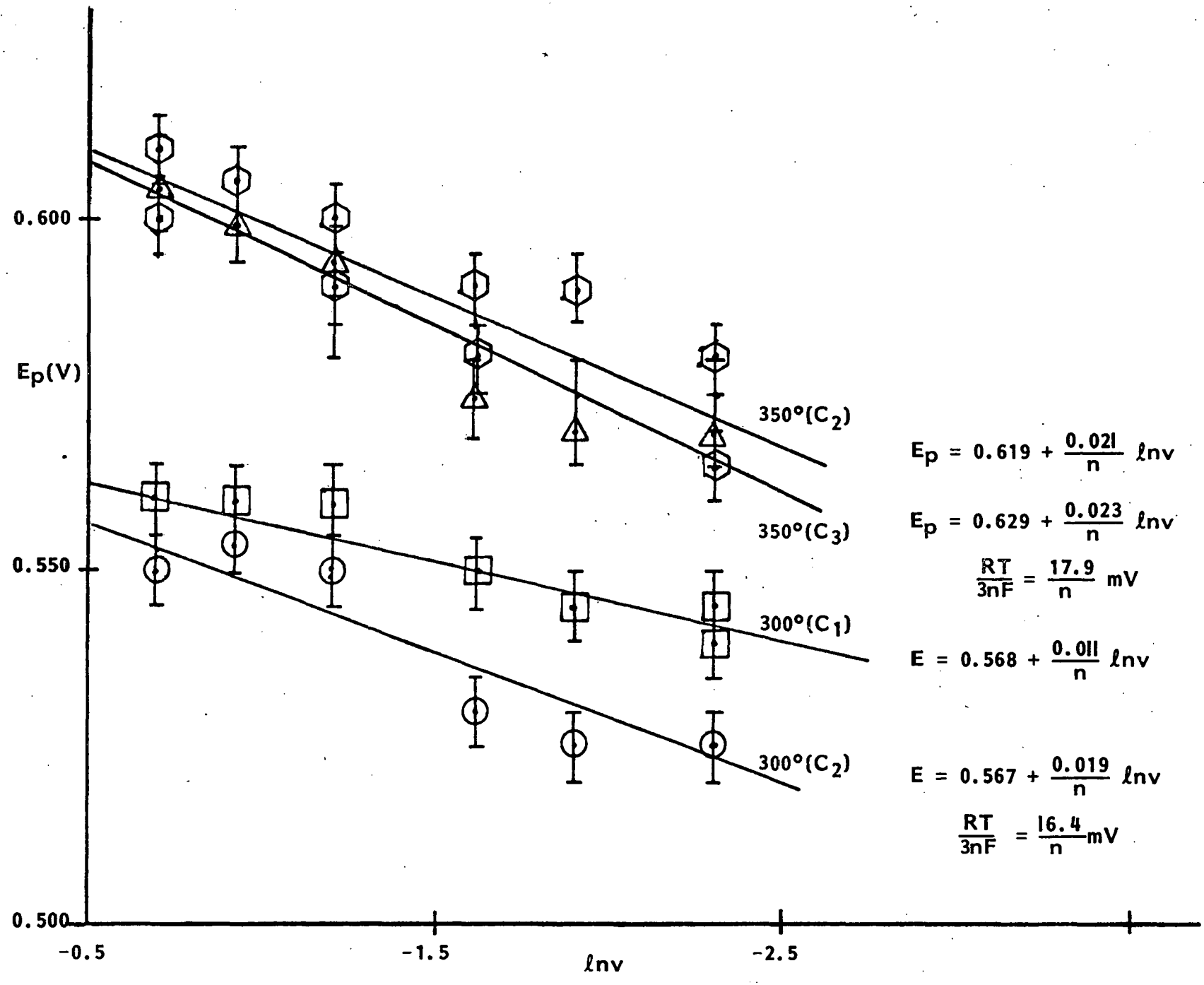

Fig. 14. Plot of peak potential versus logarithm of the scan rate at different concentrations and temperatures for the oxidation of nitrite ions on gold electrodes.

TABLE 9

COMPARISON OF THE OBSERVED HALF PEAK WIDTH WITH THE VALUE FOR A REVERSIBLE PROCESS (SOLUBLE PRODUCT) AT SEVERAL DIFFERENT TEMPERATURES

Temp., °C	$E_p^a - E_{p/2}^a$ (mV)	$2.2\left(\frac{RT}{F}\right)$ (mV)
400	167 ± 6	127.5
350	145 ± 17	118.1
300	127 ± 6	108.6

TABLE 10

ESTIMATE OF THE LINEAR SWEEP VOLTAMMETRIC FUNCTION BASED ON EXPERIMENTALLY MEASURED $i_p v^{-\frac{1}{2}}$ AND THE EXPERIMENTAL SAND CONSTANT $i\tau^{\frac{1}{2}}$

Temp., °C	$\left(\frac{i \cdot v^{-\frac{1}{2}}}{i\tau^{\frac{1}{2}}}\right)$	$\sqrt{\pi}\ \chi_{max}$
275	2.078 ± 0.003	0.399 ± 0.001
300	2.015 ± 0.127	0.396 ± 0.025
325	1.818 ± 0.127	0.365 ± 0.026
350	1.883 ± 0.162	0.386 ± 0.033
375	1.995 ± 0.053	0.417 ± 0.019
400	1.845 ± 0.166	0.330 ± 0.034
		(0.382 ± 0.030) Average

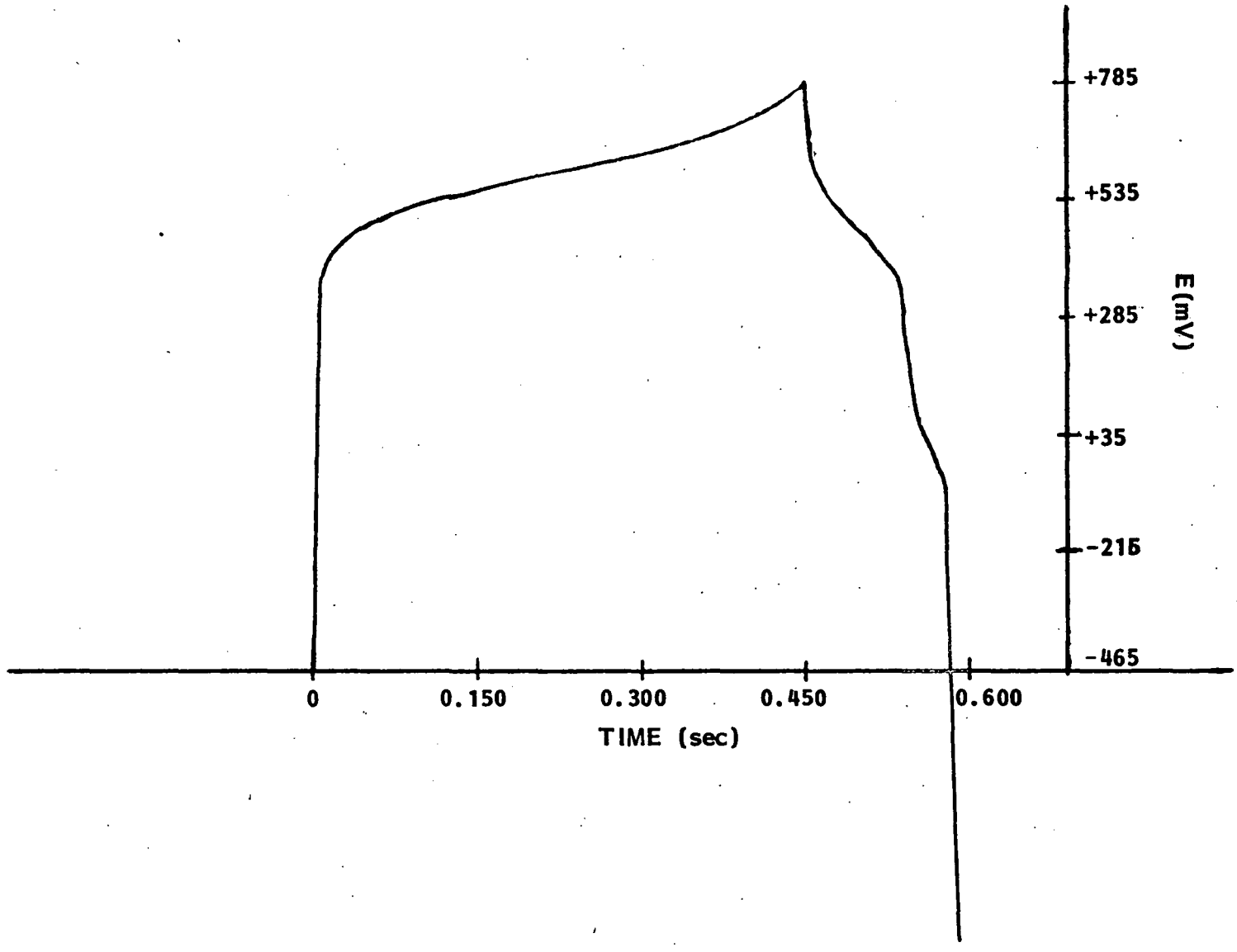

Fig. 15. Current reversal chronopotentiogram at high concentration of NO_2^- ions (17.10×10^{-3} molal) at Au electrode 0.358 cm^2, applied current 6.50 mA, t = 350°C.

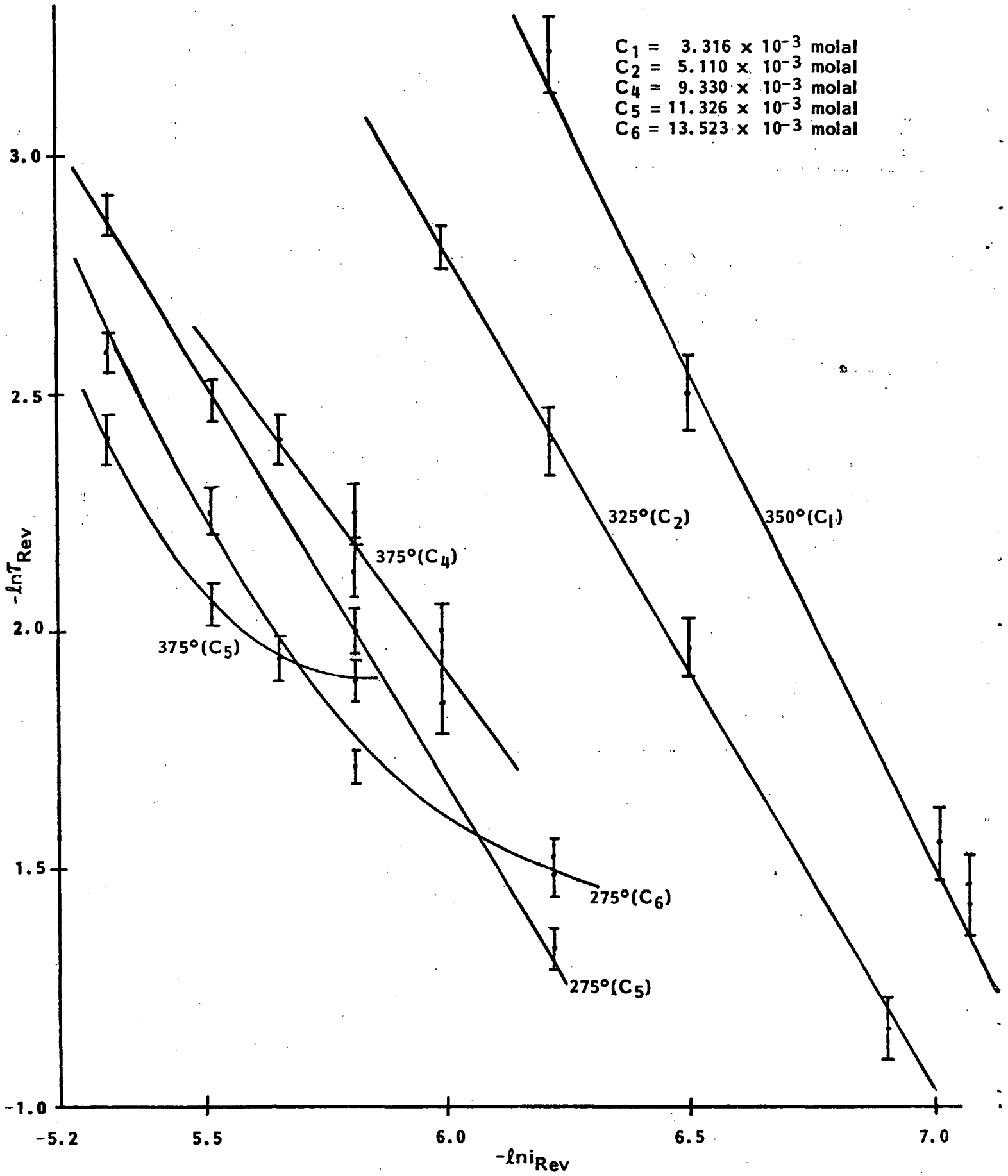

Fig. 16. Determination of order of following chemical reaction and influence of temperature and concentration.

those for a second order reaction when the chemical reaction occurs not only homogeneously but heterogeneously at or on the electrode surface (56). Examination of the boundary conditions given by him indicate that such plots will be concentration dependent and, incidentally, temperature dependent in the same sense as observed in this work. Further support for this latter mechanism is forthcoming from cyclic voltammetry.

Cyclic Voltammetry at a Stationary Electrode. Figures 17 and 18 show cyclic voltammograms for nitrite oxidation at different scan rates and concentrations. The diagnostic peak current ratio i_p^b/i_p^f never reaches the value of unity expected when no chemical complications are sensed during the scan. Plots of the peak current ratio versus scan rate at different concentrations and temperatures are shown in Figure 19. The increase of this function with increasing scan rate is characteristic of an irreversible following chemical reaction. The dependence of the ratio on concentration suggests that the order of reaction is greater than unity, but the limited dependence of peak potential on concentration is consistent with the electrode surface modifying the homogeneous reaction (see above). The well-defined second cathodic peak (under some conditions) is characteristic of the removal of surface products. From Figure 19, rather less than 50% of the electrochemical product is lost to the following chemical reaction. However, the second cathodic peak (Figure 18) is large compared to the first peak which suggests that it is not diffusion controlled. This, together with its shape, implies some surface related process supporting the model proposed above.

At the higher temperature (>450°C) where the concentration of nitrite is large, the anodic peaks became distorted and required high scan rates, v >10 V-sec^{-1}, to obtain relatively smooth peaks.

This distortion of the anodic process can be attributed to a concentration rather than a temperature effect. This is deduced from the fact that, when NO_2^- ions were removed by NO_2 treatment (at 500°C), during the subsequent reestablishment of nitrite ions under argon/or oxygen, monitored electrochemically, well-defined peaks at concentration less than 3 x 10^{-2} molal were observed. It is interesting to note that platinum electrodes showed no second peak.

4.2.3 Mechanism of the Nitrite Oxidation

The melts employed in these studies had been purified and were handled under controlled conditions. Water was absent and the blanketing gases had been passed through molecular sieves and carbon dioxide traps so that reaction pathways such as those reported by Zambonin and coworkers (53), where water behaves catalytically in a follow-up reaction, can be discounted.

The studies of Arvia et al. (26,27) on pure nitrites and solutions of nitrite ion in $NaNO_3$-KNO_3 50 mol% suggested a follow-up sequence of

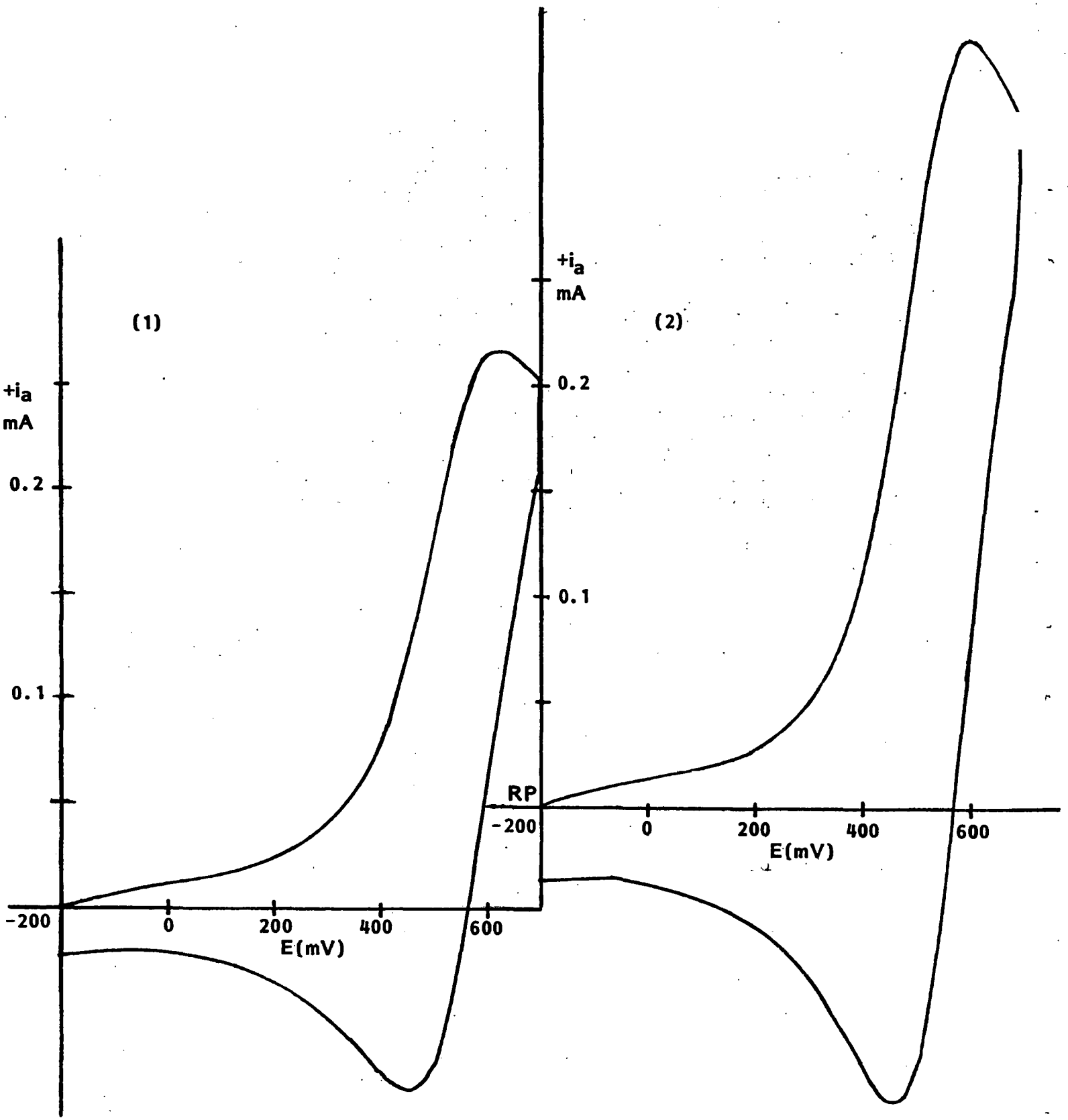

Fig. 17. Cyclic voltammogram for nitrite ion process at low concentration (3.316×10^{-3} molal) for different scan rates at Au electrode 0.365 cm^2. 1 = 0.100 V-sec^{-1}; 2 = 0.200 V-sec^{-1}, t = 350°C.

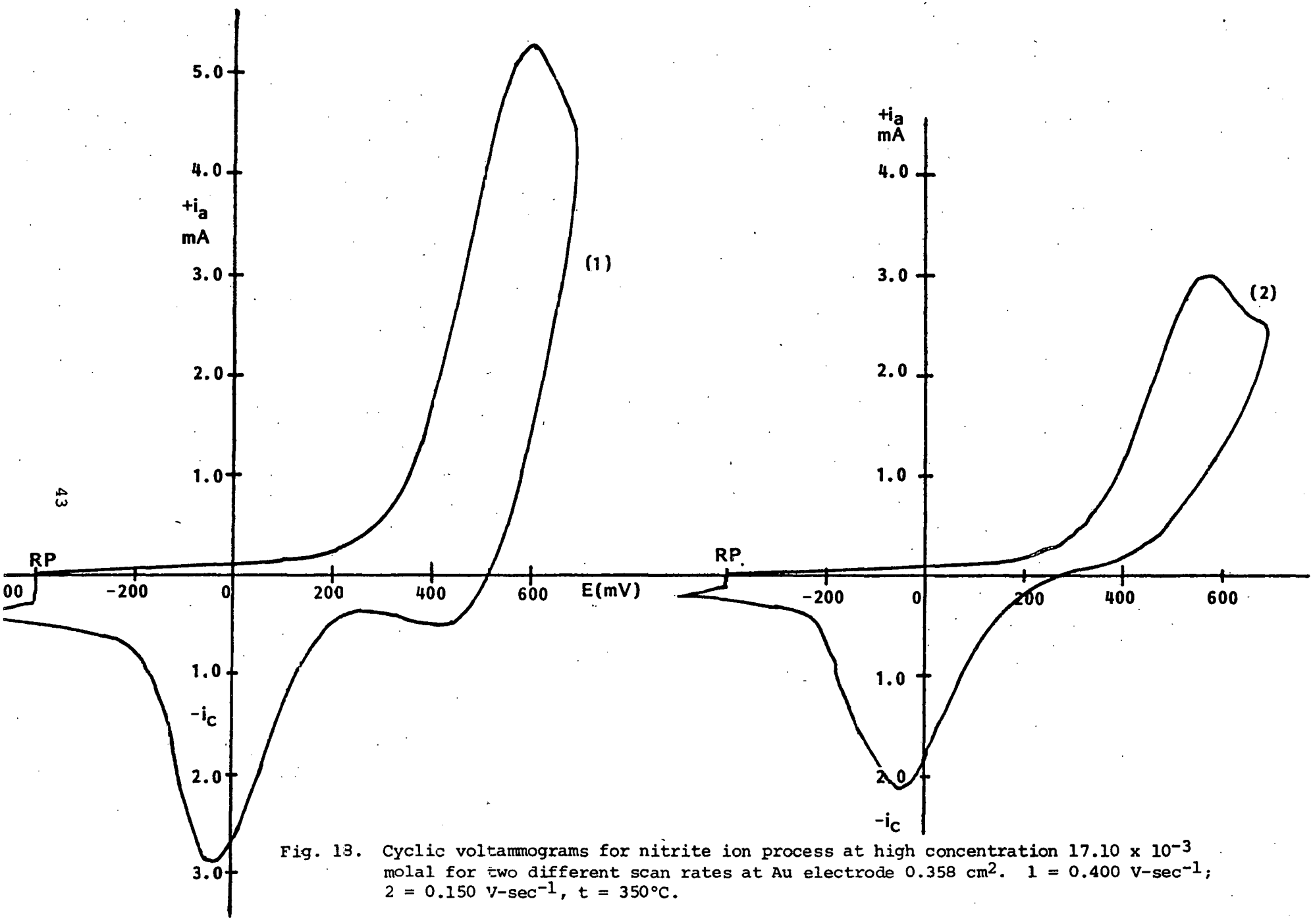

Fig. 18. Cyclic voltammograms for nitrite ion process at high concentration 17.10 x 10^{-3} molal for two different scan rates at Au electrode 0.358 cm^2. 1 = 0.400 V-sec^{-1}; 2 = 0.150 V-sec^{-1}, t = 350°C.

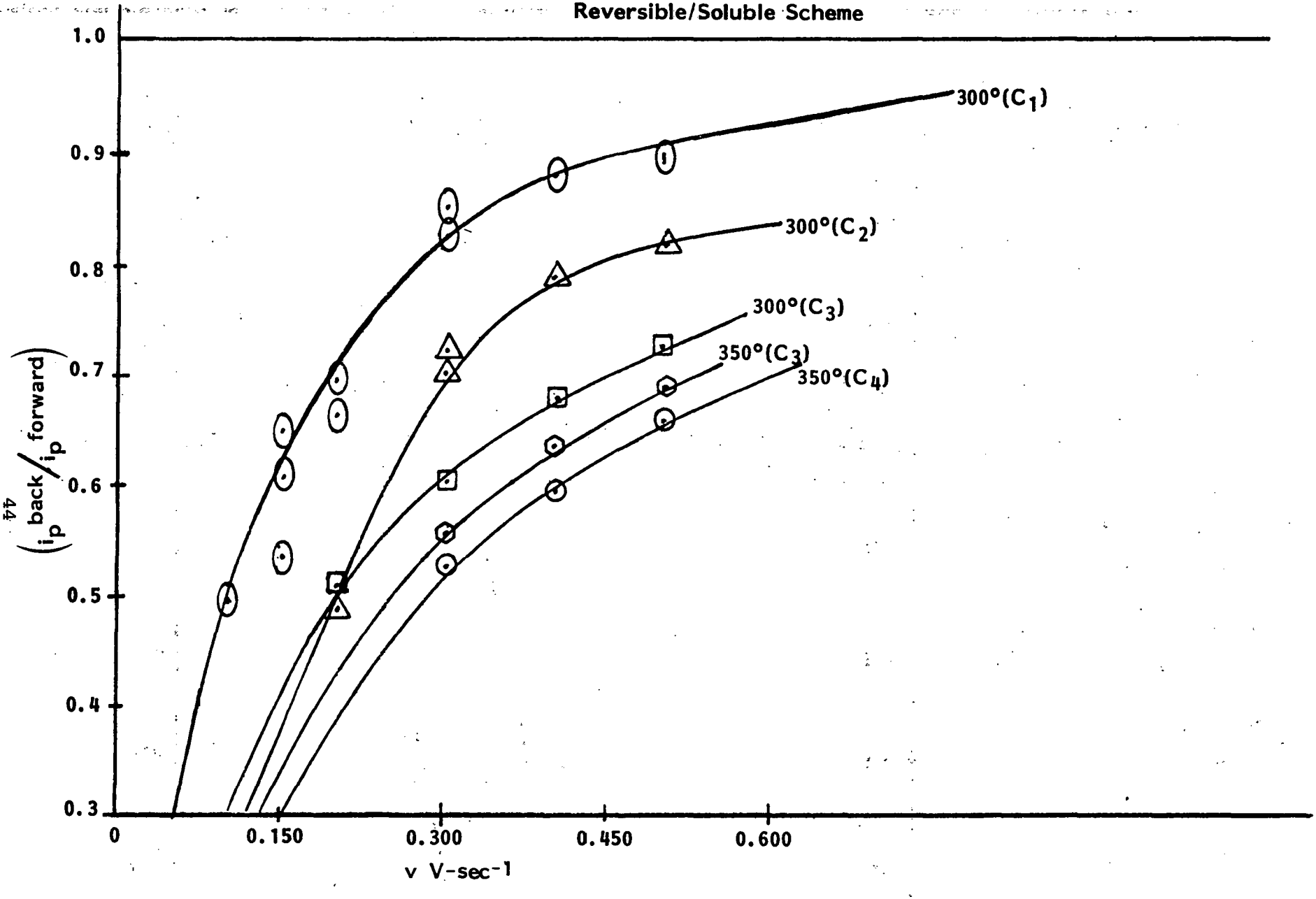

Fig. 19. Influence of concentration and temperature on the ratio of reverse peak current/forward peak current for nitrite oxidation.

reactions. Arvia's work was carried out on platinum and graphite electrodes. On platinum, changes in the "Tafel" slope were observed at lower overvoltage, an RT/nF slope was reported which changed to RT/2nF. At higher temperatures, >345°C, the slope was RT/nF. These slopes are consistent with mechanistic pathways in which only slow chemical reactions occur at or on the surface. The dimerization reaction

$$2NO_2 \rightleftarrows N_2O_4 \qquad (33)$$

was proposed which involved surface related reactions. It is unlikely that such a reaction can take place at these temperatures since the dissociation of N_2O_4 is complete above 140°C (52). Attempts to interpret the present results by a dimerization follow-up reaction either at equilibrium (57) or irreversible (58,59) were unsuccessful.

Several other possible chemical reactions, in the absence of extraneous impurities, and the known chemistry of nitrogen, can be proposed.

(a) The reaction of nitrogen dioxide with nitrite ions diffusing into the electrode viz,

$$NO_2 + NO_2^- \rightleftarrows NO + NO_3^- \qquad (34)$$

(b) The decomposition of nitrogen dioxide to nitrous oxide and oxygen

$$2NO_2 \rightleftarrows N_2O + 3/2\ O_2 \qquad (35)$$

(c) The decomposition of nitrogen dioxide to nitric oxide and oxygen

$$2NO_2 \rightleftarrows 2NO + O_2 \qquad (36)$$

The initial electron transfer reaction has been assumed to be the de-electronation of NO_2^-

$$NO_2^- \rightleftarrows NO_2 + e \qquad (37)$$

which occurs with a high heterogeneous rate constant. Other reactions can be written, for example,

$$2NO_2^- \rightleftarrows NO_3^- + NO + 2e \qquad (38)$$

but are likely combinations of (37) with follow-up reactions such as (34). Consequently, the observations for the chronopotentiometric results without current reversal are consistent with such a view, i.e., reaction (37).

The current reversal and cyclic voltammetric experiments require a more detailed examination of the mechanistic pathways following electron transfer. It is likely that reaction scheme (a) can be discounted because it fails to account for the observed second peak (Figure 18) if the results of Topol et al. (25) concerning the electroinactivity of NO are correct. On the other hand, both schemes (b) and (c) produce oxygen which may interact with the gold surface resulting in subsequent reduction peaks. Although gold oxides at high temperatures are thermodynamically unstable, there have been reports of their existence (60), and in the temperature range 250-350°C may be significant. From a thermodynamic viewpoint, reaction scheme (b) is favored over (c) because of the favorable free energy change per 2 mol nitrogen dioxide (Table 11). Nevertheless, reaction (b) is unknown and (c) is the most likely follow-up reaction. The role of the gold surface in some parallel heterogeneous reaction may be that suggested by the reverse current chronopotentiometric data. A mechanism such as

$$NO_2^- \rightleftarrows NO_2 + e$$

$$2NO_2 \rightarrow 2NO + Au(O)_2 \qquad \text{Surface}$$

and

$$2NO_2 \rightarrow 2NO + O_2 \qquad \text{Solution}$$

and may be appropriate, and leads to the overall reaction

$$2NO_2^- \rightleftarrows 2NO + O_2 + 2e \qquad (39)$$

Combination of this with the nitrate electrode

$$NO_3^- \rightleftarrows NO_2 + 1/2\ O_2 + e \qquad (40)$$

leads to the conclusion that the overall electrode process may be reaction (39). It is clear that the simple electro-oxidation of nitrite ion proposed by earlier workers was somewhat naive and the studies reported here present some insight into the possible reaction mechanisms. The subtle effect of the mechanistic pathway on in situ analysis should be noted!

4.2.4 The Chemical Behavior of Nitrite Ions

The electrochemical studies carried out in this work have confirmed that thermal decomposition of nitrate is indeed an intrinsic process although extrinsic effects may be seen. The melting of laboratory grade nitrates leads to the formation of nitrite ions in excess of the equilibrium concentration predicted from thermodynamics and at rates exceeding those observed at higher temperature. Such results, as seen from background currents in unpurified material, can be explained on the assumption that nitrite ion arises from the oxidative action of nitrate ions on residual impurities arising from manufacture and/or contamination during handling.

TABLE 11

SOME THERMODYNAMIC DATA RELATING TO REACTIONS (35) AND (36) OVER THE TEMPERATURE RANGE 230°C TO 600°C

Temp, °C	ΔG°_R (35) kcal per 2 mols NO_2	ΔG_R (36) kcal per 2 mols NO_2
230	-2.49	10.48
300	-3.11	7.90
400	-4.51	4.18
500	-5.72	0.48
600	-6.91	-3.22

Trace organic materials are most likely reductants. Melts purified by NO_2 treatment showed lower background currents. In one experiment, a melt was treated with NO_2 at 500°C to remove NO_2^-, $CO_3^=$, etc. After the removal of the NO_2 by vacuum treatment and oxygen bubbling, the nitrite ion concentration was monitored electrochemically. Figure 20 shows the increasing nitrite concentration with time. The buildup rate at this temperature is consistent with the rate of decrease of excess nitrite ions under oxygen (4). Because of the relative slowness of the reaction

$$2NO_2^- + O_2 \not\rightleftarrows 2NO_3^- \qquad (41)$$

excess NO_2^- (above the equilibrium value) becomes "locked in" when a melt at high temperature, e.g., 525°C is cooled to 425°C during a 12 hour period. Rapid cooling cycles may therefore produce melts at lower temperatures rich in nitrite and the physical and chemical properties of such liquids may differ somewhat from those of the pure nitrate. Nitrate processing to remove carbonate/hydroxide will require lower temperatures (300-400°C) unless O_2 is mixed with the NO_2 gas, since the thermal decomposition of NO_2 to NO occurs readily above 500°C. See Table 11 and reference (52).

4.3 Water - The Chemical and Electrochemical Behavior of Water in Equimolar Sodium Nitrate-Potassium Nitrate Mixture

It has been known for many years that water has a significant solubility in molten salts, particularly molten alkali metal nitrate mixtures at low temperatures (120-150°C). Water is electroactive and studies of its properties in molten nitrates appeared feasible by electrochemical techniques. Indeed some successful attempts were made to obtain water solubilities in $LiNO_3$, $NaNO_3$, KNO_3 (40) and $LiNO_3$-KNO_3 (36,61). The solubility measurements required some calibration, and Peleg (40) used direct additions of water as well as calibration involving gas phase calculations, whereas Morachevskii (61) used additions of hydrated ammonium carbonate. None of these procedures is entirely satisfactory, and in this work it has been proposed (39) that the combination of hydrodynamic voltammetry and linear sweep voltammetry would enable the water solubility to be obtained independent of a calibration procedure. For a reversible diffusion controlled process

$$\frac{i_L}{\omega^{\frac{1}{2}}} = 0.62\ nFAC\ \nu^{-1/6}\ D^{2/3} \qquad (42)$$

and

$$\frac{i_p}{\nu^{\frac{1}{2}}} = \left(\frac{nF}{RT}\right)^{\frac{1}{2}} nFAC\ \sqrt{\pi}\ \chi(i)\ D^{\frac{1}{2}} \qquad (43)$$

From the ratio of these equations, D can be evaluated and hence C is obtained (n is measured from E_p-$E_{p/2}$ of the voltammogram).

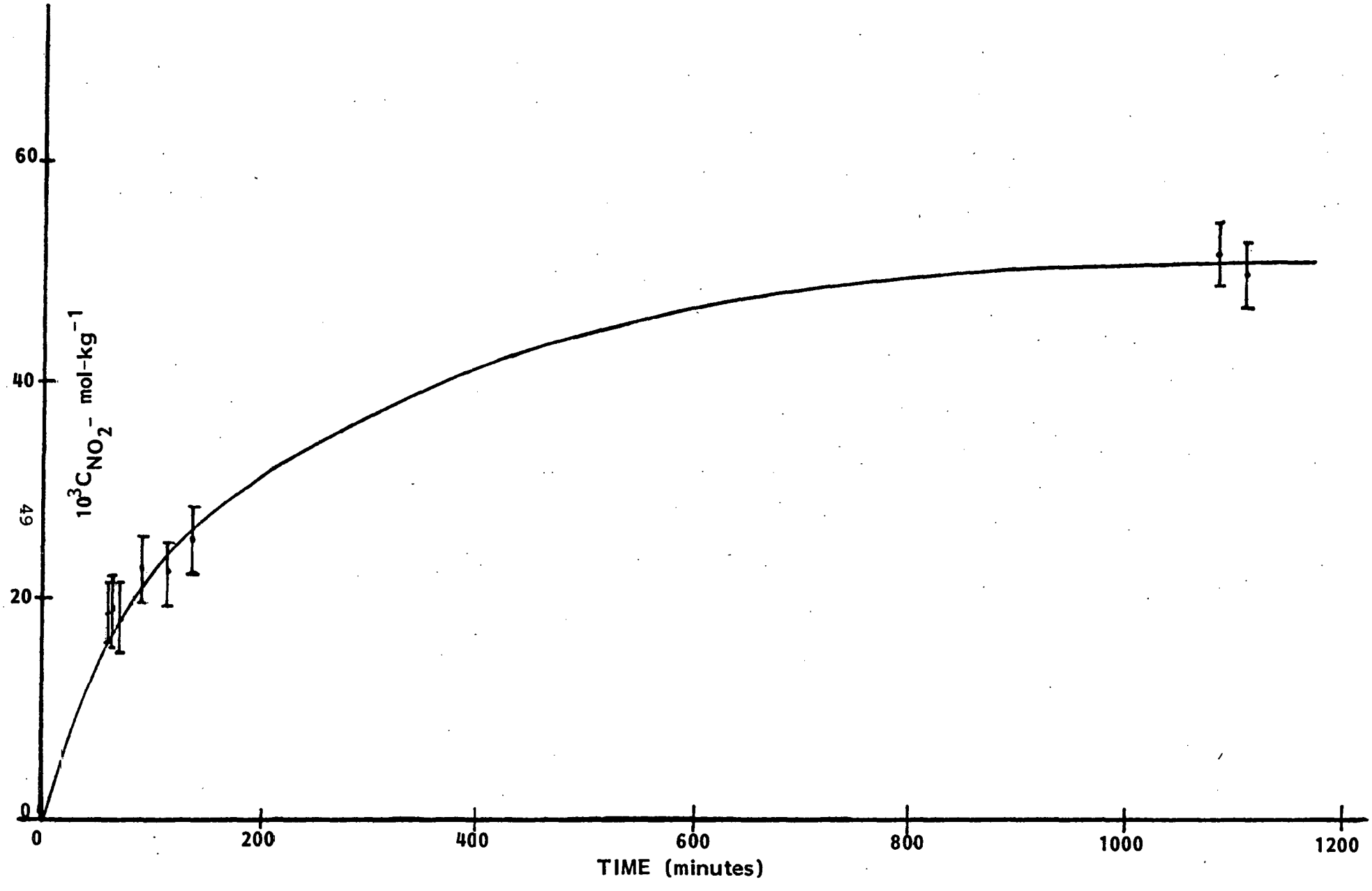

Fig. 20. Growth of nitrite ion concentration after purging nitrate melt with NO_2 gas at 500°C oxygen atmosphere.

This analysis implies that the electroreduction mechanism is that of simple diffusion control. Previous work (30) had shown that at low water concentrations i_L was proportional to the water concentration and the overall reaction had been deduced as

$$H_2O + NO_3^- + 2e \rightleftarrows NO_2^- + 2OH^- \qquad (44)$$

in spite of recent suggestions to the contrary (36).

Analysis of the data obtained in the course of the present work has shown that the electrochemical reduction of water is a more complicated process than that implied by the simple overall reaction (44). Consequently, in order to employ the electrochemical methods to evaluate the properties of water dissolved in the sodium nitrate-potassium nitrate equimolar mixture at temperatures of concern in thermal storage, it is first necessary to elucidate the reduction mechanism. Subsequently, the properties of water and its chemical behavior may be assessed.

4.3.1 Electrochemical Study of the Reduction of Water

The water reduction process appears close to the cathodic limiting process for the nitrate solvent. Under these conditions, chronopotentiograms were poorly resolved (better at higher temperatures), but limiting currents at the rotating disc electrode and cyclic voltammograms on the stationary disc electrode were well-defined. Pulse voltammograms and DPV also gave well-defined limiting currents and peaks, respectively. Figures 21 through 25 illustrate these results and Tables 12 and 13 show some typical data obtained. Addition of $LiNO_3$-$3H_2O$ confirmed these processes are due to water.

Cyclic Voltammetric Results for Stationary Electrodes. Voltammetric data were obtained as a function of scan rate, partial pressure of water in the argon gas phase above the melt, and melt temperature. Figure 23 shows typical cyclic voltammograms at three different scan rates, at 350°C. At a given melt temperature at high scan rates, the peak current function $i_p/v^{\frac{1}{2}}$ is proportional to the water vapor pressure in the gas phase, and since Henry's law is obeyed (30), proportional to the concentration of water in the melt. The peak labeled B only appears at high scan rates >0.5 V-sec^{-1}, the ratio $i_p{}^a/i_p{}^c \rightarrow 0$ at scan rates below this value. During the reverse scan following the cathodic process, the redox system C/D appears and is strongly dependent upon the scan rate (Fig.24).

The peak current function $i_p/v^{\frac{1}{2}}$ is a diagnostic characteristic in resolving reaction mechanisms. For a simple reversible reaction, this function is independent of the scan rate but depends upon concentration and temperature (Equation 43). In the case of water reduction, this quantity is shown as a function of scan rate at constant temperature, Figure 26, and at constant partial pressure of water, Figure 27. At a given water partial pressure and at temperatures around 300°C,

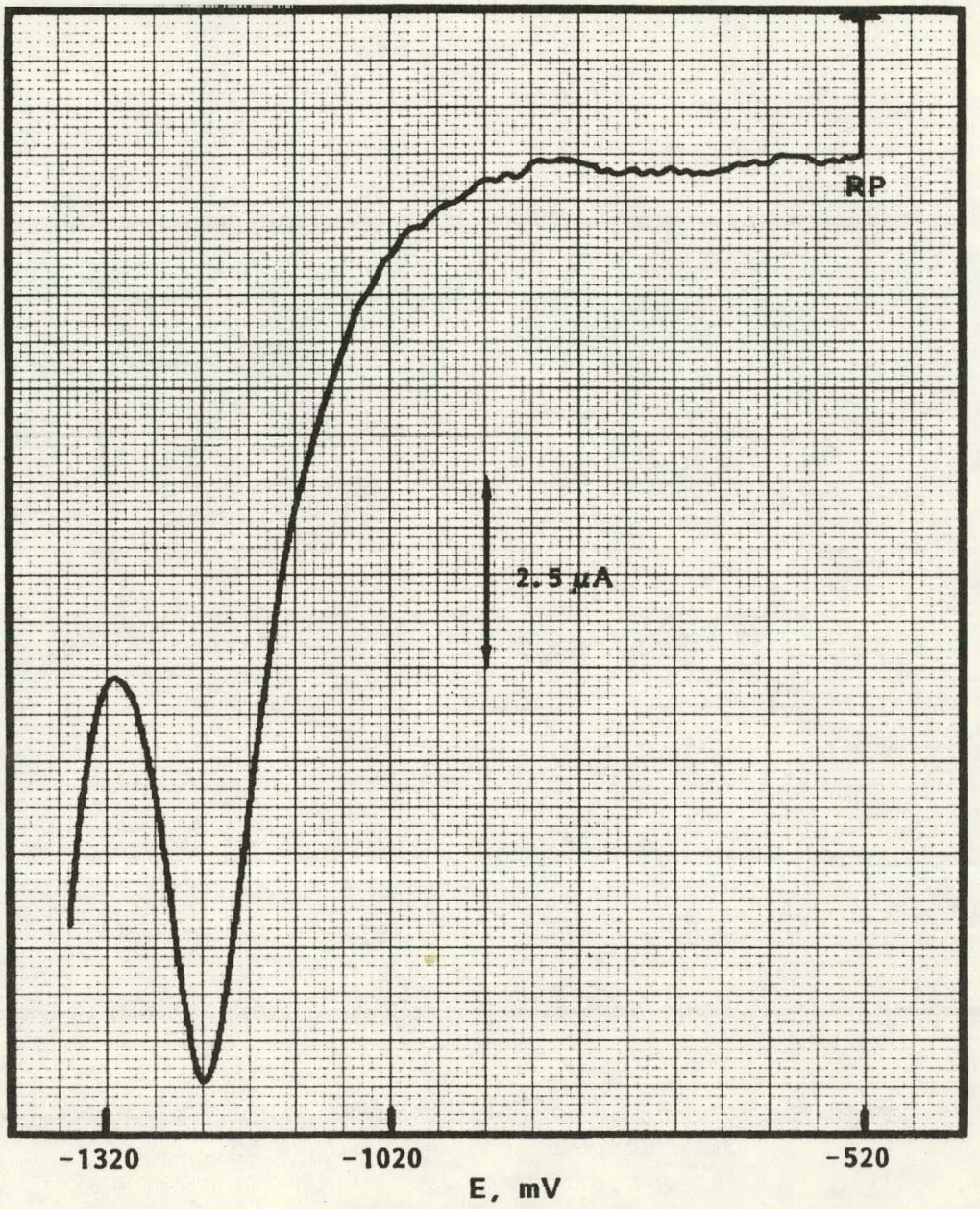

Fig. 21. Differential pulse voltammogram for water reduction at 300°C, p_{H_2O} = 19.35 mm. Au electrode 0.06 cm^2, amplitude 5 mV, scan rate 2 mV-sec^{-1}, drop time 1 sec. RP = -0.520V vs. 0.07m Ag(1)/Ag reference.

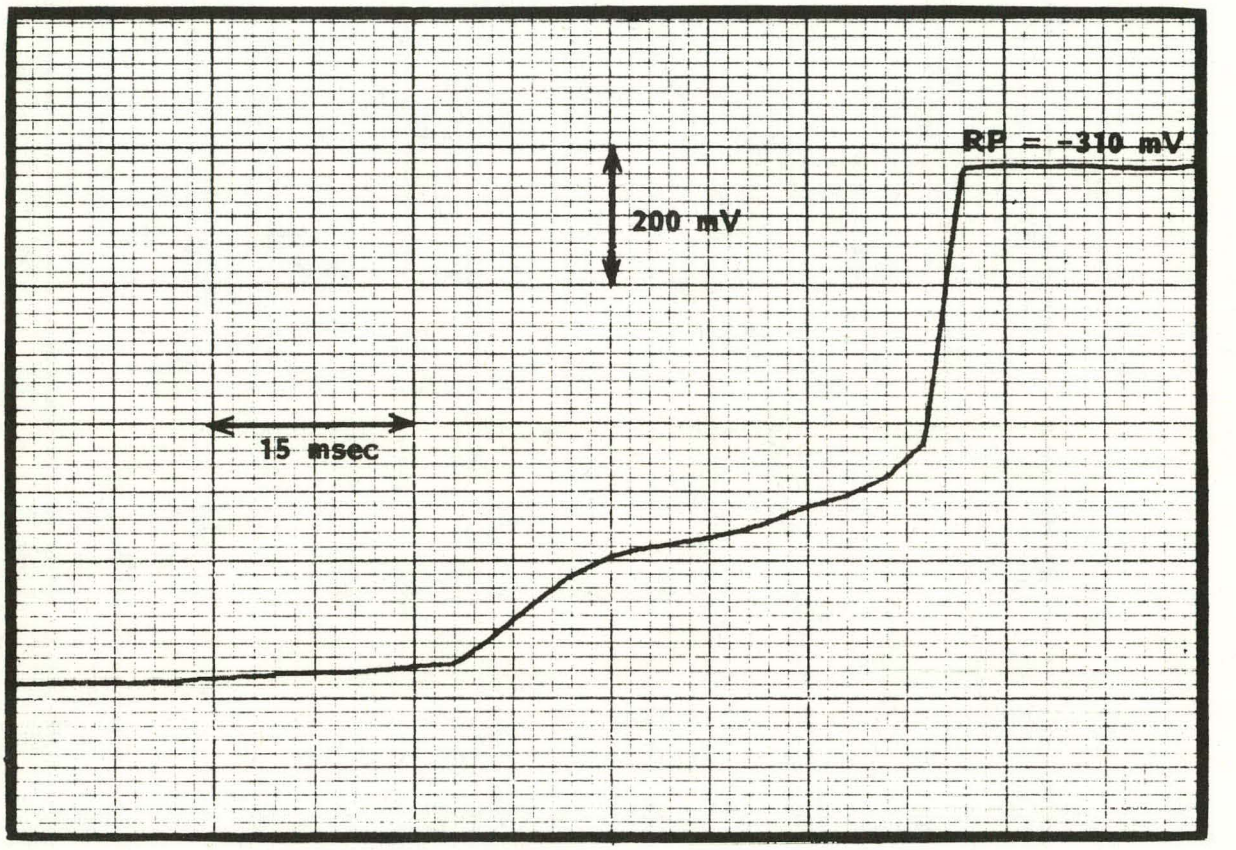

Fig. 22. Chronopotentiogram for the reduction of water on Au electrode at 525°C, P_{H_2O} = 19.3 mm.

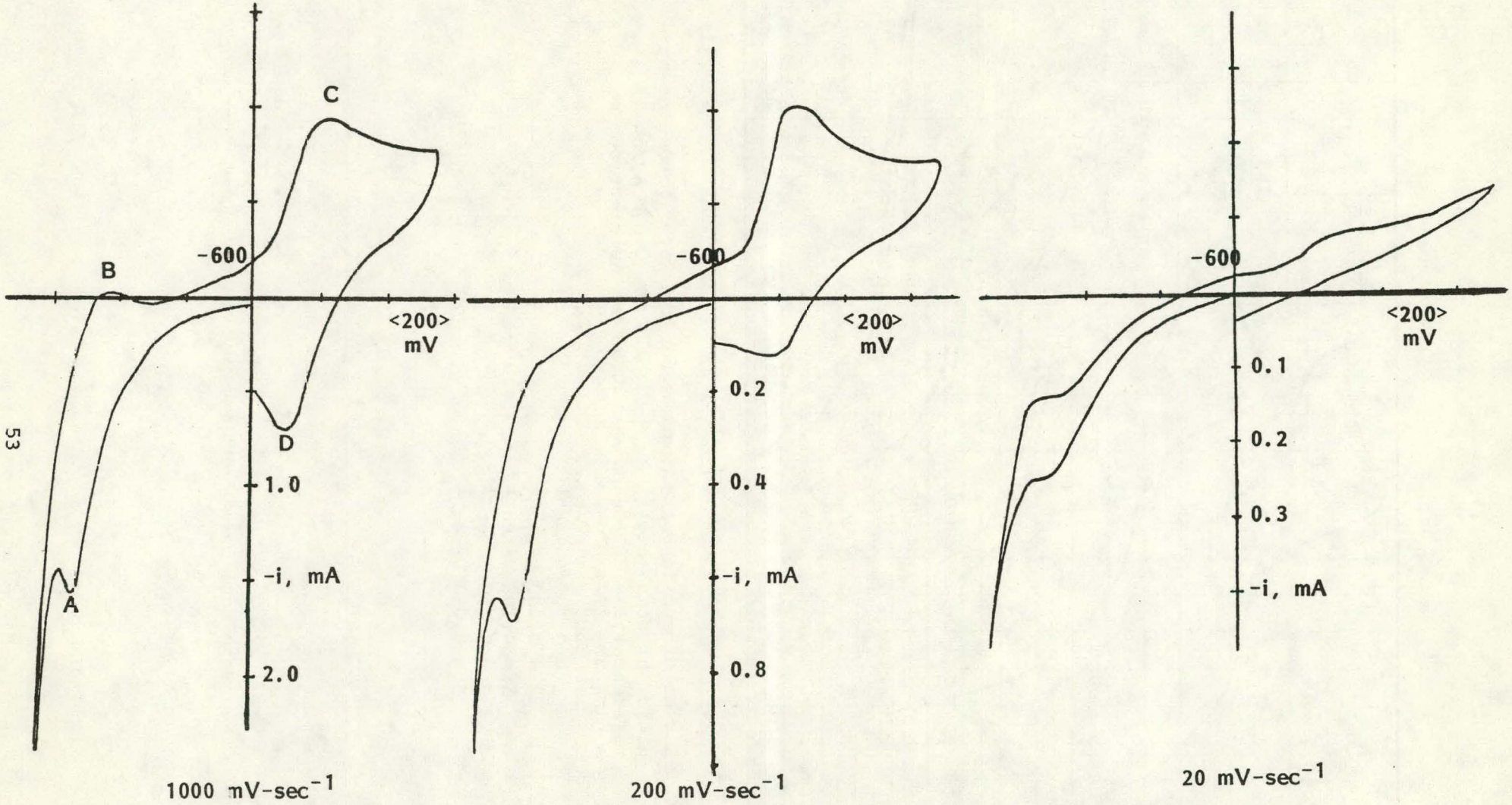

Fig. 23. Cyclic voltammograms for water reduction as a function of scan rate. Gold electrode, 350°C water partial pressure = 21 mm. E versus $Ag/AgNO_3$ 0.07m $NaNO_3$-KNO_3 reference electrode.

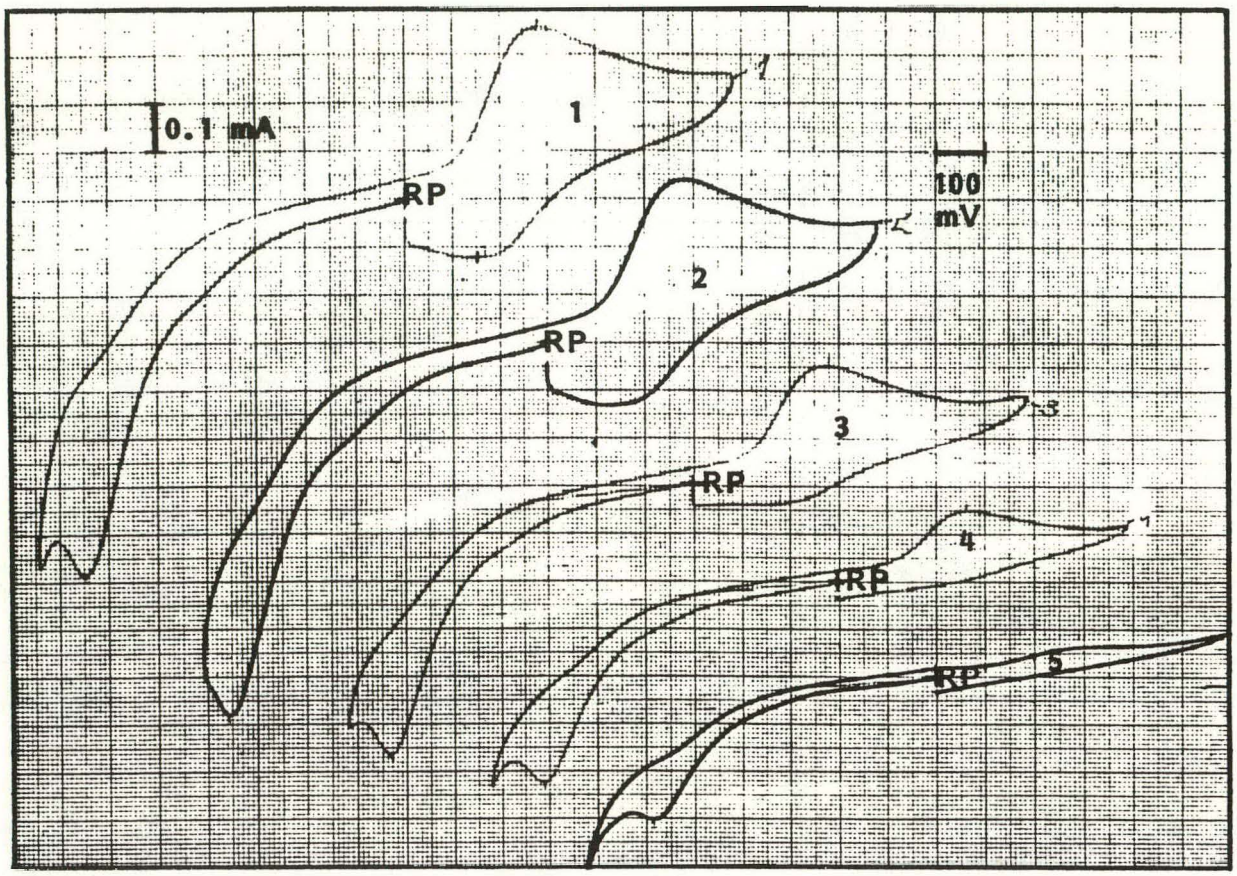

Fig. 24. Series of cyclic voltammograms for the water processes at different scan rates. RP = -0.612V vs. 0.07m Ag/Ag(1) reference; t = 325°C; P_{H_2O} = 20.85 mm; Au electrode = 0.06 cm^2.

1 = 0.200 V-sec^{-1}
2 = 0.200 V-sec^{-1}
3 = 0.100 V-sec^{-1}
4 = 0.050 V-sec^{-1}
5 = 0.020 V-sec^{-1}

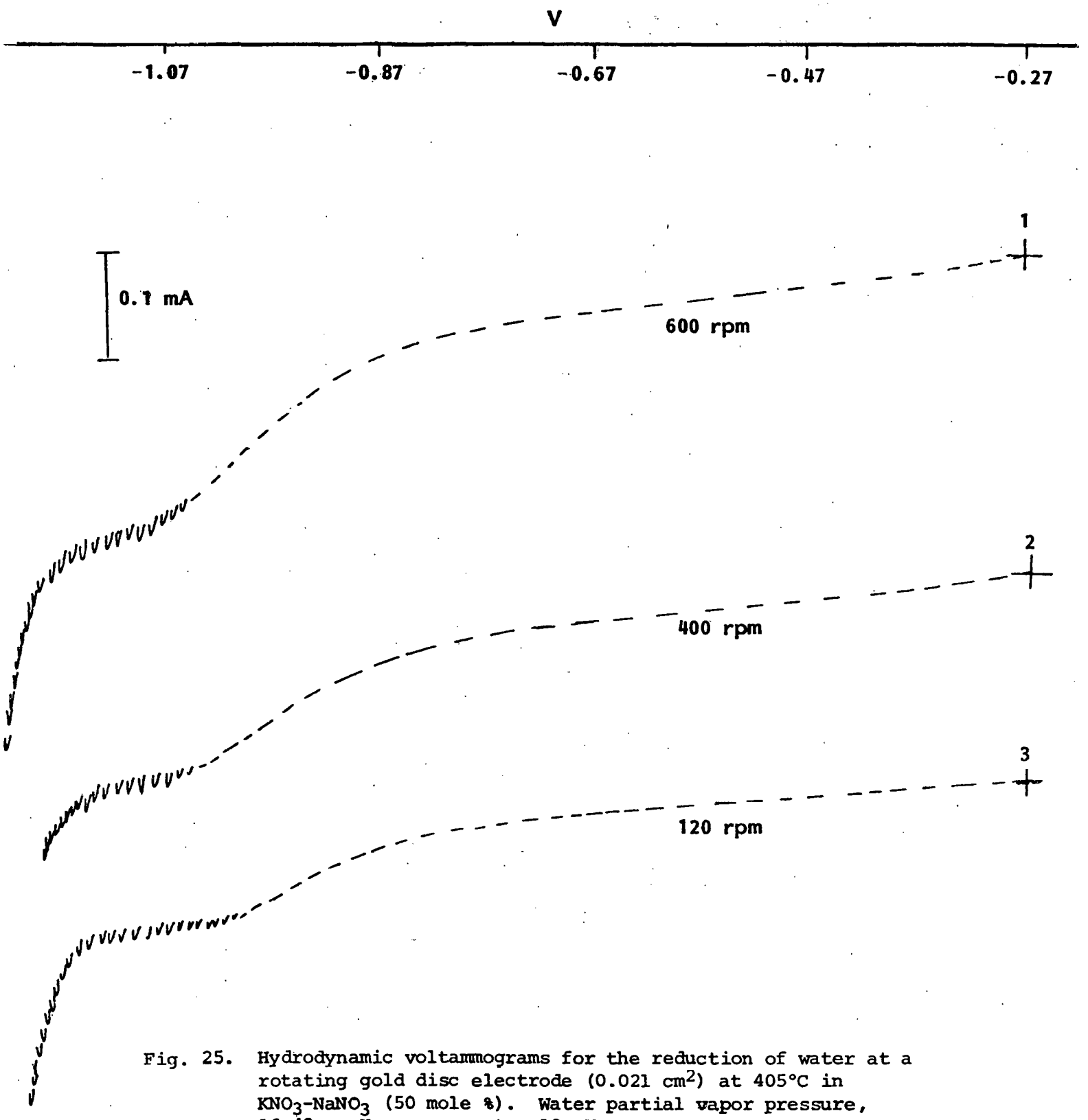

Fig. 25. Hydrodynamic voltammograms for the reduction of water at a rotating gold disc electrode (0.021 cm^2) at 405°C in KNO_3-$NaNO_3$ (50 mole %). Water partial vapor pressure, 16.48 mm Hg; sweep rate, 10 mV-sec.

TABLE 12

CV DATA FOR THE REDUCTION OF WATER IN MOLTEN $NaNO_3$-KNO_3 (50-50 mol%) MIXTURE AT 295°C ON STATIONARY GOLD ELECTRODE (0.021 cm^2)

P_{H_2O} (mm Hg)	E_p (V)	Scan Rate (V/sec)	$i_p \cdot V^{-\frac{1}{2}}$ ($\mu A \cdot V^{-\frac{1}{2}} sec^{\frac{1}{2}}$)	$E_p - E_{p/2}$ (mV)	P_{H_2O} (mm)	E_p (V)	V ($V \cdot sec^{-1}$)	$i_p / V^{\frac{1}{2}}$ ($\mu A \cdot V^{-\frac{1}{2}} sec^{\frac{1}{2}}$)	$E_p - E_{p/2}$ (mV)
18.20	-	0.030	8.22	-	12.38	-	0.030	569	-
	-1.235	0.050	7.88	-80		-1.185	0.050	553	- 95
	-1.242	0.075	7.62	-72		-1.200	0.075	515	-100
	-1.250	0.100	7.78	-87		-1.205	0.100	494	-100
	-1.265	0.150	7.48	-85		-1.220	0.150	491	-100
	-1.275	0.200	7.40	-83		-1.230	0.300	486	-100
	-1.290	0.300	7.26	-82					

TABLE 13

HDV DATA FOR REDUCTION OF WATER ON Au DISC, 0.021 cm^2 AND A SCAN RATE 2 $mV \cdot sec^{-1}$, t°C = 295

P_{H_2O} (mm Hg)	$E(i_{L/2})$ (V)	RPM (ω)	$i_L \cdot \omega^{-\frac{1}{2}}$ ($\mu A \cdot rad^{-\frac{1}{2}} \cdot sec^{\frac{1}{2}}$)	P_{H_2O} (mm)	$E(i_{L/2})$ (V)	RPM (ω)	$i_L \cdot \omega^{-\frac{1}{2}}$ ($\mu A \cdot rad^{-\frac{1}{2}} \cdot sec^{\frac{1}{2}}$)
18.20	-	-	-	12.38	-1.180	550	46.1
	-1.205	480	56.8		-1.170	480	45.8
	-1.203	400	56.8			400	46.3
	-1.195	300	58.8			300	47.2
	-1.182	200	60.1			120	56.4
	-1.175	120	67.7			60	62.8

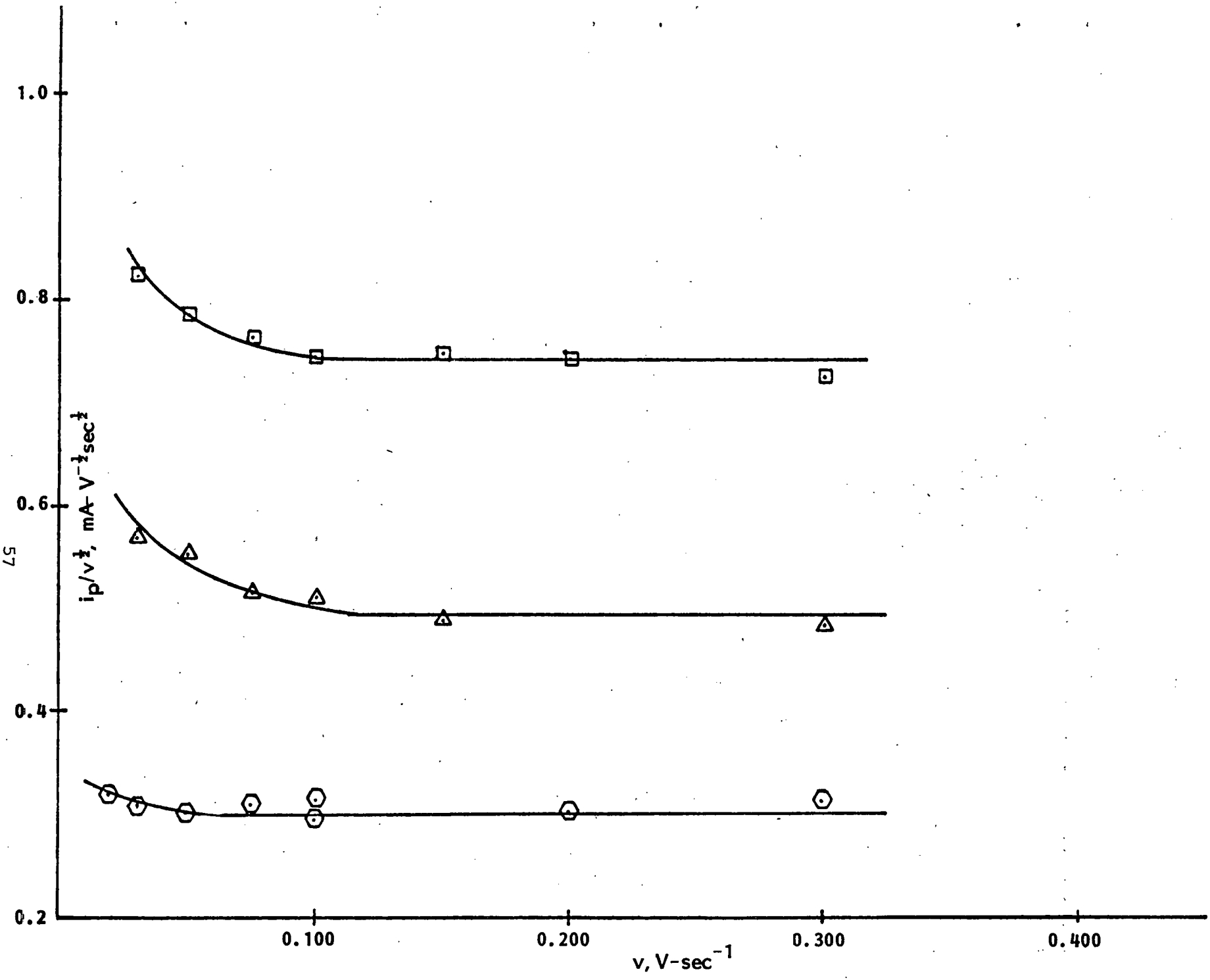

Fig. 26. Current function versus scan rate at constant temperature (t = 295°C) at three water partial pressures (mm). ⊡ = 18.20; ▲= 12.38; ⊙= 7.51 gold electrode = 0.021 cm^2.

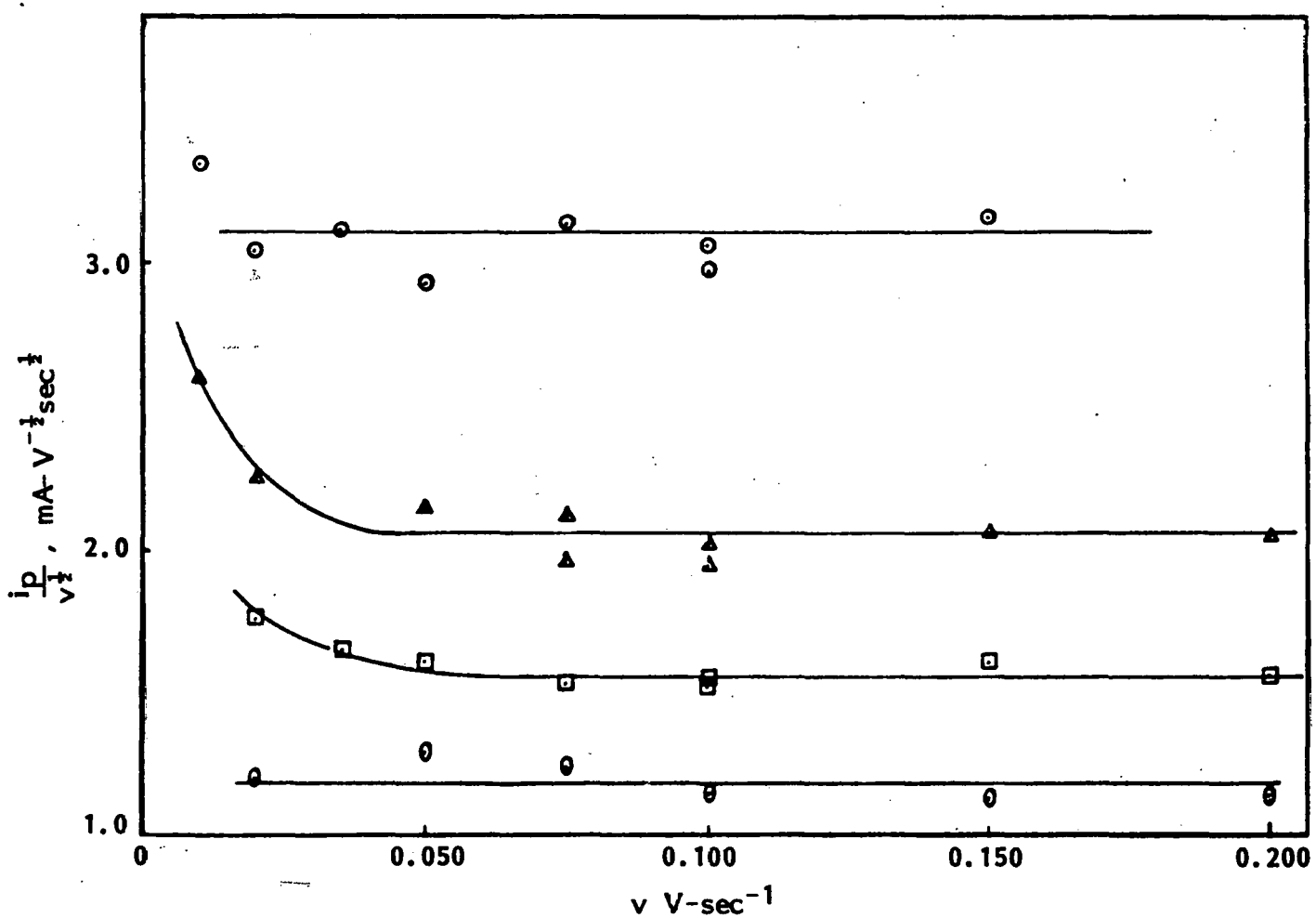

Fig. 27. Peak current function versus scan rate for four different temperatures.

⊙ 250°C ⊡ 325°C p_{H_2O} = 22.94 mm
Δ 300°C θ 346°C A_{Au} = 0.06 cm^2

$i_p/v^{\frac{1}{2}}$ is scan rate dependent at lower scan rates, becoming constant at higher scan rates. At higher (>350°C) and lower temperatures (250°C) the current function is independent of scan rate even at the lower scan rates.

The peak potential E_p of peak A is also a function of scan rate at all temperatures and water vapor pressures. E_p is a linear function of lnv with a slope of RT/2nF. Figure 28 shows this dependence for three different partial pressures. These results imply that the peak potential is a function of the water concentration in the nitrate melt becoming more cathodic as the water concentration increases. Table 14 show that the half peak width $E_p-E_{p/2}$ depends on the temperature but within a large experimental error is independent of water partial pressure.

The above results and observations, especially at ∿300°C, imply that the reduction of water is not a simple diffusion controlled process. The potential data suggest that either an irreversible charge transfer process is involved (62) or that a following irreversible chemical reaction is coupled to a reversible charge transfer process (63). The irreversible charge transfer mechanism can be discounted because of the concentration dependence of E_p, the growth of anodic peak (Figure 23) as the scan rate increases, and the behavior of the peak current function.

The appearance of the redox couple C/D, the dependence of E_p on concentration and characteristically, the increase of $i_p/v^{\frac{1}{2}}$ at low scan rate, suggest that an E.C. process is followed by a second reduction reaction involving the product of the chemical reaction, i.e., the mechanism is of the type E.C.E. (64,65).

On the basis of these results and the overall reaction reported for massive electrolysis of water by Zambonin and the absence of H or N in the mass spectra of the supernatant gases during electrolysis (37), the following mechanism is proposed to explain the results at 300°C:

$$H_2O + e \rightleftarrows H + OH^- \qquad E_1^\circ \qquad (45)$$

$$H + NO_3^- \xrightarrow{k_f} OH\cdot + NO_2^- \qquad C_1 \qquad (46)$$

$$OH\cdot + e \rightleftarrows OH^- \qquad E_2^\circ \qquad (47)$$

where $E_2^\circ > E_1^\circ$.

It is known that a reaction similar to C_1 proceeds in nitrate melts at such a temperature (17) and the free energy of this reaction

$$H_2 + NO_3^- \rightleftarrows NO_2^- + H_2O \qquad (48)$$

is negative, lending support to this mechanism. It is not clear from these results whether or not the electrode surface (through surface

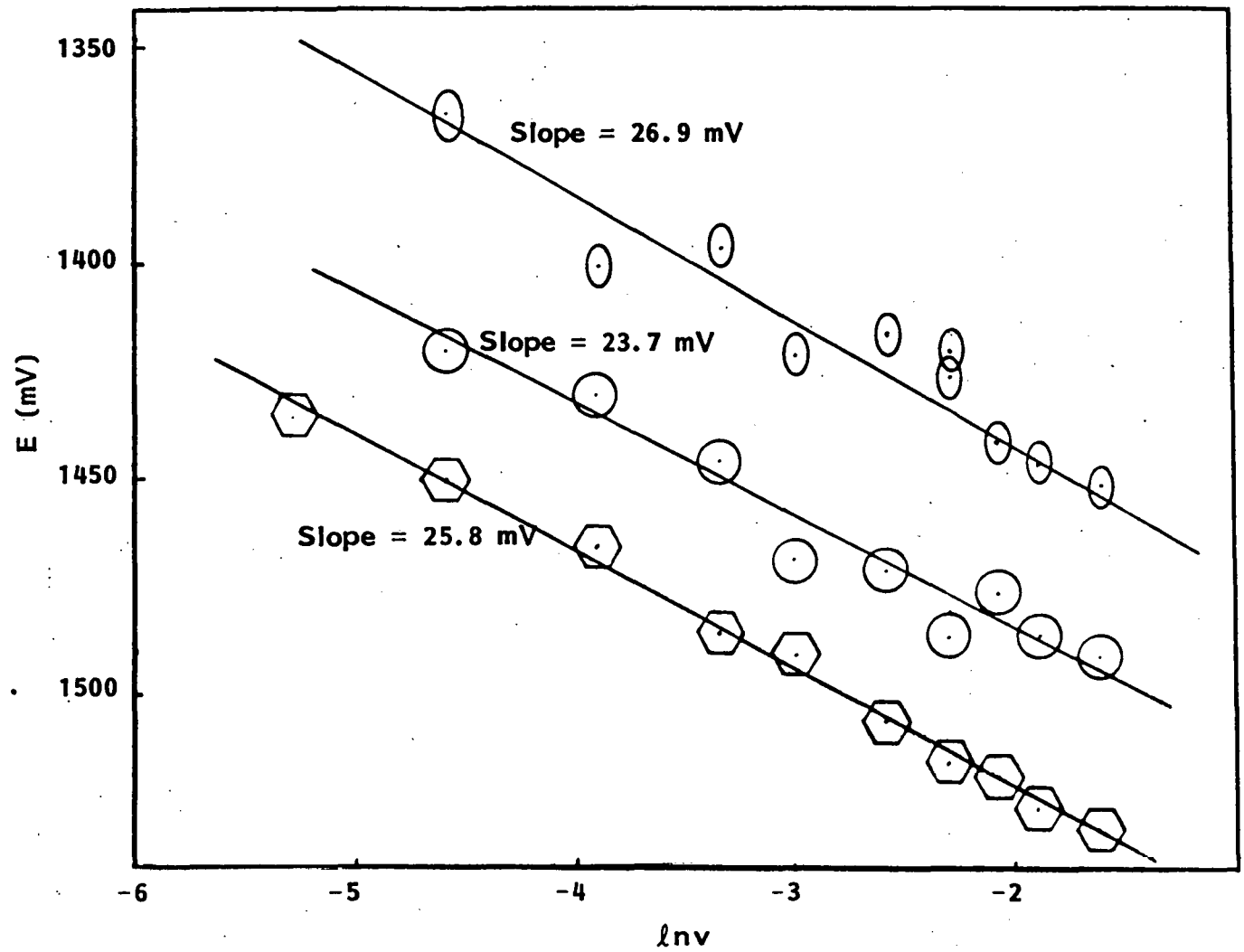

Fig. 28. Plot of peak potential as function of ℓn scan rate for three different water partial pressures and constant temperature (300°C). θ 9.21 mm; ⊙ 19.35 mm; ⊙ 31.81 mm. Lines are least squares fit.

TABLE 14

HALF PEAK WIDTH DATA (E_p-$E_{p/2}$) FOR WATER REDUCTION PEAK COMPARED WITH THAT EXPECTED FOR REVERSIBLE-IRREVERSIBLE/CHEMICAL COMPLICATION AT SEVERAL TEMPERATURES

T, (°C)	$1.857 \frac{RT}{F}$[1] (mV)	$2.2 \frac{RT}{F}$[2] (mV)	E_p-$E_{p/2}$ (mV)
346	-99	-117	-147 ± 12
325	-95	-113	- 94 ± 4
300	-91.6	-108	- 82 ± 7
295	-90.8	-107.6	- 94 ± 16
250	-86.3	-99	- 80 ± 6

[1]Irreversible/chemical complication
[2]Reversible

coverage by H) plays a part, but hydrogen atom adsorption does not occur readily on gold in aqueous solutions.

Hydrodynamic Voltammetric Results. Further support for this mechanism at 300°C comes from the hydrodynamic voltammetric results (rotating disc electrode). Typical voltammograms are shown in Figure 25. From such results, the plots of i_L versus $\omega^{\frac{1}{2}}$ shown in Figure 29 were constructed. At lower rotation rates, the limiting currents are greater than expected on the basis of the Levich equation (42), at all observed partial pressures. The potential at $i_L/2$ is also a function of rotation rate, Figure 30. These results are consistent with an E.C. mechanism. For an E.C. mechanism (66)

$$E(i_{L/2}) = E'_{\frac{1}{2}} - \frac{RT}{2nF} \ln\omega \qquad (49)$$

when the rate constant for the chemical reaction is high. Observed slopes are close to those predicted by equation (49).

Filinovskii (67) showed that for an E.C.E. mechanism in which k_f is large, the limiting current observed, $i_L(k_f)$, is given by

$$\frac{i_L(k_f)}{i_L(k_f=0)} = 0.94\left[\left(1 + \frac{n_2}{n_1}\right) - \frac{n_2}{n_1}\left(\frac{D}{1.9\gamma^2 k_f}\right)^{\frac{1}{2}} \omega^{\frac{1}{2}} + \cdots\right] \qquad (50)$$

where

$$\gamma = 1.61 D^{1/3} \nu^{1/6} \qquad (51)$$

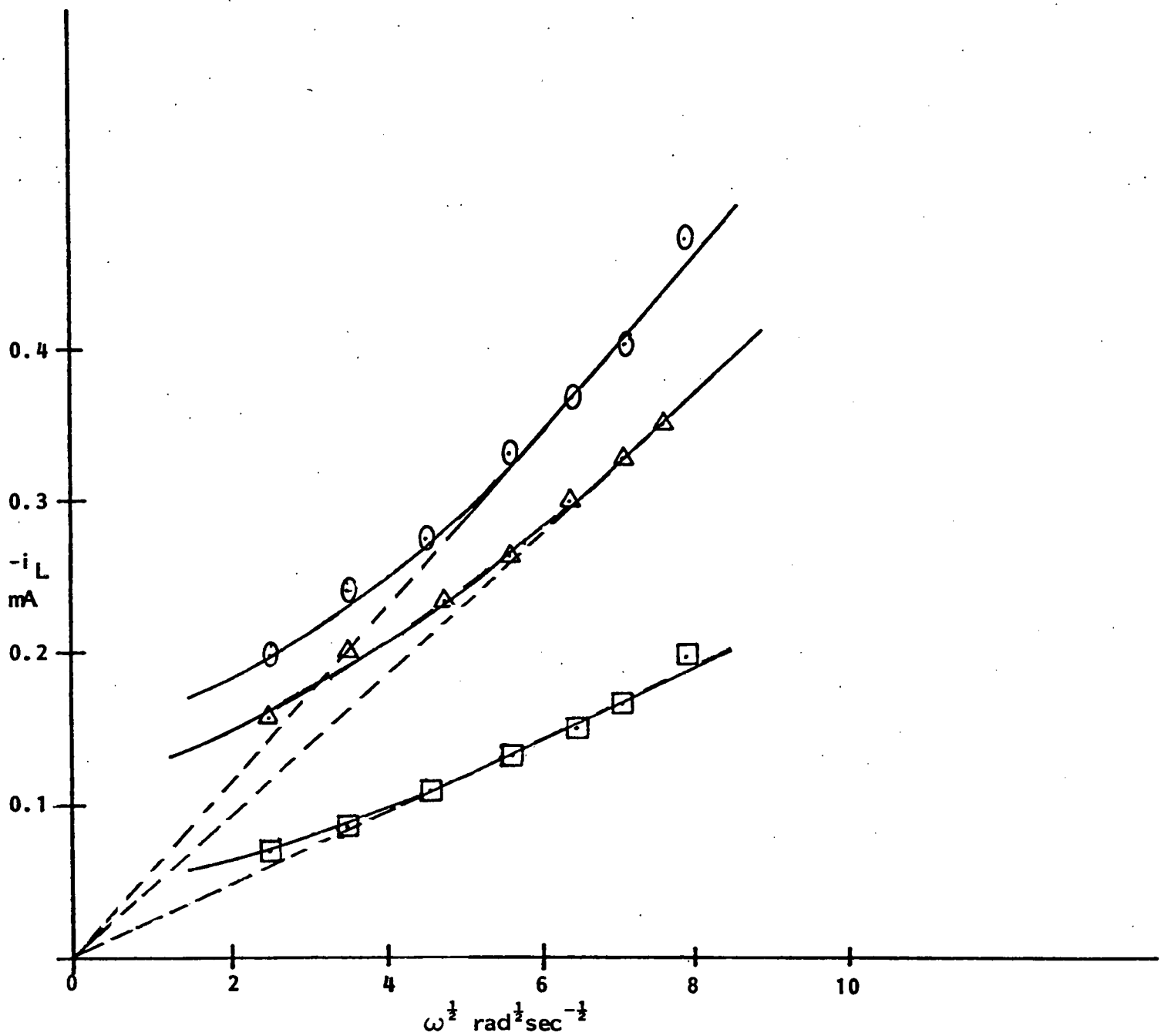

Fig. 29. Plot of $-i_L/mA$ versus the square root of the rotation rate at 295°C and three water partial pressures: θ, 18.20 mm; Δ, 12.38 mm; and ⊡, 7.51 mm. Au disc = 0.021 cm^2.

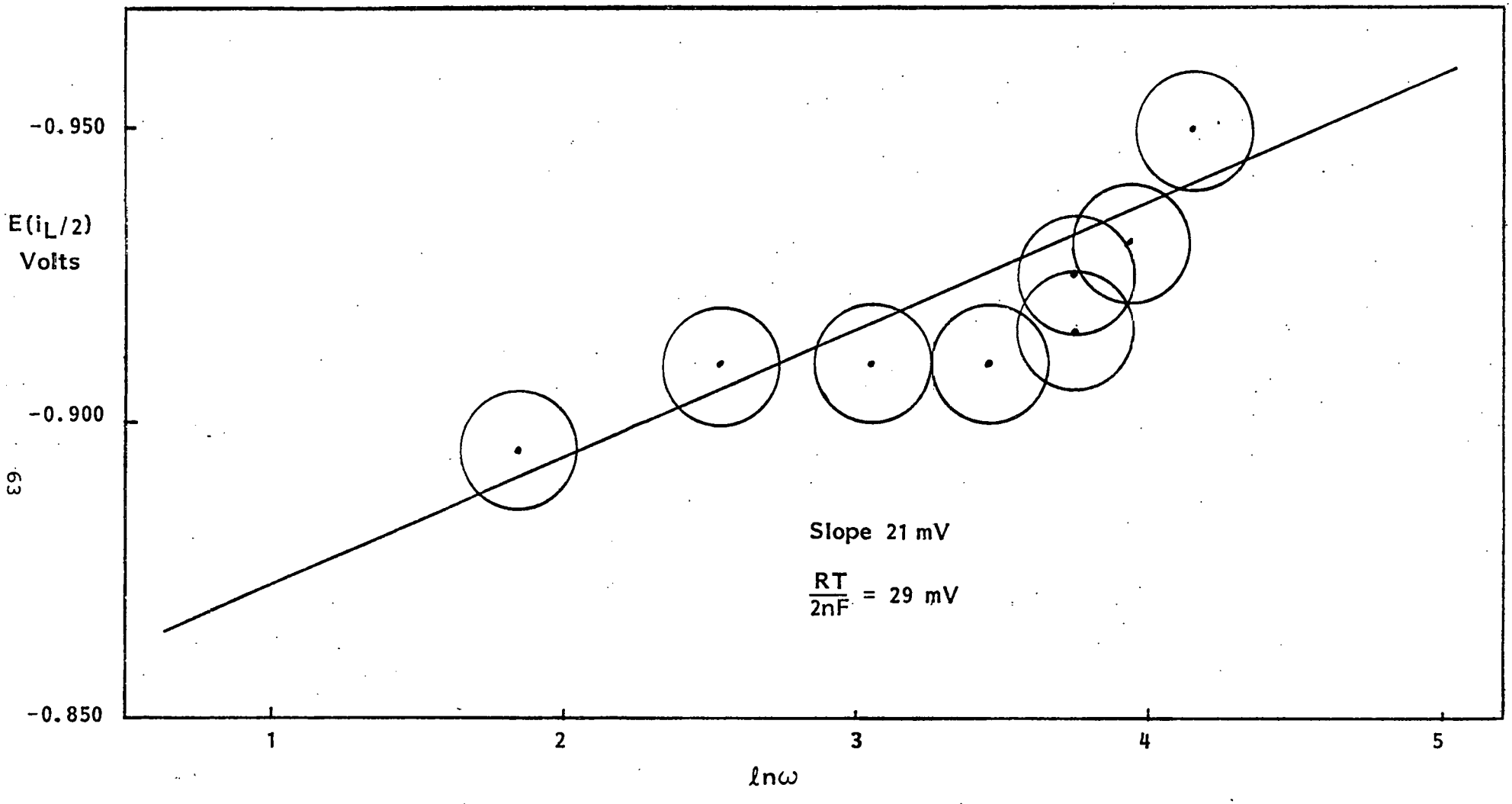

Fig. 30. Plot of $E(i_{L/2})$ versus $\ell n\omega$ at 405°C and a partial pressure of 16.48 mm. Theoretical slope for EC mechanism.

Substituting the Levich equation (42) for $i_L(k_f = 0)$, equation (50) becomes

$$\frac{i_L(k_f)}{\omega^{\frac{1}{2}}} = 0.573\ AFCD^{2/3}\nu^{-1/6}(n_1 + n_2) - \left[\frac{0.2586\ n_2\ AFCD^{5/6}}{k_f^{\frac{1}{2}}\ \nu^{1/3}}\right]\omega^{\frac{1}{2}} \qquad (52)$$

Plots of $i_L/\omega^{\frac{1}{2}}$ versus $\omega^{\frac{1}{2}}$ are shown in Figure 31. For the cyclic voltammetric peak currents at a stationary electrode, Nicholson and Shain showed that for similar E.C.E. conditions (64)

$$i_p = 0.4958\ (n_1 + n_2)F(n_1F)^{\frac{1}{2}}ACD^{\frac{1}{2}}(RT)^{-\frac{1}{2}}v^{\frac{1}{2}} \qquad (53)$$

Combination of the hydrodynamic data with those presented earlier for cyclic voltammetry (Figure 26) (only the results at high scan rate were used) enables the water concentration in the nitrate melt to be evaluated. At the same time, the diffusion coefficient for water and the rate constant for reaction C_1 are also obtained. Finally, since the partial pressure of water is known, the Henry's Law constant K_H is obtained. These results are summarized in Table 15 and compared through the Henrian constant with

TABLE 15

RESULTS OF THE COMBINED ANALYSIS OF HYDRODYNAMIC AND VOLTAMMETRIC DATA FOR WATER AT 295°C

P_{H_2O} (mm)	C x 10^{+3} (mol-kg^{-1})	D x 10^{+5} (cm^2-sec^{-1})	k_f (sec^{-1})	$K_H \cdot 10^{+4}$ (mol-kg^{-1}mm^{-1})	$K_H \cdot 10^4$ * (mol-kg^{-1}mm^{-1})
7.51	3.39	2.58	21.4	4.52	3.41
12.38	4.09	5.23	49.0	3.31	3.41
18.20	8.19	2.86	12.67	4.50	3.41

*Literature data.

those of Zambonin (30). The good agreement between K_H values supports the electrochemical mechanism through which these results were obtained. The chemical rate constant for reaction C_1 is of a reasonable magnitude consistent with the limiting conditions of the theory for the E.C.E. mechanism. The diffusion coefficient obtained is also of a magnitude expeced at this temperature. The calculation of diffusion coefficients based upon Zambonin's solubility data and the appropriate cyclic voltammetric function enabled the activation energy for diffusion of water to be calculated. The Arrhenius plot is shown in Figure 32 and the data used in Table 16. The diffusion coefficient expressed as a function of temperature is given by the least squares equation

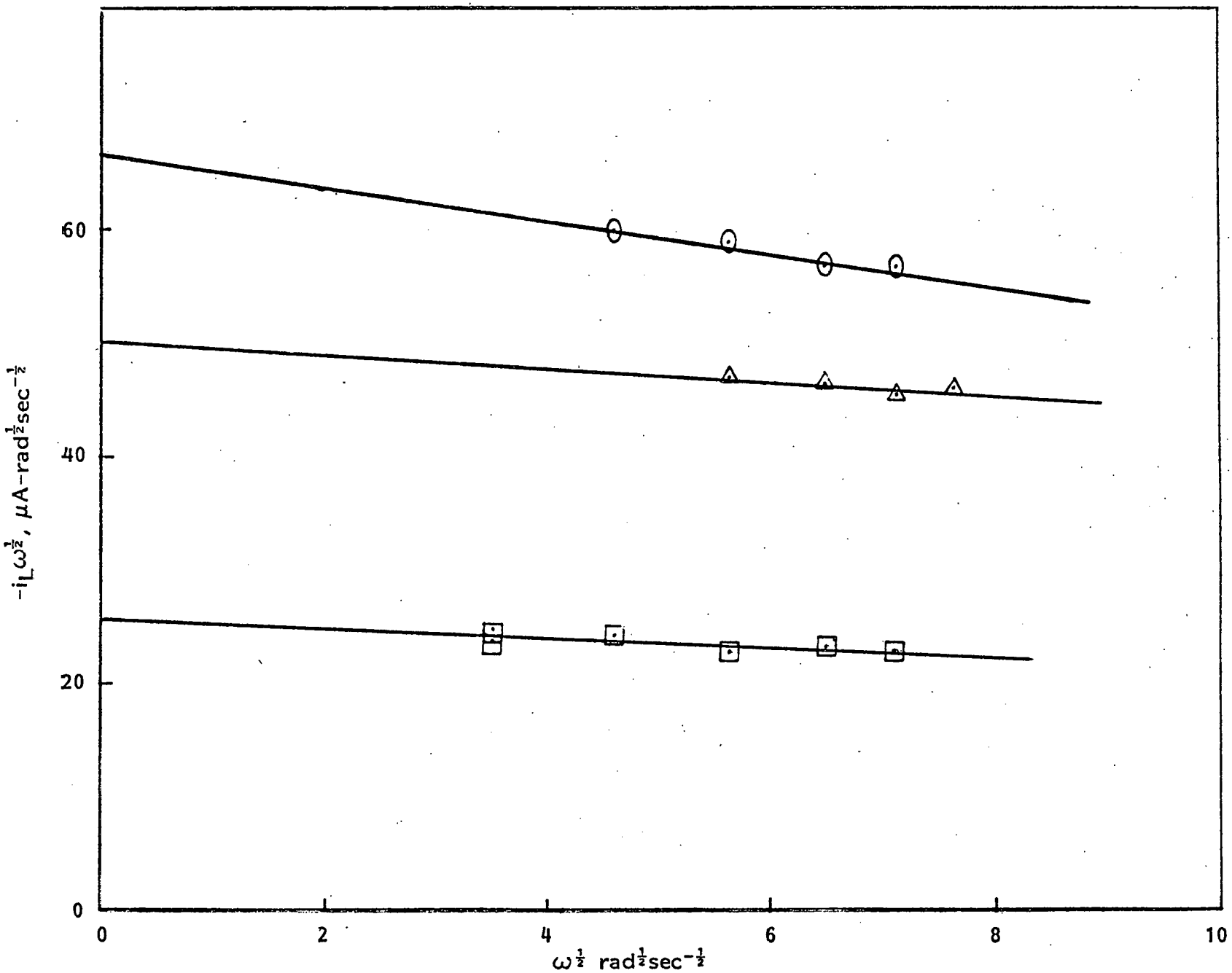

Fig. 31. Limiting current data analysis for E.C.E. mechanism. Three different partial pressures: θ 18.20 mm; Δ12.38 mm; ⊡ 7.51 mm, t = 295°C.

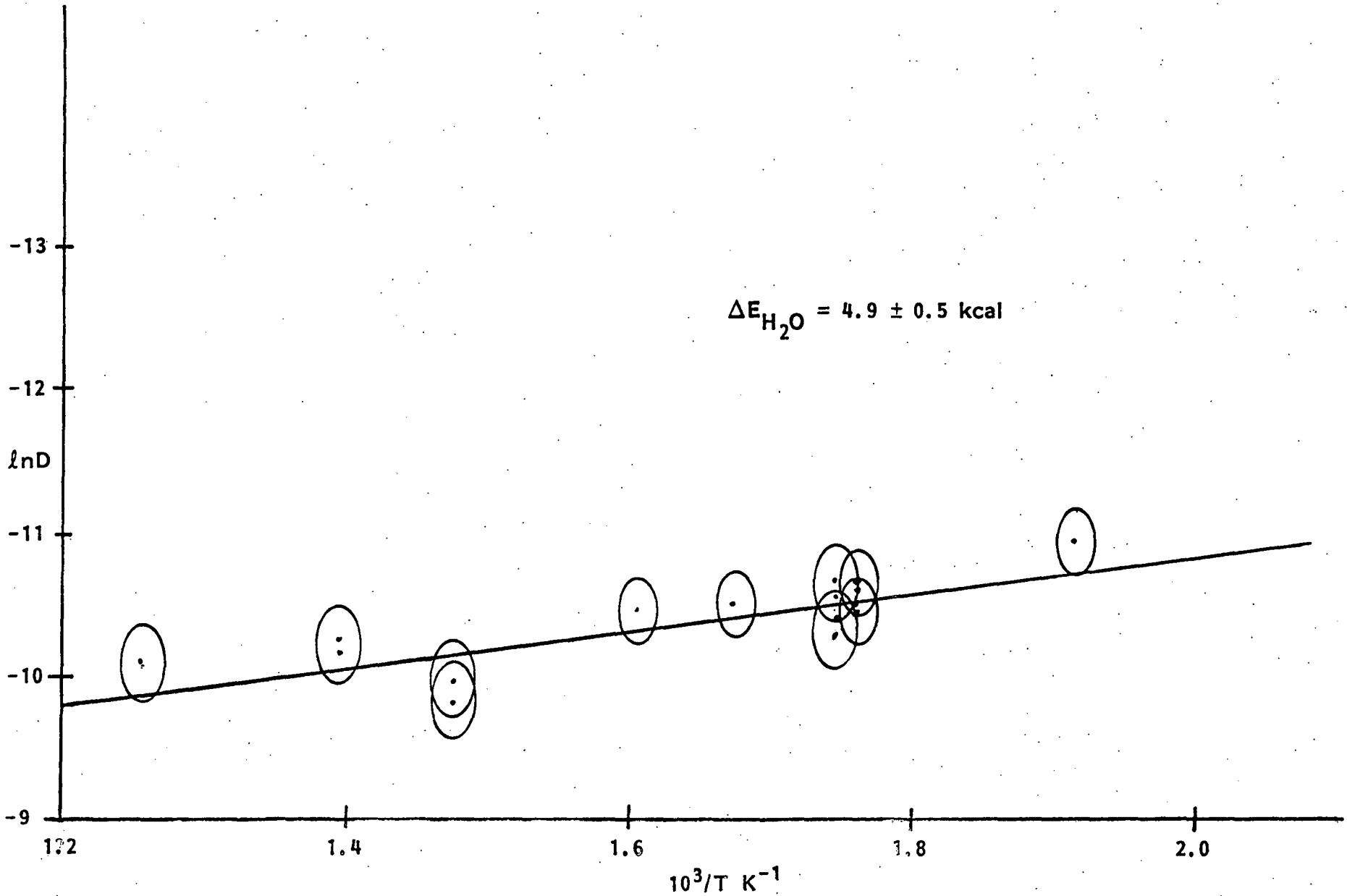

Fig. 32. Temperature dependence of the diffusion coefficient of water.

TABLE 16

DIFFUSION COEFFICIENT OF WATER RELEVANT DATA

Method Used	T (°C)	P_{H_2O} (mm)	D x 10^5 (cm^2-sec^{-1})	lnD	$10^3/T$ ($°K^{-1}$)
1	250	20.94	1.92	-10.861	1.912
	300	20.84	4.14	-10.092	1.745
	325	20.94	4.50	-10.009	1.672
	350	20.94	4.92	- 9.920	1.605
	300	9.21	6.64	- 9.620	1.745
	300	19.35	5.49	- 9.810	1.745
	300	31.81	3.19	-10.353	1.745
	295	7.51	4.54	-10.00	1.760
	295	12.38	3.55	-10.246	1.760
	295	18.20	5.00	- 9.903	1.760
2	295	7.51	4.52	-10.004	1.760
	295	12.38	3.31	-10.315	1.760
	295	18.20	4.50	-10.008	1.760
3	405	7.51	18.10	- 8.614	1.475
	405	16.48	13.01	- 8.946	1.475
4	445	16.45	7.4	- 9.51	1.392
	445	27.50	8.9	- 9.32	1.392
5	525	19.3	9.8	- 9.230	1.253

$$i_p/v^{\frac{1}{2}} = 0.4958(n_1)^{\frac{1}{2}}\ (n_2+n_1)\ F^{3/2}\ A\ D^{\frac{1}{2}}C\ (RT)^{-\frac{1}{2}} \qquad (1)$$

$$i_p/v^{\frac{1}{2}} = 0.446(n)^{3/2}\ F^{3/2}\ A\ D^{\frac{1}{2}}C\ (RT)^{-\frac{1}{2}}(n = 2) \qquad (2)$$

Methods of calculating D_{H_2O}:

1 Concentration H_2O calculated on the basis of Zambonin's K_H and ΔH for water and the CV data obtained using equation (1)

2 From the combination of CV and HDV data (see text).

3,4 Concentration of water calculated from Zambonin's K_H and ΔH data and then using CV data and equation (2).

5 Concentration of water calculated from Zambonin's K_H and ΔH data and this combined with chronopotentiometric data.

$$\ell nD = -5.762 - 2.458 \times 10^3 T^{-1} \quad (54)$$

and the activation energy $\Delta E = 4.9 \pm 0.5$ kcal-mol^{-1}.

At temperatures above 300°C, the rate constant k_c will increase rapidly (2-3 times k_c for each 10° rise in temperature). Thus, it is expected that the predominating mechanism will be one in which the cathodic current of the voltammogram results from a fast two-electron process (reversible). Nevertheless, it should be recognized that the oxidizable component of E_1° is consumed chemically and thus the anodic cycle only shows the oxidation of hydroxyl ion (the product of E_2°) at much more anodic potentials. Under these circumstances, the peak current is given by equation (43) where n = 2, and this was used appropriately to obtain D_{H_2O} at temperatures above 350°C.

At temperatures in excess of 450°C, the background currents for the voltammograms increase significantly, whereas the water reduction currents decrease because of the decreasing solubility with increasing temperature. The net result is that the water reduction current must be obtained by taking the difference between two large numbers, i.e., i_p = (background current + i_p water current) - (background current) with all the well-known problems associated with such a procedure. Attempts to obtain i_p graphically confirmed the continued presence of water but allowed no quantitative results to be obtained. The application of microprocessor techniques inherent in the Bascom-Turner 8000 recorder would aid these measurements.

Additionally, at high water vapor pressures and in the presence of oxygen, a more anodic peak was detected probably arising from the process

$$O_2 + 2H_2O + 4e \rightleftarrows 4OH^- \quad (55)$$

thus leading to further complications in the "main" water reduction process at these high temperatures.

At temperatures around 250°C, the cyclic voltammograms show that the redox couple C/D no longer appears and a new reverse peak is visible, perhaps involving oxide ions (Figure 33). Consequently, this implies a modification of the reduction pathway for the water. That this is possible can be deduced from the fact that the peak potential is much more cathodic especially at high water partial pressures and may now be in a region where the hydroxyl ions are reduced. At the same time, the chemical rate constant k_c will have decreased by about two orders of magnitude. Thus, it might be expected that the E.C.E. mechanisms may undergo modification. The limited data at this temperature do not enable a more detailed interpretation to be given.

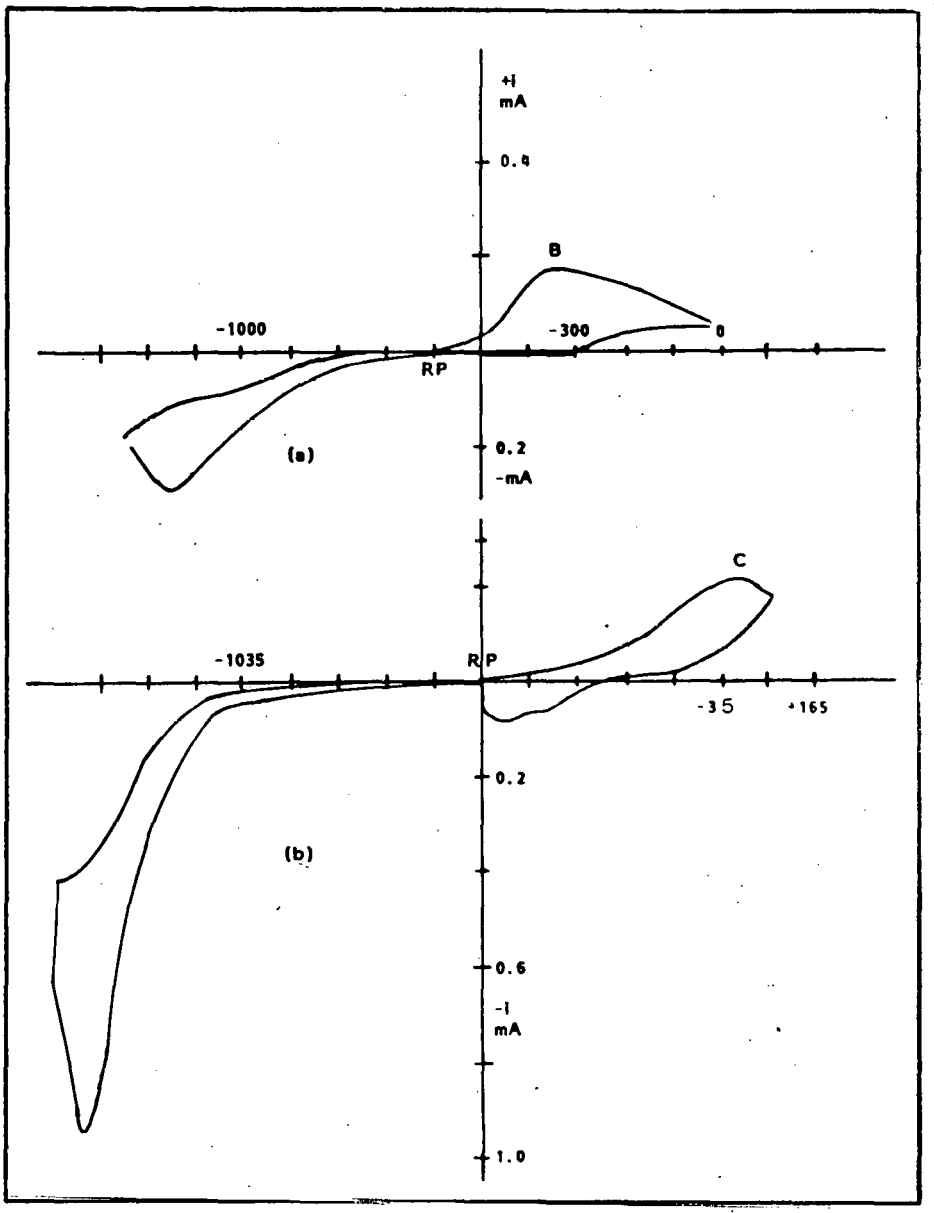

Fig. 33. Cyclic voltammograms on gold electrodes for water. Area of electrode = 0.06 cm^2, scan rate = 0.1 $V\text{-}sec^{-1}$, water partial pressure 20.8 mm. (a) Temperature 350°C, RP -0.600V vs. Ag/Ag(1) 0.07m reference electrode. (b) Temperature 250°C, RP -0.535 vs. Ag/Ag(1) 0.07m reference electrode.

4.3.2 The Physical and Chemical Properties of Water in Contact with the Nitrate Mixture

Peleg reported that water could be removed from pure sodium nitrate and potassium nitrate melts by displacement with dry inert gas. On the other hand, water was not completely removed from molten lithium nitrate (40). Swofford and Laitinen (41) suggested that residual water in sodium nitrate-potassium nitrate mixture could be removed similarly and showed polarograms before and after inert gas bubbling. These observations, albeit at temperature below 350°C for single salts and around 250°C for the binary mixture, suggest that in the absence of lithium ions, water is dissolved in the nitrate melt without irreversible chemical changes occurring. The solubility increases as the alkali cation radius decreases. This suggests that ion-dipole interactions may be important in determining the properties of water in the nitrate melt. The large negative heats of solution reported by Peleg (40) and Zambonin (30) are consisten with this view. At the highest temperatures likely to be encountered in thermal storage application, the reduced solubility is consistent with only ion-dipole interactions. Thermodynamic data in Table 3 also confirm the likely absence of specific chemical interaction leading to chemical decomposition of water. However, the additional presence of carbon dioxide may require reconsideration of this situation (Section 4.4).

Experiments were carried out during the course of this work to observe not only the removal of water but also its uptake under different conditions. The changes of water content were monitored *in situ* by measuring the water peak current at a constant scan rate (Section 4.3.1) in a voltammetric sweep. The gas flow was interrupted (10-30 sec) during the actual running of the voltammogram.

Water Uptake by the Nitrate Melt. In these experiments, saturation of the melt was achieved by passing argon with a known water vapor pressure at flow rates between 100-300 cm^3-min^{-1} either over the melt surface or through the molten mixture. The volume of the gas space above the melt was 1400 cm^3. The time to establish equilibrium conditions in the gas phase (e.g., from dry argon to wet argon) was flow rate dependent and in the conditions used in this study was between 5 and 15 min.

Figures 34 and 35 illustrates the typical time dependence of the water buildup in the melt under quiescent conditions. These results are for a particular depth into the melt represented by the position of the monitor electrode. Typically the melt had a surface area of 24 cm^3 and a depth of 2-3 cm. Under stirred conditions, water equilibrated in 5-10 min and water uptake profiles were not obtained.

The shape of the buildup curves is similar to that expected from a diffusion layer model but displaced on the time axis to shorter times. This may be due to the effect of thermal convective stirring aiding the dispersal of water through the melt.

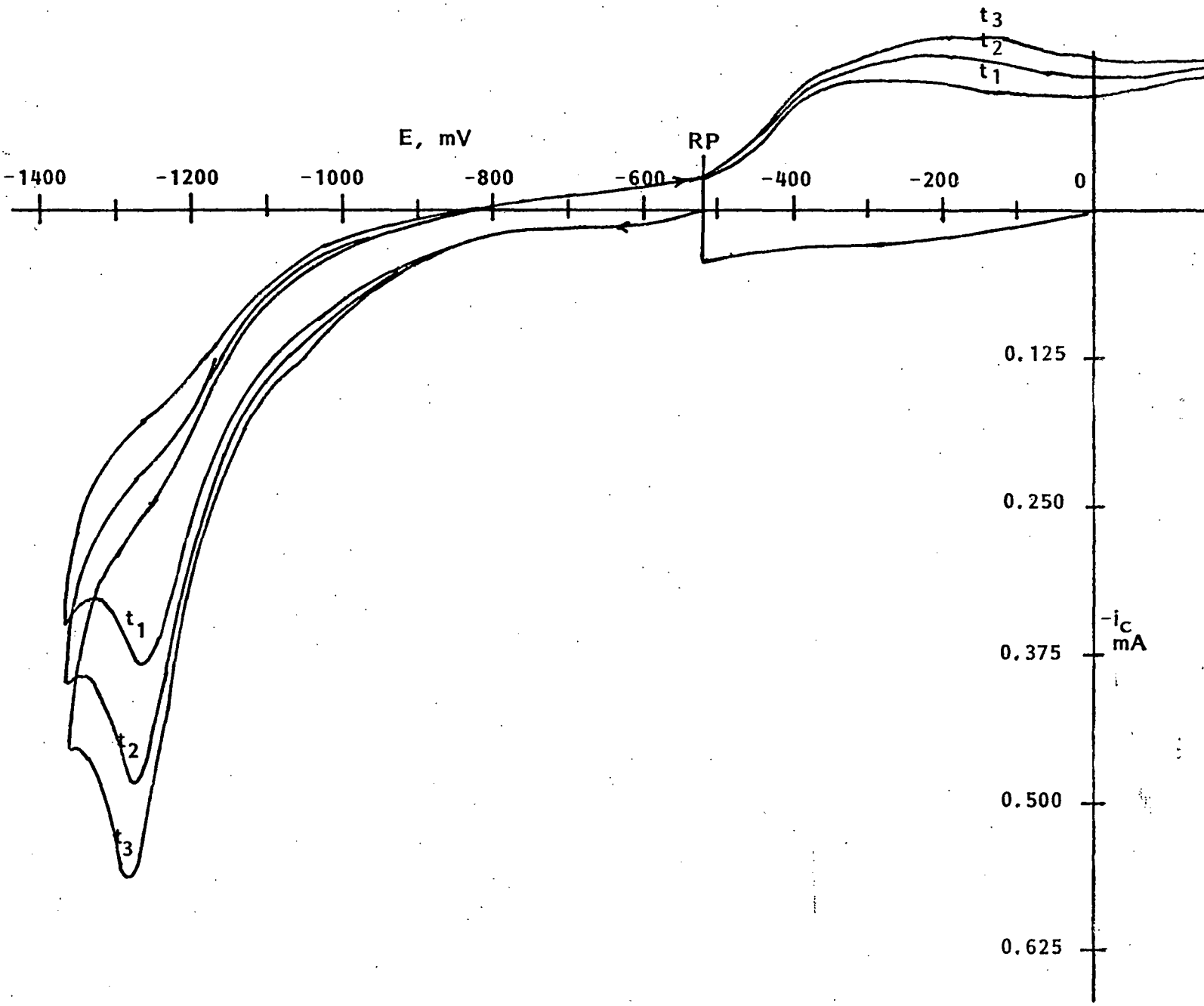

Fig. 34. Development of water peak, 300°C p_{H_2O} = 19.35 mm. Au electrode 0.06 cm^2, scan rate = 100 $mV\text{-}sec^{-1}$, E scale versus 0.07m $AgNO_3$ 50 mol% $NaNO_3$-KNO_3. Time after starting flow of wet argon over melt t_1 = 37 min, t_2 = 56 min, t_3 = 69 min.

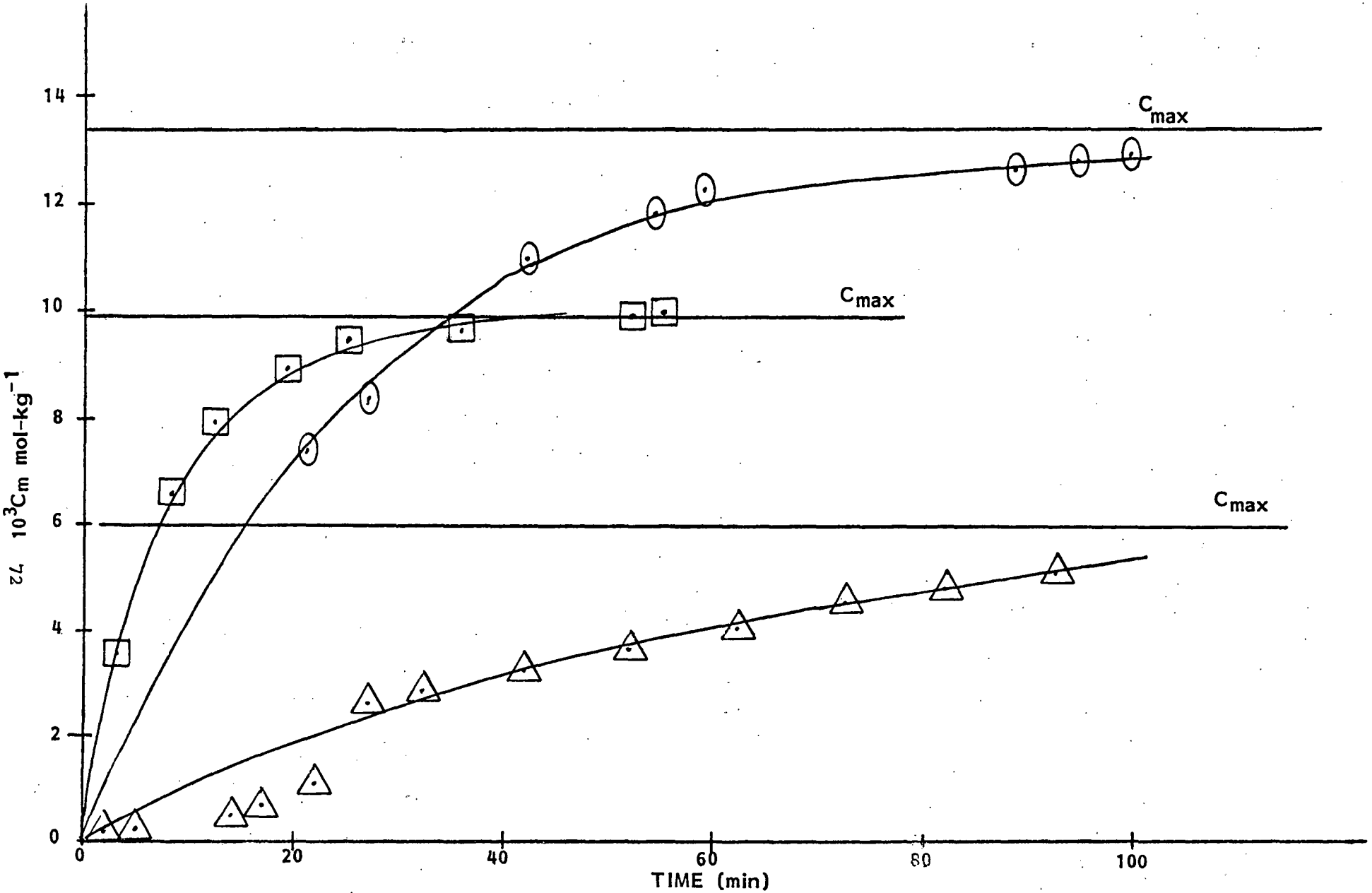

Fig. 35. Increase of water content during equilibration process under different conditions.

θ p_{H_2O} = 20.91 mm, t = 250°C
⊡ p_{H_2O} = 31.81 mm, t = 300°C
△ p_{H_2O} = 19.35 mm, t = 300°C

Water Removal from the Melt. After equilibrating the nitrate melt with an argon stream containing a known partial pressure of water and establishing the voltammetric response at the monitoring electrode, the wet argon was replaced by dry argon flowing either over the melt or with the gas bubbling through the melt. Figure 36, curve A, shows water removal without bubbling to point X after which gas was bubbled through the melt and stopped only for the 30 sec or so required to obtain the voltammetric measurement. Curve C shows water removal by gas bubbling from time zero. The removal of water when gas is passed above the melt surface is analogous to an electrochemical total electrolysis. Thus, the time dependence of the water concentration is given by

$$C(t) = C_{max} \exp -Bt \tag{56}$$

where

$$B = \frac{A}{V} m_o = \frac{A}{V} \frac{D_{H_2O}}{\delta} \tag{57}$$

Using the experimental values of A, V, the value of D_{H_2O} obtained in this work and the experimental slope, the diffusion layer thickness δ is 0.14 cm. This value is totally consistent with that expected for a quiescent liquid. Stirring increases the slope and consequently decreases the diffusion layer thickness as would be predicted for a diffusion controlled reaction.

These results then confirm the ease by which water is taken up by the binary molten nitrate system. Conversely, water is rapidly removed by inert gas bubbling, even at the higher temperatures. No evidence of chemical reaction products were detected to 500°C.

It may be concluded that water, in the absence of carbon dioxide, has little or no short time deleterious effects on molten nitrates held in ceramic (Al_2O_3) containers.

Analytically, water is readily detected by hydrodynamic voltammetry or cyclic voltammetry either through the limiting current or peak current dependence.

The present work has established the following relationship between peak potential E_p, temperature T°K, v sweep rate, and p (mm) partial pressure of water, viz,

$$E_p = -2.419 + 2.2745 \times 10^{-3}T - 4.485 \times 10^{-5}T \ln v - 1.1698 \times 10^{-4}T \ln p \tag{58}$$

The peak potential can be used to obtain analytically the water content of the melt. E_p for the data presented here is referred to the Ag/Ag(1) 0.07 molal $NaNO_3KNO_3$/reference electrode. The use of the peak potential avoids the difficulties associated with measurements of peak currents and could provide a simple automated method for water detection. Table 17 shows a number of peak potentials calculated from this equation at different temperatures and partial pressures relevant to the present studies.

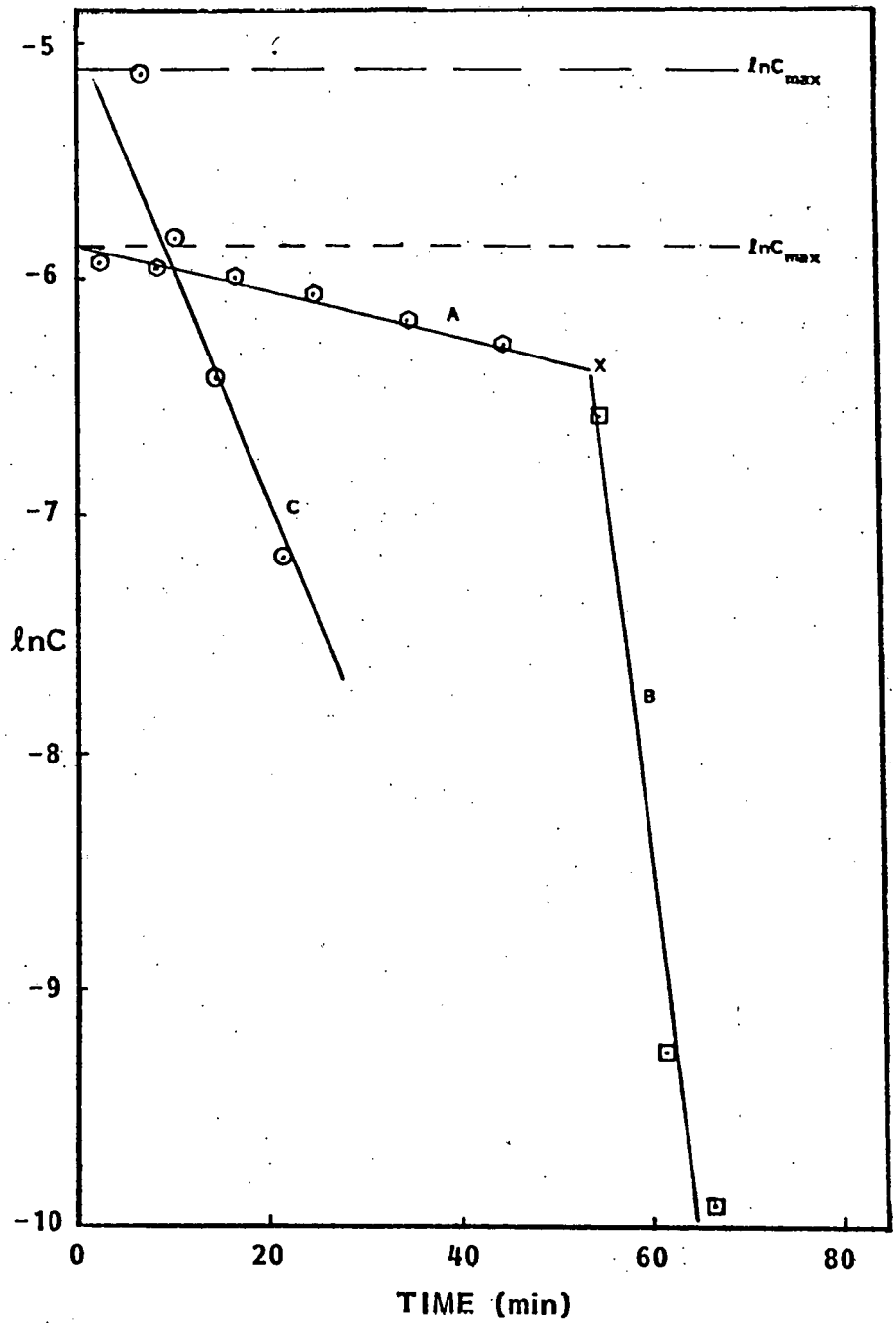

Fig. 36. Plot of log water concentration (mol-kg^{-1}) versus time in min.

Curves A & B, C_{max} = 2.88 x 10^{-3} mol-kg^{-1} water removal dry argon gas above melt; slope A = 1.46 x 10^{-4} sec^{-1} at X argon gas bubbling into melt, slope B = 4.74 x 10^{-3} sec^{-1}.

Curve C, C_{max} = 6.06 x 10^{-3} mol-kg^{-1}. Dry argon bubbling through melt from time t = 0.

From slope A, diffusion layer thickness calculated

$$\text{Slope} = \frac{D_{H_2O}\, A_{surface}}{\delta\, V_{melt}} = 1.46 \times 10^{-4}$$

V = 48 cm^3; A = 23.75 cm^2

D_{H_2O} = 4.2 x 10^{-5} cm^2-sec^{-1} at 300°C

$\therefore$ $\underline{\delta = 0.14 \text{ cm}}$

TABLE 17

EXAMPLES OF E_p VERSUS Ag/0.07m AgNO, $NaNO_3$-KNO_3 REFERENCE ELECTRODE CALCULATED FROM THE RELATIONSHIP

$$E_p = -2.419 + 2.2745 \cdot 10^{-3}T - 4.485 \cdot 10^{-5}T \ln v - 1.1698 \cdot 10^{-4}T \ln p$$

AT SCAN RATE 0.100 V-sec^{-1} OVER THE TEMPERATURE INTERVAL 250-600°C FOR RANGE OF TYPICAL WATER PARTIAL PRESSURE

P_{H_2O} T, °C	20 mm E_p, V	10 mm E_p, V	5 mm E_p, V
250	-1.358	-1.316	-1.274
300	-1.257	-1.210	-1.164
350	-1.156	-1.105	-1.055
400	-1.055	-1.000	-0.945
450	-0.953	-0.895	-0.836
500	-0.852	-0.789	-0.726
525	-0.801	-0.737	-0.672
550	-0.751	-0.684	-0.617
600	-0.649	-0.579	-0.508

4.4 Carbon Dioxide - The Interaction of Carbon Dioxide with the Equimolar Molten Sodium Nitrate-Potassium Nitrate Mixture

4.4.1 Introduction

The solubility of carbon dioxide in a number of nitrate melts has been reported at low temperatures (<400°C). These experimental measurements were generally carried out over a time period measured in hours and no chemical reactivity between gas and melt was observed. The measurements reported here were carried out over the temperature range 250-505°C and involved a much longer period (1-4 days) of contact between melt and either pure gas or CO_2 mixed with oxygen or water. Carbonate ions were detected electrochemically, and in order to use the electrochemical methodology to study these gas-melt interactions, a preliminary study of the oxidation of carbonate ions was carried out. Again, the electrochemical behavior was complicated by the aggressive nature of the nitrate/nitrite solvent signalling caution in the application of electrochemical methods of detecting carbonate ions in these solutions. Nevertheless, it turns out that chronopotentiometry is very effective for in-situ analysis of carbonate ions under carefully defined conditions.

4.4.2 Electrochemistry of Carbonate Ion Oxidation on Stationary Gold Electrodes

Figure 37 shows a typical chronopotentiogram obtained in a solution containing added potassium carbonate at 530°C. Figure 38 shows a corresponding voltammogram. Chronopotentiometric measurements were made for the oxidation of carbonate ions as a function of current density concentration and temperature. These results are presented in Figures 39 and 40. in the form of Sand plots ($\tau^{\frac{1}{2}}$ versus i^{-1}) and demonstrate that equation (29) is applicable, i.e., the oxidative process is diffusion controlled. The plot of $i\tau^{\frac{1}{2}}$ versus C supports this conclusion (Figure 41). Further support for a fast electrochemical step is obtained from Karaoglanoff plots made for potential-time data. The linearity of the function

$$E = E_{\tau/4} - \frac{RT}{nF} \ln \left(\frac{\tau^{\frac{1}{2}}}{t^{\frac{1}{2}}} - 1 \right) \qquad (59)$$

(Figure 42 and Table 18) support this simple interpretation. The obvious concentration and transition time dependence of $E_{\tau/4}$ suggest that there are complicating features in the reaction pathway. The slope of plots in Figure 42 suggest that n = 2.

Both current reversal chronopotentiometry and cyclic voltammetry confirm that the oxidation process is indeed rather complex, because of the absence of reverse transition times and peak currents as illustrated in Figure 38. At high concentrations (Figure 43), reverse chronopotentiograms indeed exhibit a rather cathodic transition time in the region where

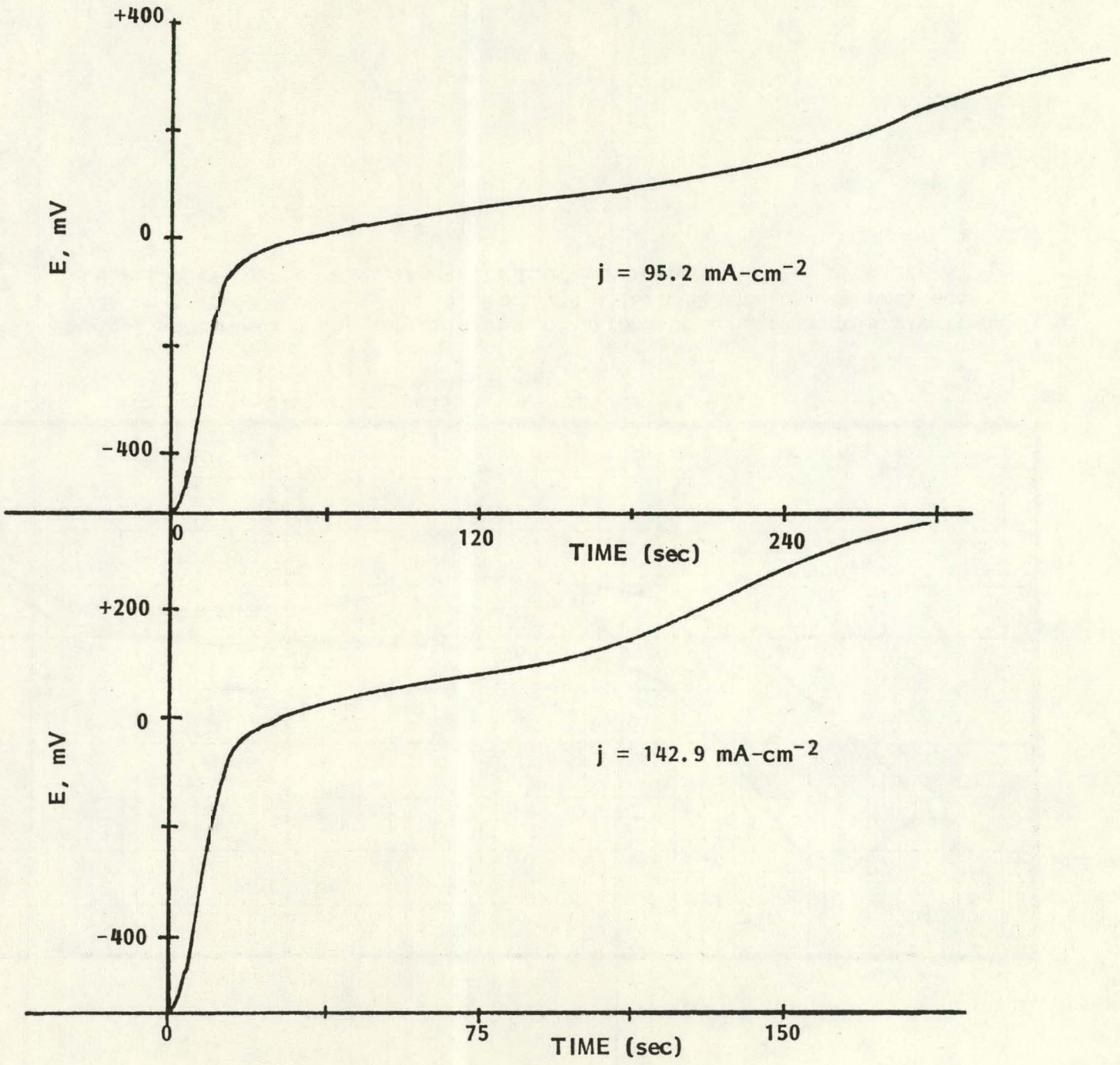

Fig. 37. Two chronopotentiograms at different current densities for the oxidation of carbonate ions at 530°C and 20.69 x 10^{-3} molal.

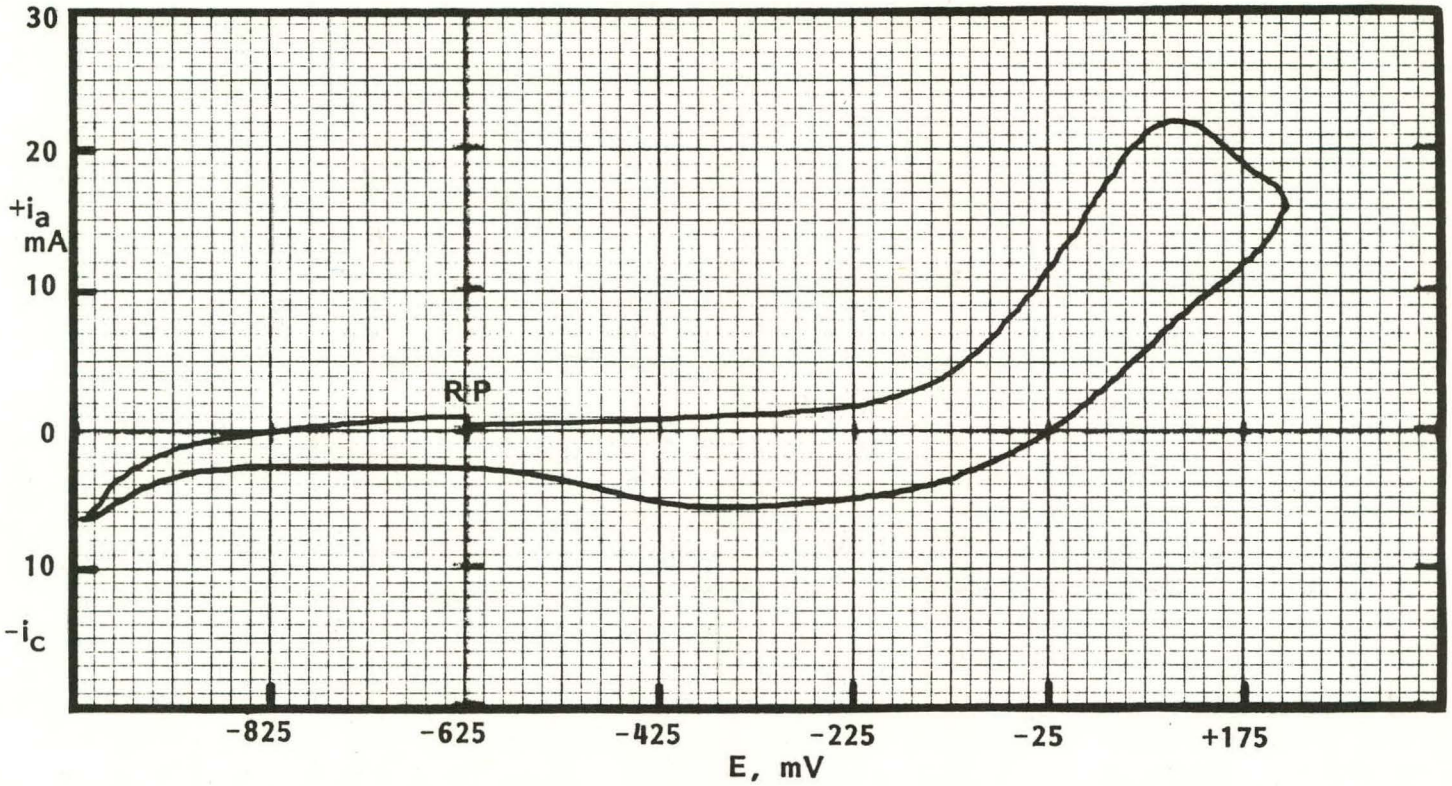

Fig. 38. Typical voltammogram for the oxidation of carbonate ions on a gold electrode (0.21 cm^2) at 530°C. $C_{CO_3^=}$ = 20.69 x 10^{-3} molal. Oxygen atmosphere, scan rate = 1.00 V-sec^{-1}. E vs. Ag/Ag(1) 0.07 m reference.

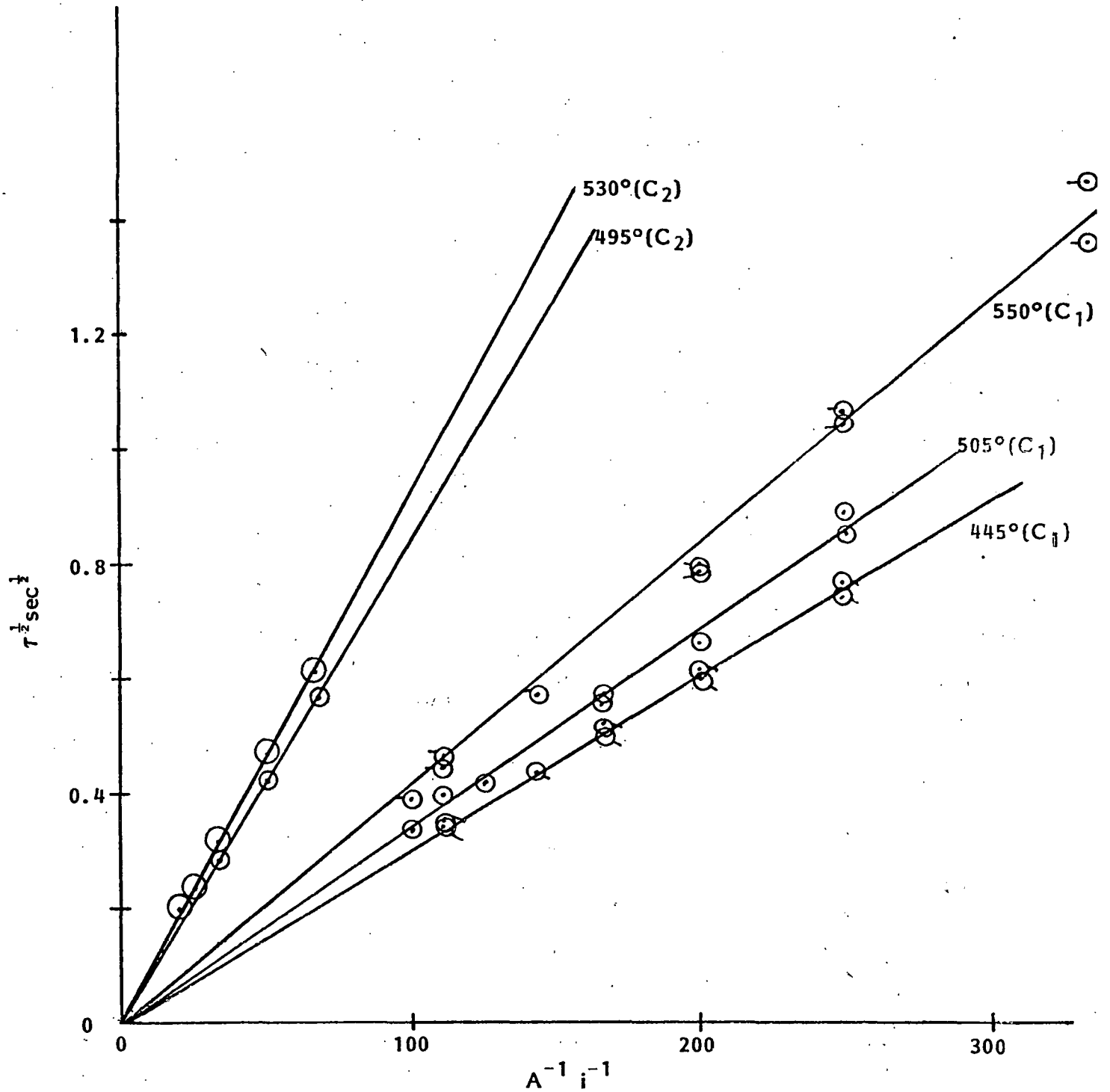

Fig. 39. Sand's plots for carbonate ion oxidation as a function of temperature and concentration. Gold electrode 0.21 cm^2.

C_1 = 8.295 x 10^{-3} molal
C_2 = 20.692 x 10^{-3} molal

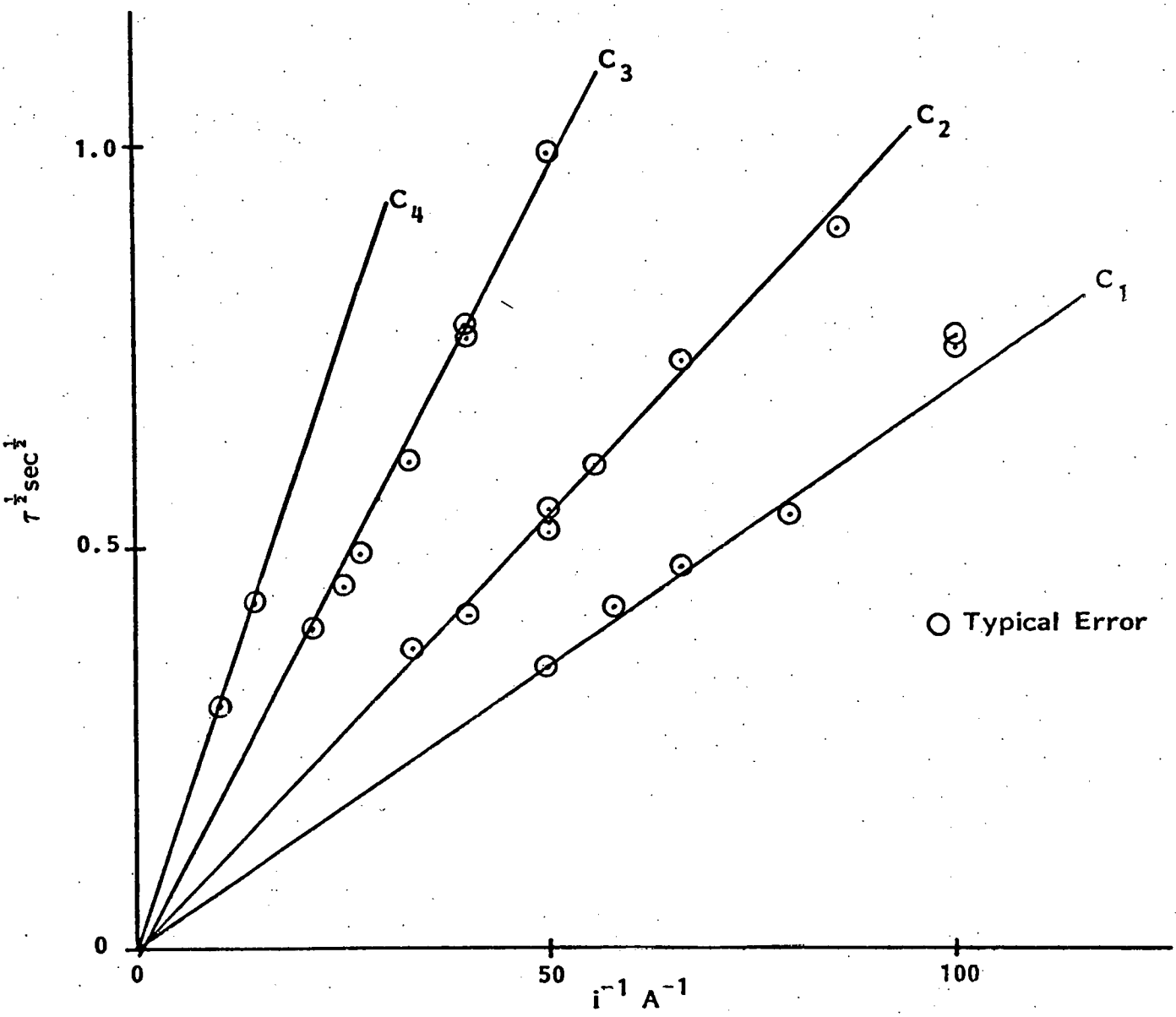

Fig. 40. Sand's plot for carbonate ion oxidation at 505°C. Gold electrode, 0.21 cm^2.

$C_1 = 15.42 \times 10^{-3}$ molal $C_3 = 44.42 \times 10^{-3}$ molal
$C_2 = 24.72 \times 10^{-3}$ molal $C_4 = 67.20 \times 10^{-3}$ molal

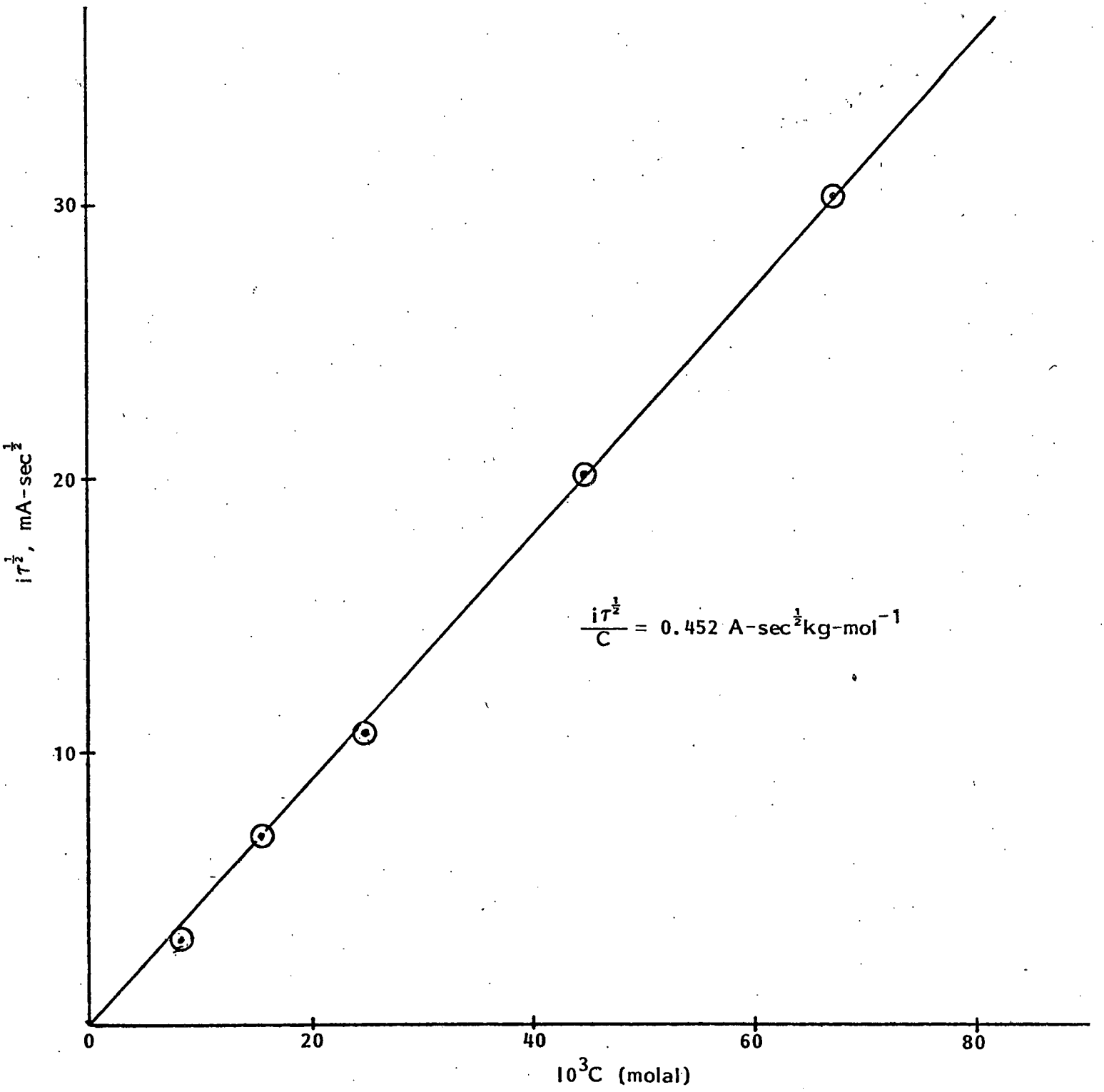

Fig. 41. Sand's constant as a function of carbonate ion concentration at 550°C. On a gold electrode, 0.21 cm^2.

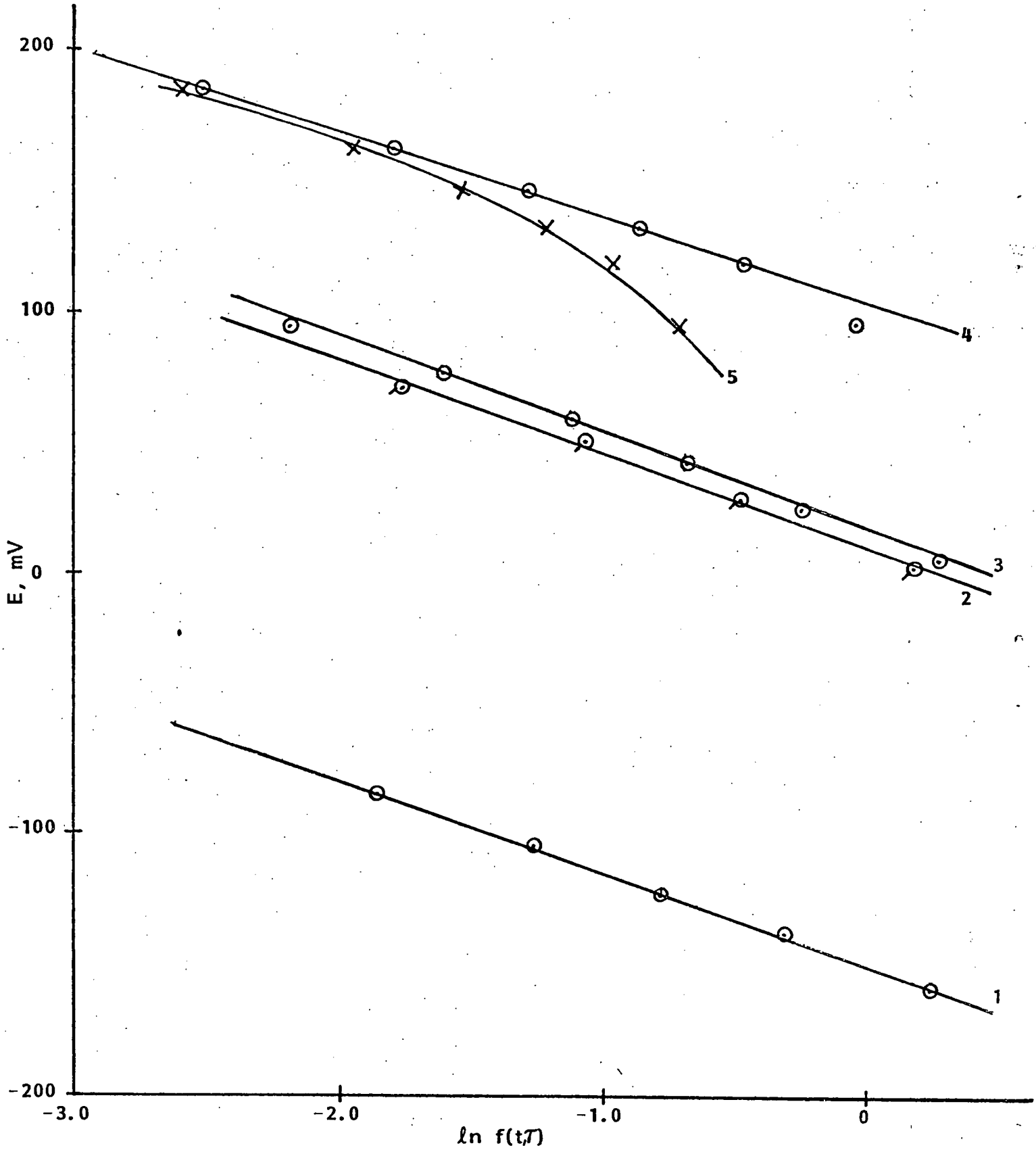

Fig. 42. Karaoglanoff plots for the oxidation of carbonate ions. Effect of concentration and transition time.

$$1 \text{ to } 4 = E \text{ v } \ln \frac{\tau^{\frac{1}{2}} - t^{\frac{1}{2}}}{t^{\frac{1}{2}}}$$

$$5 = E \text{ v } \ln \tau^{\frac{1}{2}} - t^{\frac{1}{2}}$$

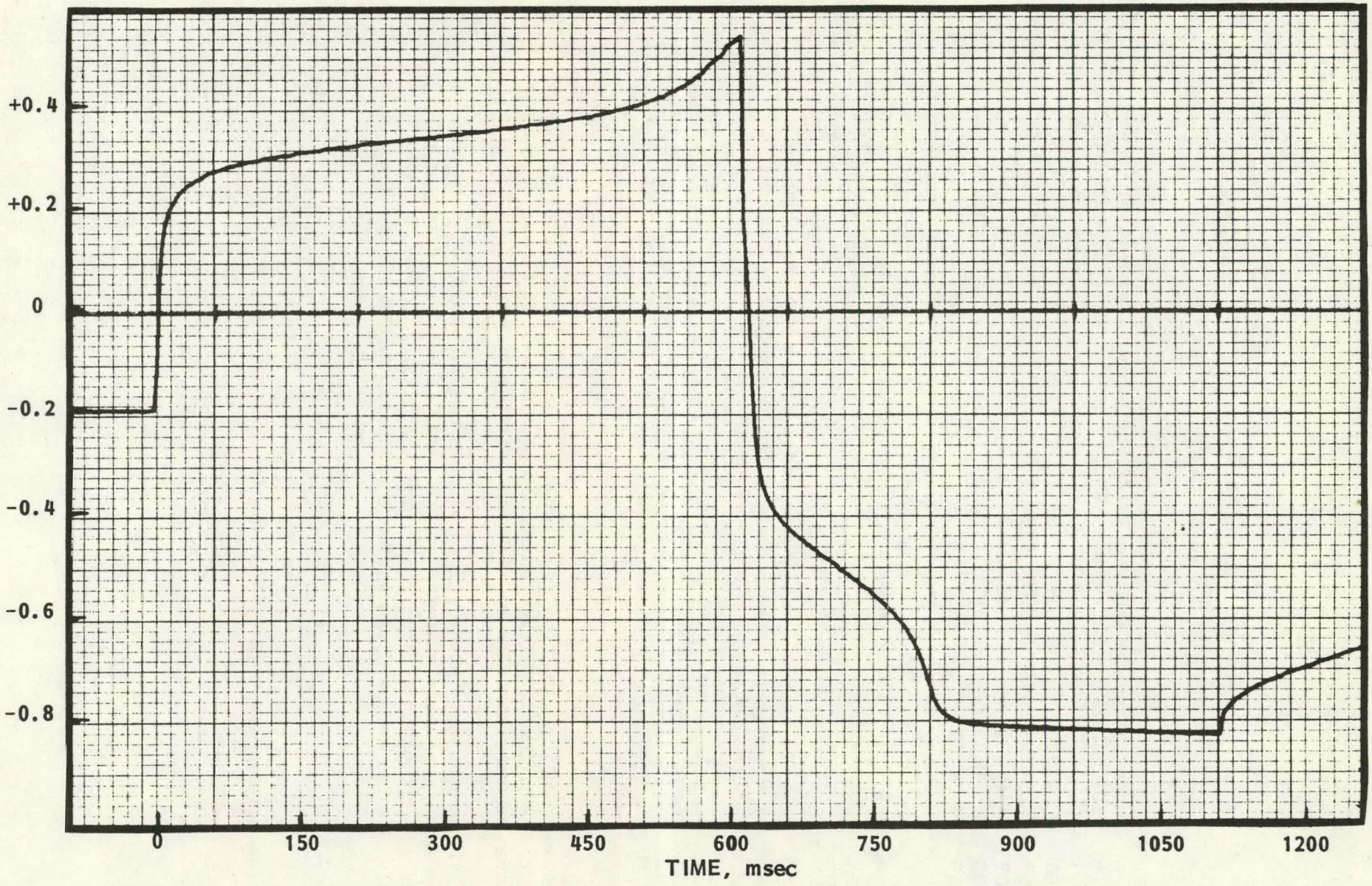

Fig. 43. Current reversal chronopotentiogram at gold electrode 0.21 cm^2 and 505°C. C = 24.72 x 10^{-3} molal carbonate, $i_a = i_c$ = 15 mA.

TABLE 18

RESULTS FOR KARAOGLANOFF PLOTS
FOR CARBONATE OXIDATION

t,°C	Concentration (10^3 molal)	Transition Time (m-sec)	RT/2F (mV)	L.S. Slope (mV)	Correlation Coefficient	$E_\tau/4$ (mV)
550	8.295	108	35.4	-34.5	0.9994	-151
505	8.295	750	33.0	-36.5	0.9987	+ 16
505	8.295	430	33.0	-34.5	0.9977	+ 10
505	20.69	315	33.0	-32.6	0.9998	+103
505	20.69	315	-	-	-	-

Zambonin, albeit at ∿250°C, reported the reduction process

$$CO_2 + NO_3^- + 2e \rightleftarrows CO_3^= + NO_2^- \qquad (60)$$

Thus it is deduced that only CO_2 is produced during the oxidation of carbonate ions. On this basis and using the value of n = 2 measured from Karaoglanoff plots, the overall reaction

$$CO_3^= + NO_2^- \rightleftarrows CO_2 + NO_3^- + 2e \qquad (61)$$

rather than

$$CO_3^= \rightleftarrows CO_2 + \tfrac{1}{2}O_2 + 2e \qquad (62)$$

is proposed for the oxidation of carbonate. In all experiments at around 500°C, the equilibrium nitrite ion concentration was in excess of the carbonate ion concentration by at least a factor of two to one.

The mechanistic pathway involved has not been deduced from the present data. A number of pathways are possible which lead to rather complex electrochemical situations. The essential features, however, probably involve a fast dissociation equilibrium for carbonate ions

$$CO_3^= \underset{k_b}{\overset{k_f}{\rightleftharpoons}} CO_2 + O^{2-} \qquad (63)$$

where the equilibrium K is

$$K = \frac{k_f}{k_b} << 1 \qquad (64)$$

and $k_f >> 1$.

Subsequent electro-oxidation of oxide ions results in follow-up reactions such as

$$O^{2-} \rightleftarrows O^{-} + e \tag{65}$$

then $$O^{-} + NO_2^{-} \underset{\text{FAST}}{\rightleftharpoons} NO_3^{-} + e \tag{66}$$

or $$O^{-} \rightleftarrows [O] + e \tag{67}$$

and $$[O] + NO_2^{-} \xrightarrow[\text{FAST}]{} NO_3^{-} \tag{68}$$

More studies are required to completely resolve this interesting fundamental problem. Cyclic voltammetry is sensitive to the mechanistic pathways as would be expected and is precluded from analytical applications. Chronopotentiometry which is singularly suitable for carbonate ion determination via the Sand relationship has been used to monitor some of the chemical effects of carbon dioxide on this melt.

To aid the analytical detection of carbonate ions at these temperatures, the diffusion coefficient of these ions were measured as a function of temperature from data in Figures 39 and 40. The temperature dependence of diffusion of carbonate ions is given in the Arrhenius plot in Figure 44. The least squares equation relating $D_{CO_3^{=}}$ and temperature is given by

$$\ln D = -4.445 - 4.293 \times 10^3 \, T^{-1} \tag{69}$$

and $\Delta H = 8.5 \pm 1.0$ kcal mol^{-1}. Zambonin reported a value of $\Delta H = 6.8 \pm 1.0$ kcal mol^{-1} for data over the temperature range 230-300°C. Agreement between extrapolated D values is good bearing in mind the long extrapolation and the precision of the data.

The high temperature results presented here provide, through chronopotentiometry, a means of monitoring the carbonate ion concentration in the equimolar nitrate mixture.

4.4.3 The Chemistry of Carbon Dioxide and Carbonate Formation in the Equimolar Nitrate Mixture

The influence of carbon dioxide in contact with the nitrate melt at 505°C was monitored electrochemically over a period of days. Figure 45 shows the buildup of the carbonate ion concentration as deduced from the electrochemical measurements. These data show that the rate of reaction between carbon dioxide and melt is rather slow. Even after ∿80 hr, the carbonate concentration was well below the solubility limit calculated from Zambonin's data in Table 4. The likely route for carbonate formation can be judged from the thermodynamic calculations presented in Table 3 and probably involves nitrite ions viz,

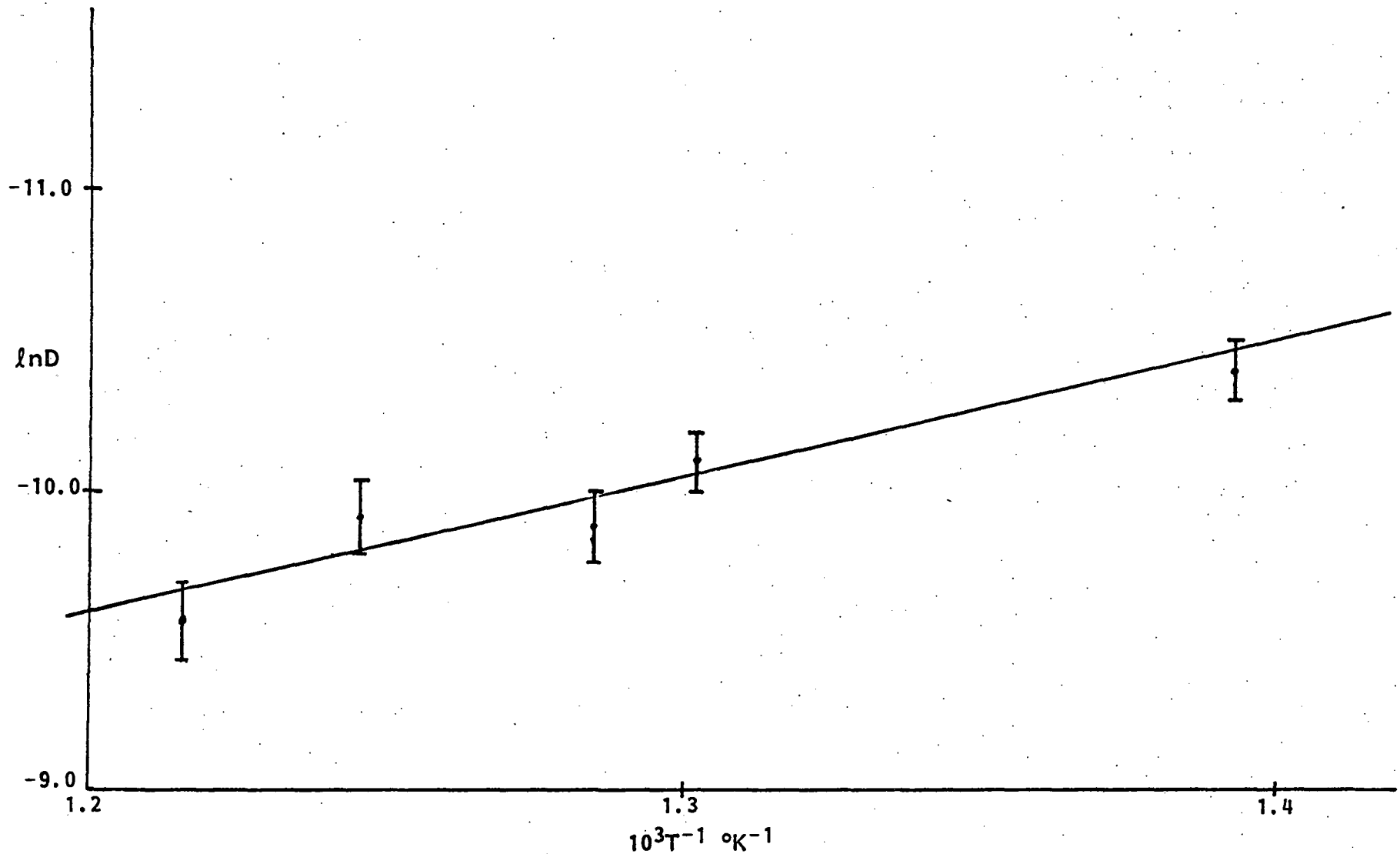

Fig. 44. Arrhenius plot for carbonate ion diffusion.

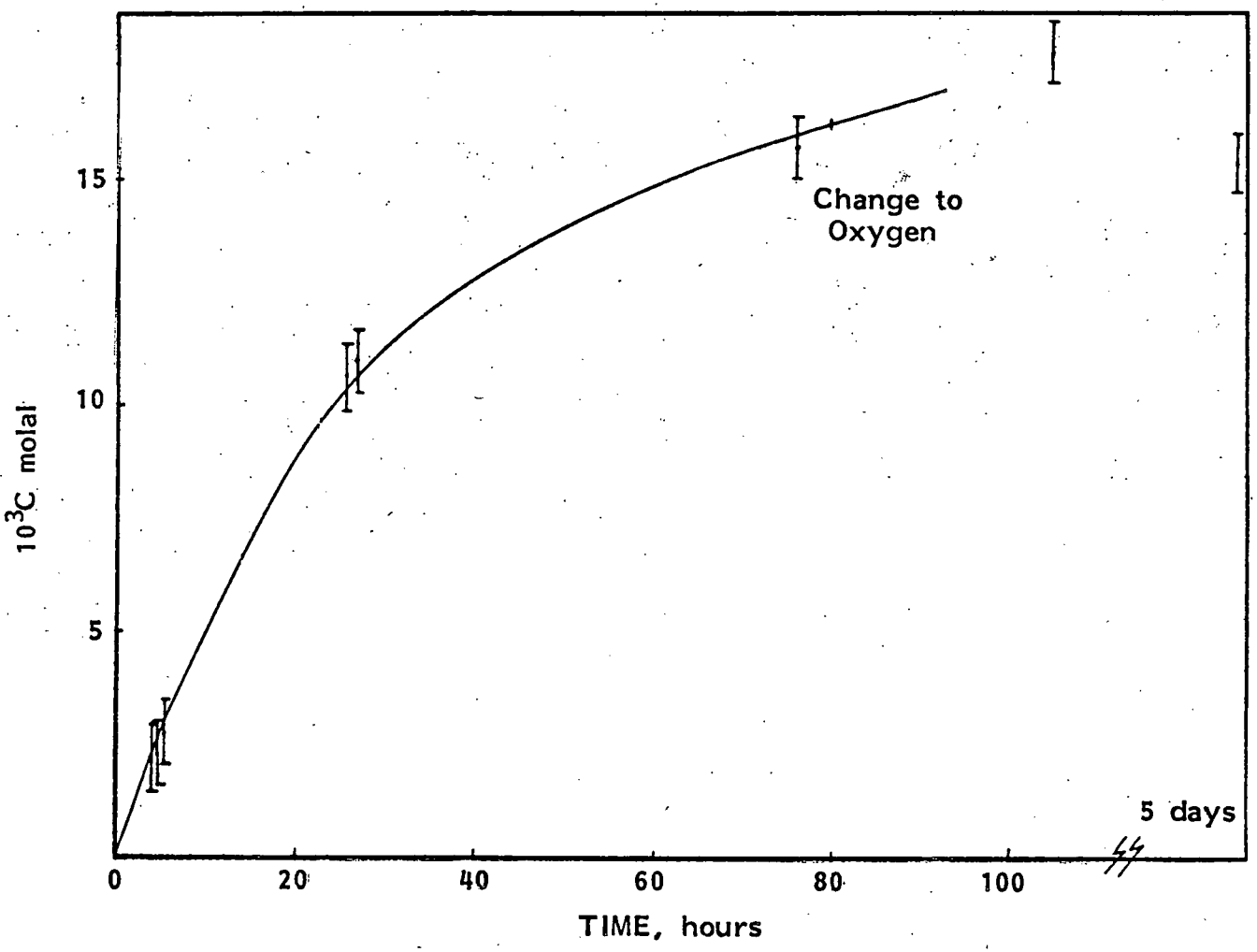

Fig. 45. Buildup of carbonate ions in the binary nitrate melt in contact with dry carbon dioxide. Carbonate ion concentration detected electrochemically.

$$CO_2 + 2NO_2^- \rightleftarrows CO_3^= + NO_2 + NO \qquad (70)$$

During the passage of CO_2, the outlet gas was tested for NO_2/NO components with starch iodide paper and a positive result was obtained. This confirmed the human sensor response! No positive result was obtained under oxygen or argon gas flow thus confirming that CO_2 and the nitrate/nitrite ions do indeed react. The rate of formation of carbonate ions is probably controlled by diffusion of CO_2 through the gas/melt interface, since the nitrite ion concentration at these temperatures was $\sim 100 \times 10^{-3}$ molal. Figure 46 shows a voltammogram under carbon dioxide atmosphere (compare with Figure 38 for added carbonate), confirming that the reaction product is indeed carbonate ion. No other new electroactivity was detected in the electroinactive range of the melt.

At no time was the solubility limit of carbonate ions detected, showing that the solubility is in excess of 80×10^{-3} molal at 505°C (compare Table 4). The buildup of carbonate ions in a thermal storage system would arise from the interaction of carbon dioxide in the air with the melt. Lower rates of buildup might be anticipated to be slow in view of the low partial pressure of carbon dioxide in air. Measurements with carbon dioxide-oxygen mixtures contain a few percent carbon dioxide showing increasing carbonate ion contents in this work. Because of the high solubility of carbonate at these high temperatures and the long contact (years) times, carbonate formation may become a significant problem in thermal storage where the melt is cycled between high and low temperatures. Comparison of carbonate solubilities in Table 4 suggest the magnitude of the problem.

Consideration may be given to blanketing the melt with inert gas to prevent carbonate buildup or alternatively, periodic removal of carbonate might be required. In the latter case, treatment of the melt with nitrogen dioxide or NO_2/O_2 mixture would probably be the mode of action.

An experiment was carried out in which a melt containing $\sim 80 \times 10^{-3}$ molal carbonate was treated with NO_2 gas for $\sim$1 hour. The melt was monitored prior to and after treatment. Figure 47 illustrates the results. No problem was detected for this process and the resultant melt was quite free of $CO_3^=$ and NO_2^- ions.

At low temperatures the reaction between CO_2 or wet CO_2 and the nitrate melt certainly occurs, Figure 48. However, the much lower solubility, nitrite ion concentrations, and diffusional rates suggest that carbonate formation will be much less of a problem at temperatures below 300°C.

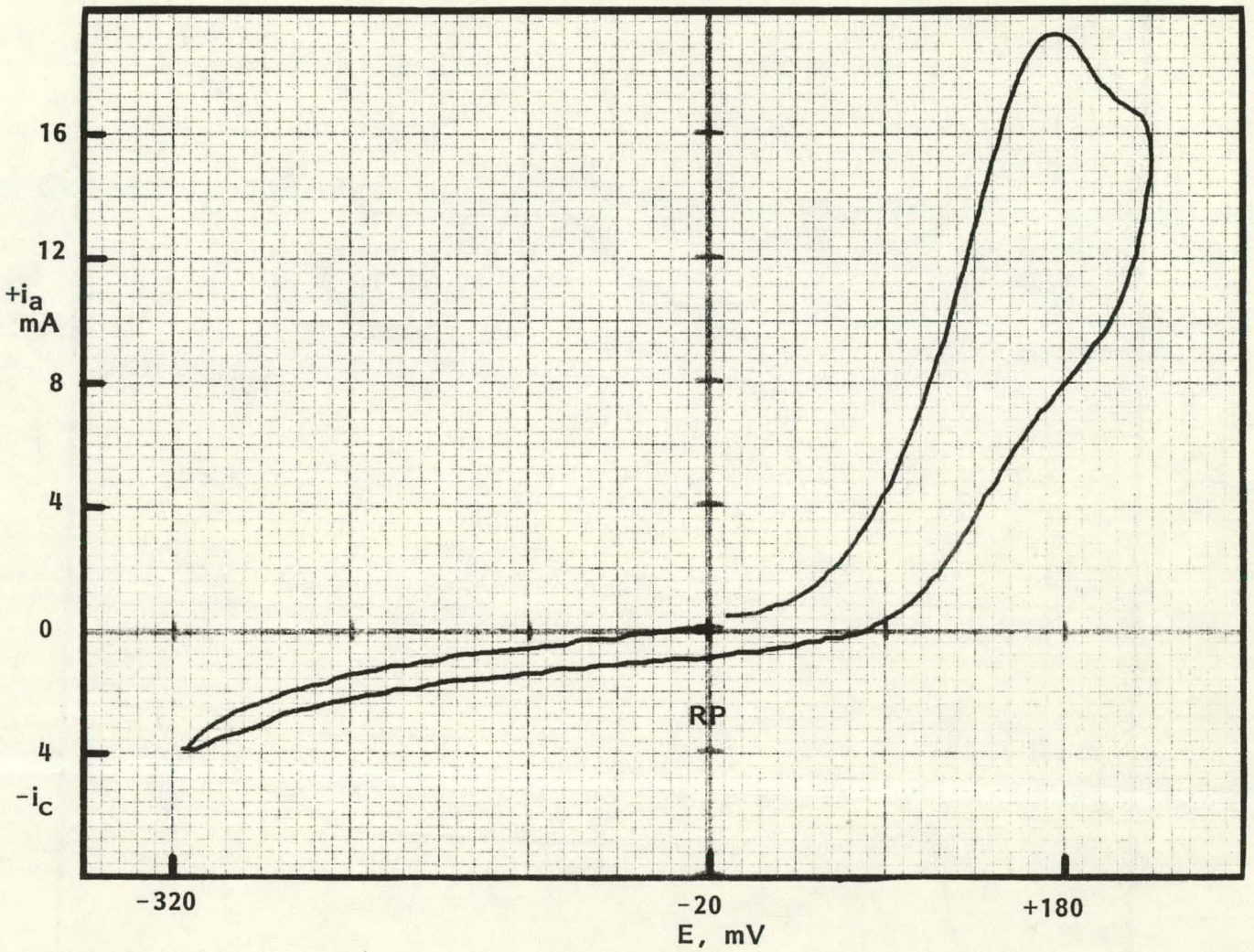

Fig. 46. Anodic peak observed after CO_2 in contact with nitrate melt after 3 days. E vs. Ag/Ag(1) 0.07m reference. Scan rate = 1.0 V-sec^{-1}.

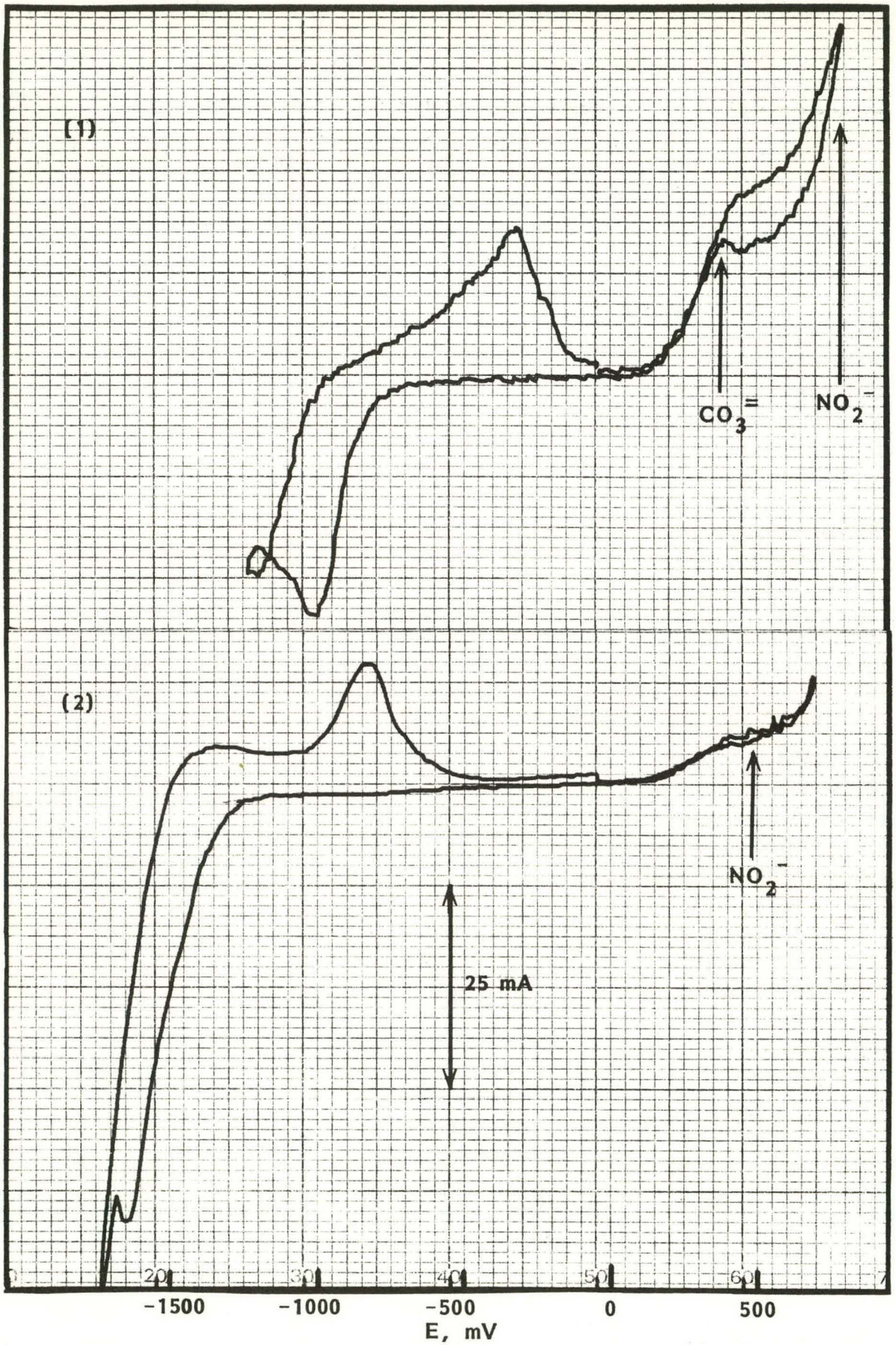

Fig. 47. Voltammograms showing the melts (1) containing carbonate and nitrate ions before NO_2 treatment and (2) after NO_2 treatment and showing developing NO_2^- ion peak, E vs. Ag/Ag(1) 0.07m reference electrode.

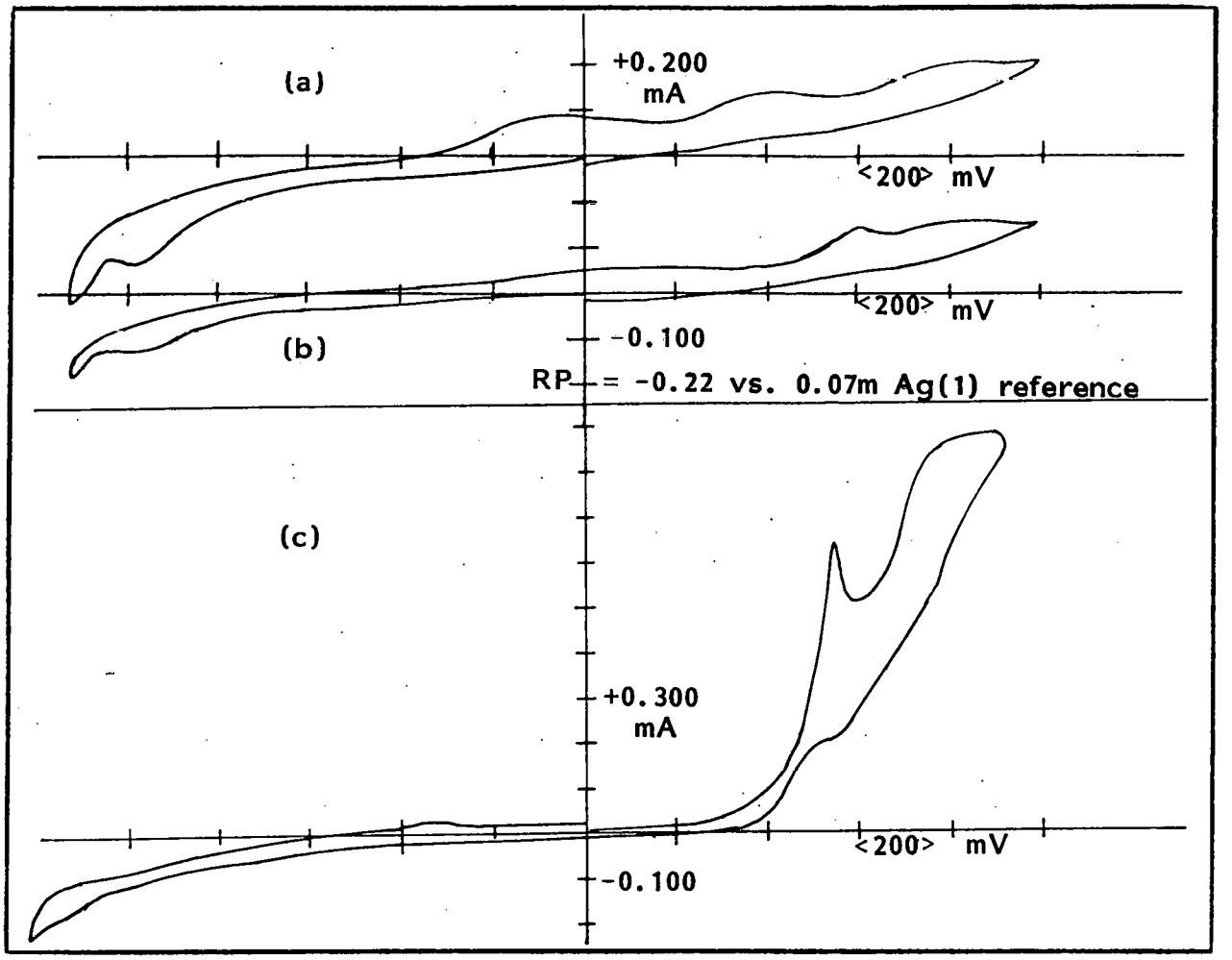

Fig. 48a. Cyclic voltammogram showing background during removal of CO_2/water: v = 0.100 V-sec^{-1}, T = 300°C (20 min after dry argon introduced).

48b. Cyclic voltammogram showing background 15 hours after dry argon: v = 0.100 V-sec^{-1}, T = 300°C.

48c. Cyclic voltammogram after addition of 30.8 x 10^{-3} molal $NaNO_2$ and 12.5 x 10^{-3} molal K_2CO_3: v = 0.100 V-sec^{-1}, T = 300°C.

REFERENCES

1. G. J. Janz et al., "Physical Properties Data Compilations Relevant to Energy Storage," Vol. II, p. 396, U.S. Department of Commerce, April 1979.

2. D. A. Nissen in Molten Nitrate Salt Technology Workshop, Sandia National Laboratory, October 1980.

3. E. Desimoni, P. Paniccia and P. G. Zambonin, J. Electroanal. Chem., 38, 373 (1972).

4. D. A. Nissen, Sandia Report, SAND81-8007, June 1981.

5. P. G. Zambonin, Anal. Chem., 43, 1571 (1971).

6. P. G. Zambonin and J. Jordan, Anal. Letters, 1, 1 (1967).

7. P. G. Zambonin and J. Jordan, J. Am. Chem. Soc., 89, 6365 (1967).

8. E. Desimoni, F. Paniccia, L. Sabbatini and P. G. Zambonin, J. Appl. Electrochem., 6, 445 (1976).

9. F. Paniccia and P. G. Zambonin, J. Chem. Soc., Faraday Trans. 1, 69, 2019 (1973).

10. P. G. Zambonin, Anal. Chem., 44, 763 (1972).

11. R. W. Foreman, Abstract 663, Fall Meeting of The Electrochem. Soc., Florida, October 1980.

12. E. Sada, S. Katoh, H. Beniko, H. Yoshii and M. Kayano, J. Chem. Eng. Data, 25, 45 (1980).

13. P. E. Field and W. J. Green, J. Phys. Chem., 75, 821 (1971).

14. P. E. Field, Advances in Molten Salt Chemistry, Chapter 2 (Plenum Press, 1975), Vol. 3, p. 75.

15. M. Amadori, Atti Reale Accad. Lincei Sez 11, 22, 336 (1913).

16. M. M. Karnowsky, R. M. Biefeld and N. J. Norem, Sandia Report, SAND80-8052, March 1981.

17. E. Desimoni, F. Paniccia and P. G. Zambonin, J. Chem. Soc., Faraday Trans. 1, 69, 2014 (1973).

18. A. G. Keenan, C. G. Fernandez and T. R. Williamson, J. Electrochem. Soc., 121, 885 (1974).

19. K. A. Romberger, Thesis, The Pennsylvania State University, PA, 1967.

20. H. S. Swofford and P. G. McCormick, Anal. Chem., 37, 970 (1965).

21. P. G. Zambonin, Anal. Chem., 41, 868 (1969).

22. D. Inman and J. Braunstein, Chem. Comm., 148 (1966).

23. D. Inman, R. Spencer and S. H. White, unpublished work, see B.Sc. Thesis, City University, London, 1967.

24. G. G. Bombi, R. Freddi and M. Fiorani, Ann. Chim. (Rome), 56, 759 (1966).

25. L. E. Topol, R. A. Osteryoung and J. H. Christie, J. Phys. Chem., 70, 2857 (1966).

26. A. J. Calandra and A. J. Arvia, Electrochim. Acta, 11, 1173 (1966).

27. A. J. Calandra and A. J. Arvia, Electrochim. Acta, 12, 95 (1967).

28. D. Neiswander, see Ref. 2.

29. S. H. White, in Ionic Liquids, ed. by D. Inman and D. G. Lovering (Plenum Press, 1981), Ch. 12, p. 185.

30. P. G. Zambonin, V. L. Cardetta and G. Signorile, J. Electroanal. Chem., 28, 237 (1970).

31. G. Bertozzi, Z. Naturforsch, 22a, 1748 (1967).

32. H. Haug and L. F. Albright, Ind. Eng. Chem. Press Dess. Develop., 4, 241 (1965).

33. H. S. Hull and A. G. Turnbull, J. Phys. Chem., 74, 1783 (1970).

34. J. P. Frame, E. Rhodes and A. R. Ubbelohde, Trans. Faraday Soc., 57, 1075 (1961).

36. T. Kozlowski and R. F. Bartholomew, J. Electrochem. Soc., 114, 937 (1967).

36. D. G. Lovering and R. M. Oblath, in Ch. 11, Ref. 29.

37. T. E. Geckle, Thesis, Pennsylvania State University, 1969.

38. J. Jordan, J. Electroanal. Chem., 29, 127 (1971).

39. S. H. White, Proposal to Sandia, Contract 20-2991, 1980.

40. M. Peleg, J. Phys. Chem., 71, 4553 (1967).

41. H. S. Swofford and H. A. Laitinen, J. Electrochem. Soc., 110, 814 (1963).

42. S. H. White, unpublished work.

43. C. R. Wolfe and R. D. Caton, Anal. Chem., 43, 663 (1971).

44. D. Inman, J. Sci. Instr., 39, 391 (1962).

45. A. Weissberger and B. W. Rossiter, eds, Physical Methods of Chemistry, IIA. Electrochemical Methods (Wiley, 1971).

46. K. Vetter, Electrochemical Kinetics (Academic Press, 1967).

47. A. J. Bard and L. R. Faulkner, Electrochemical Methods (Wiley, 1980).

48. H. E. Bartlett and K. E. Johnson, Can. J. Chem., 44, 2119 (1966).

49. G. J. Hills and K. E. Johnson in Proceedings of the 2nd International Congress on Polarography, Cambridge, 1959 (London: Pergamon Press, 1961), p. 974.

50. J. M. deJong and G. H. J. Broers, Electrochim. Acta, 21, 605, 893 (1976).

51. A. F. J. Goeting and J. A. H. Ketelaar, Electrochim. Acta, 19, 267 (1974).

52. F. A. Cotton and G. Wilkinson, Advanced Inorganic Chemistry (Interscience, 1972).

53. F. Palmisano, L. Sabbatini, E. Desimoni and P. G. Zambonin, J. Electroanal. Chem., 89, 311 (1978).

54. T. Berzins and P. Delahay, J. Am. Chem. Soc., 75, 4205 (1953).

55. O. Dracka, Coll. Czech. Chem. Comm., 26, 2144 (1961).

56. O. Dracka, Coll. Czech. Chem. Comm., 41, 953 (1973).

57. J. M. Saveant and E. Vianello, Electrochim. Acta, 12, 1545 (1967).

58. R. S. Nicholson, Anal. Chem., 37, 667 (1965).

59. M. L. Olmstead, R. G. Hamilton and R. S. Nicholson, Anal. Chem., 41, 260 (1969).

60. N. S. Wrench and D. Inman, J. Electroanal. Chem., 17, 319 (1968).

61. S. B. Aganesova, P. Ladani, V. P. Yurkinskii and A. G. Morachevskii, Zhur. Prik. Khim., 48, 1164 (1975).

62. P. Delahay, J. Am. Chem. Soc., 75, 1190 (1953).

63. R. S. Nicholson and I. Shain, Anal. Chem., 36, 706 (1964).

64. R. S. Nicholson and I. Shain, Anal. Chem., 37, 178 (1965).

65. D. S. Polcyn and I. Shain, Anal. Chem., 38, 370 (1966).

66. Z. Galus, Fundamentals of Electrochemical Analysis (Horwood, 1976).

67. V. Yu. Filinovskii, Elektrokhimiya, 5, 635 (1969).

68. W. O'Deen and R. A. Osteryoung, Anal. Chem., 43, 1879 (1971).

69. H. S. Swofford and P. G. McCormick, Anal. Chem., 41, 146 (1969).

UNLIMITED RELEASE

INITIAL DISTRIBUTION

Division of Thermal and Mechanical Energy Storage Systems
MS 6B025 Room 1G-100
Forrestal Building
U.S. Department of Energy
Washington, D. C. 20585
Attn: M. Gurevich
S. Strauch
J. H. Swisher

Division of Solar Thermal Energy Systems
600 E Street N.W., Room 419
U.S. Department of Energy
Washington, D.C. 20585
Attn: W. Auer
G. W. Braun
C. Manngold
C. McFarland
J. E. Rannels
D. Stogoski

Albuquerque Operations Office
Special Programs Division
P. O. Box 5400
U.S. Department of Energy
Albuquerque, NM 87115
Attn: D. Schueler

San Francisco Operations Office
1333 Broadway
U.S. Department of Energy
Oakland, CA 94612
Attn: D. Elliott

Dr. Robert A. Osteryoung
Department of Chemistry
State University of New York at Buffalo
Buffalo, NY 14214

Prof. Harald A. Oye
Institutt for uorganisk kjemi
Norges tekniske hogskole
Universitetet i Trondheim
N-7034 Trondheim - NTH
NORWAY

John Neill
Advanced Energy Concepts
Suite I
11722 Sorrento Valley Rd.
San Diego, CA 92121

Aerospace Corporation
2350 El Segundo Blvd.
El Segundo, CA 90009
Attn: P. Mathur
L. R. Sitney

Steve P. Harnden
Arizona Public Service Company
P. O. Box 21666
Phoenix, AZ 85036

William F. Clancey
Babcock and Wilcox Company
P. O. Box 351
Barberton, OH 44203

Bill Oberjohn
Babcock and Wilcox
Box 835
Alliance, OH 44601

C. A. Bolthrunis
Badger Energy, Inc.
One Broadway
Cambridge, MA 02142

Robert L. Lessley
Bechtel
50 Beale
San Francisco, CA 94119

James P. Maddox
Biphase Energy Systems
2800 Airport Ave.
Santa Monica, CA 90405

George H. Rowe
Combustion Engineering
1000 Prospect Hill Road
Windsor, CT 06095

Sydney H. White (10)
EIC Labs., Inc.
55 Chapel Street
Newton, MA 02158

EPRI
P. O. Box 10412
3412 Hillview Ave.
Palo Alto, CA 94303
Attn: J. Bigger

Donald C. Erickson
Energy Concepts Co.
627 Ridgely
Annapolis, MD 21401

Patrick Joy
Solar Thermal Systems
Divisin of Exxon Enterprises, Inc.
P. O. Box 592
Florham Park, NJ 07932

T. V. Narayanan
Foster Wheeler
12 Peach Tree Hill Road
Livingston, NJ 07039

Donald J. Spellman
Gas Cooled Reactor Assoc.
3344 N. Torrey Pines Road
La Jolla, CA 92137

General Atomic Co.
P. O. Box 81608
San Diego, CA 92138
Attn: James Kaae
Daniel L. Vrable

Soeren S. Nielsen
Gould, Inc.
40 Gould Center
Rolling Meadows, IL 60008

JPL
4800 Oak Grove Dr.
Pasadena, CA 91103
Attn: J. Becker
V. Truscello

Martin Marietta Corporation
Box 179
Denver, CO 80201
Attn: David W. Neiswander
Tom Tracey

McDonnell Douglas
5301 Bolsa Ave.
Huntington Beach, CA 92647
Attn: Donald L. Endicott
George F. Greenwald

C. M. Kramer
Code 6130
Naval Research Lab
Washington, D. C. 20375

J. H. DeVan
Oak Ridge National Laboratory
Oak Ridge, TN 37830

Olin Corporation
275 Winchester Ave.
New Haven, CT 06511
Attn: Louis C. Fiorucci
Stephen L. Goldstein

Olin Corporation
120 Long Ridge Road
Stamford, CT 06904
Attn: Norman Christopher

Pacific Gas and Electric
3400 Crow Canyon Road
San Ramon, CA 94583
Attn: Jay Raggio

Dr. R. W. Foreman
Park Chemical Company
8074 Military Avenue
Detroit, MI 48204

Robert J. Walter
Rocketdyne
6633 Canoga Ave.
Canoga Park, CA 91360

Rockwell International
8900 De Soto Ave.
Canoga Park, CA 91304
Attn: Jerry B. Brukiewa, ETEC
Rick L. Howerton, ETEC
Ted Johnson, ESG
Anarg Z. Frangos

SERI
1536 Cole Blvd.
Golden, CO 80401
Attn: B. Butler
B. P. Gupta
R. G. Nix
R. Ortiz (SERI Library)

Kenneth Ladd
Southwestern Public Service Co.
P. O. Box 1261
Amarillo, TX 79170

Donald J. Liffengren
Stearns-Roger
4500 S. Cherry Creek Drive
Denver, CO 80217

United Engineers and Construction
30 S. 17th Street
Philadelphia, PA 19103
Attn: A. E. Rosica

Stuart A. Shiels
Westinghouse Electric Corporate
Advanced Reactors Division
Box 158
Madison, PA 15663

C. Winter, 400
A. Narath, 4000
J. H. Scott, 4700
G. E. Brandvold, 4710; Attn: J. F. Banas, 4716
J. A. Leonard, 4717
D. G. Schueler, 4720; Attn: J. V. Otts, 4721
J. K. Galt, 5000
R. S. Claassen, 5800
R. G. Kepler, 5810
M. J. Davis, 5830
N. J. Magnani, 5840
T. B. Cook, 8000; Attn: D. M. Olson, 8100
R. J. Gallagher, 8124
A. N. Blackwell, 8200
B. F. Murphey, 8300
D. M. Schuster, 8310
D. A. Nissen, 8312
R. W. Bradshaw, 8313
R. W. Mar, 8313
S. H. Goods, 8316
J. C. Swearengen, 8316
R. L. Rinne, 8320
L. Gutierrez, 8400
R. A. Baroody, 8410
R. C. Wayne, 8430
R. W. Carling, 8431 (5)
P. J. Eicker, 8431
L. G. Radosevich, 8431
C. S. Selvage, 8450
C. T. Yokomizo, 8451
A. C. Skinrood, 8452
D. B. Dawson, 8453
W. G. Wilson, 8453
C. M. Tapp, 8460
D. L. Hartley, 8500
Publications Division, 8265, for TIC (27)
Publications Division, 8265/Technical Library Processes Division, 3141
Technical Library Processes and Systems Division, 3141 (3)
M. A. Pound, 8214, for Central Technical Files (3)